UNSTEADY FLOWS IN DISTRIBUTED-OUTFLOW SYSTEMS

David C. Wiggert

A dissertation submitted in partial fulfillment
of the requirements for the degree of
Doctor of Philosophy in the
University of Michigan
Department of Civil Engineering
1967

April, 1967

To my parents with sincere gratitude

ACKNOWLEDGEMENTS

TABLE OF CONTENTS

TABLE OF CONTENTS (CONT'D)

LIST OF FIGURES

LIST OF FIGURES (CONT'D)

LIST OF TABLES

LIST OF PLATES

NOMENCLATURE

Symbol	Meaning	Dimensions (M, L, T)
A	Cross-sectional area of tube	L^2
A_o	Area of an orifice	L^2
A_k, B_k	Fourier coefficients, flowmeter frequency response	
AMP_k	Component of amplitude correction, flowmeter frequency response	
B	Coefficient for orifice outflow, $q = B\sqrt{H}$	
C	Capacitance per unit length, gA/a^2	L
$\tilde{C}$	Coefficient for friction term, $h_f' = \tilde{C}\,q^n$	
C_d	Orifice discharge coefficient	
C_β	Momentum coefficient	
D	Diameter of tube	L
G	Conductance, or leakage per unit length, $mB\bar{H}^{m-1}$	LT^{-1}
H	Piezometric head as a function of x and t	L
$H(0)$	Complex number independent of time	L
H_B	Bed pressure head (Chapter VI)	L
HR	Complex pressure-head transfer function	
$\bar{H}$	Mean value of head	L
K	System bulk modulus of elasticity, $a = \sqrt{K/\rho}$	$ML^{-1}T^{-2}$
$K(x)$	Laminar outflow coefficient (Chapter VI)	LT^{-1}
L	Inertance per unit length, $1/gA$	$L^{-3}T^2$
N	Number of discrete orifices	
P	Subscript denoting point P	
PH_k	Component of phase correction, flowmeter frequency response	

NOMENCLATURE (CONT'D)

Symbol	Meaning	Dimensions (M,L,T)
Q	Flow as a function of x and t	$L^3 T^{-1}$
$\overline{Q}$	Mean value of flow	$L^3 T^{-1}$
Q'	Flow corrected for phase and amplitude error	$L^3 T^{-1}$
R	Resistance per unit length, $n \tilde{C} \overline{Q}^{n-1}$	$L^{-3} T$
R	Subscript denoting point R	
R_e	Reynolds number, $R_e = VD/\nu$	
S	Subscript denoting point S	
V	Mean cross-sectional velocity as a function of x and t	LT^{-1}
ZR	Complex input impedance	$L^{-2} T$
Z_c	Characteristic impedance	$L^{-2} T$
a	Pressure-pulse wave speed, $a = \sqrt{K/\rho}$	LT^{-1}
b	Width of continuous orifice	L
f	Darcy-Weisbach friction factor	
g	Gravitational acceleration	LT^{-2}
h'	Head perturbation	L
h_f	Frictional head loss	L
h'_f	Frictional head loss per unit length	
i	$\sqrt{-1}$	
i	Subscript	
j	Superscript denoting number of iterations within one time step	
k, kk	Subscripts	

Symbol	Meaning	Dimensions (M,L,T)
ℓ	Length of tube	L
m	Exponent for lateral outflow, $\tilde{q} = BH^m$	
m	Subscript	
n	Exponent for friction term, $h'_f = \tilde{C}\, Q^n$	
n	Subscript	
p	Pressure as a function of x and t	$ML^{-1}T^{-2}$
$q, \tilde{q}$	Lateral outflow per unit length	$L^2 T^{-1}$
q'	Flow perturbation	$L^3 T^{-1}$
q_o	Outflow from one orifice	$L^3 T^{-1}$
t	Independent variable time	T
u,v,w	Velocity components of lateral outflow	LT^{-1}
v_p	Phase velocity, or velocity of propagation	LT^{-1}
x	Independent variable distance along tube	L
α	Rate of change of D_o with respect to x (Chapter VI)	
α, η, ξ	Parameters used in characteristic equations	
β	Dimensionless pressure rise	
γ	Complex propagation constant	L^{-1}
ζ	Relative outflow parameter	
θ	Angle of outflow vector relative to tube axis	
ν	Kinematic viscosity	$L^2 T^{-1}$
ρ	Fluid density	ML^{-3}

NOMENCLATURE (CONT'D)

Symbol	Meaning	Dimensions (M, L, T)
τ_o	Wall shear stress	$ML^{-1}T^{-2}$
ϕ	Relative area parameter	
ψ	Phase angle	
ω	Frequency	T^{-1}

I. INTRODUCTION

1.1. Basis for the Study

While much literature can be cited concerning the nature of distributed outflow in steady-state conditions,[1,7,11,13] few investigations can be found which contribute toward the general understanding of the nature of unsteady flows in a fluid line which experiences leakage.

The need for such a study, described herein, can be justified on several bases. With advancing technology industrial fluid processes are becoming increasingly complex. For example, the design of manifolds is often encountered in chemical processing plants and in the manufacture of paper; when the lateral outflow is predominant, the nature of the unsteady flow in the system is analogous to the dissipation of heat in a rod of finite length, or a plate of finite width, in that the governing equation is parabolic in form. As a second illustration, it might be desirable to analyze and design the longitudinal-conduit and multilateral-port system of a navigation lock.[16] If the valve-opening rate is small, one encounters a mass-acceleration problem; however with rapid valve motion, water-hammer effects must be taken into account.

The application of fluid mechanics to the study of blood flow in the cardiovascular system has been successfully attempted in recent years. The descending aorta in the thoracic and abdominal regions is basically a tapered, elastic tube possessing numerous side branches which divert the flow of blood as it journeys from its source of energy, the heart. This energy is dissipated throughout the aorta as the blood

travels its length and is distributed laterally into the branching arteries. The mathematical synthesis of such a complex branching tree would enhance the physical understanding of blood flow systems.

The author believes that this investigation represents the first time unsteady flows in manifolds have been treated in a general manner. The field of fluid transients is rapidly expanding. It is hoped that an analysis of distributed-outflow systems will contribute to a better understanding of the discipline.

1.2. Literature

The basic equations for unsteady flow through elastic conduits including a distributed-outflow parameter have been presented by Streeter et al.[20] The one-dimensional equations of momentum and continuity are reduced to hyperbolic form, applicable to the method of characteristics solution. The authors describe flow in an arterial segment, and assume the outflow per unit length to be proportional to the head difference inside and outside the tube.

Recently Rudinger[17] has presented the characteristic equations, and has included a distributed-leakage parameter with which any type of lateral outflow may be assumed, e.g., a number of branching tubes. If one assumes the fluid to be incompressible relative to the distensibility of a vessel wall such as an artery, the three nonlinear equations required for analysis are, after Rudinger,

$$g\frac{\partial H}{\partial x} + \frac{\partial V}{\partial t} + V\frac{\partial V}{\partial x} + \Lambda = 0 \; ,$$

$$\frac{\partial}{\partial x}(AV) + \frac{\partial A}{\partial t} + X = 0 \; ,$$

$$A = A(H, \; x, \; t) \; ,$$

in which H , V , and A are the pressure head, velocity, and cross-sectional area, respectively. The first relation is the momentum balance in which Λ represents the resultant of all longitudinal body and dissipative forces. In the continuity equation X designates the volume flow removed per unit length of the vessel. The third relation is the equation of state of the vessel which represents the relationship between the cross-sectional area, the pressure, and other parameters.

By linearizing the basic equations one can obtain analytic solutions. Attinger and Anne[3] discuss the linearized Navier-Stokes equation and the continuity equation in relation to blood-flow systems. They include a leakage-flow parameter which is directly proportional to the pressure:

$$\frac{\partial H}{\partial x} + L \frac{\partial Q}{\partial t} + RQ = 0 \, ,$$

$$\frac{\partial Q}{\partial x} + C \frac{\partial H}{\partial t} + GH = 0 \, .$$

The flow is represented by Q , R is the viscous resistance term, L the fluid inertance, C the capacitance, and G the parallel conductance or leakage per unit length. These linearized equations are directly analogous to the electric transmission-line equations, and, with appropriate values of L , R , C and G , are valid for many types of fluid lines as well as arterial systems. Moore[15] presents parallelisms between the telegraphers equations and the equations for various nonelectromagnetic waves.

While this thesis is primarily concerned with unsteady flow, it is necessary to know the initial boundary-value solution in a distributed fluid line, especially if subsequent transients in the system

are of a high frequency or rapidly dissipate. For most practical situations this initial condition is of a steady-state nature. A sizeable amount of literature is available concerning the analysis of a manifold under steady-flow conditions -- a few pertinent references will be cited in this discussion.

A theoretical beginning point is a study performed by McNown and Hsu[12] in which free streamline theory is used to determine the characteristics of divided flow through two-dimensional conduits. McNown[11] has made a detailed investigation of pipe manifold flow, combining the results of experimental data with simplified theory. Included is a review of literature covering the stated field, both experimental and theoretical. Papers by Acrivos et al.,[1] Horlock,[7] and Markland[13] are of particular interest, where for the steady-state analysis of flow from pipe manifolds, the authors assume a distributed-outflow mechanism in the form of a continuous slot, thereby simulating a finite number of orifices distributed along the axis of the conduit. They simplify the energy equation which governs flow through the ports, and combining it with the one-dimensional forms of the momentum and continuity equations, obtain either analytical or step-wise solutions for the distribution of flow in the manifolds.

1.3. Objective

The primary objective of this thesis is to present a general analysis of unsteady, nonuniform flow variations in fluid lines which experience lateral outflow distributed along the axis of the tube. In particular, the distributed-outflow mechanism might be a number of

orifices, or it may be a series of lateral fluid lines branching from the main section. Both transient and steady-oscillatory flows are considered. An original contribution is the recognition of a class of flows which is governed by a parabolic partial differential equation.

The purpose of the experimental investigation is to observe and analyze low-frequency oscillating flows in a manifold system, and to verify the concomitant governing equations.

Since the equations of motion and continuity are reduced to two different forms, viz., hyperbolic and parabolic, it is necessary to show the range of applicability of these restricted forms once limiting assumptions have been imposed.

1.4. Scope and Plan

Consideration is given to various problems associated with distributed outflow, including the analysis of steady-state conditions, water-hammer surges, and steady-oscillating flows. Numerical solutions are based on the following techniques: (1) the Runge-Kutta method for steady flows, (2) the method of characteristics to solve the equations of motion and continuity in hyperbolic form, (3) a finite-difference method based on the Gauss-Seidel iteration coupled with the Crank-Nicolson approximation to the second derivative[4] which solves the nonlinear parabolic equation, a reduced form of the momentum and continuity relations, and (4) impedance methods which provide analytical solutions of the linearized equations for steady periodic flows.

The order of investigation is as follows:

1. Computer analysis of surges in a manifold system, comparing a finite-orifice line with a continuous-orifice line.

Emphasis is given to the solution of the hyperbolic form of the continuity and momentum equations. Consideration is also given to steady-state or initial conditions.

2. The analysis of experimental data of low-frequency, oscillating flows in an orifice manifold. It is shown that the behavior of system variables (i.e., heads and flows) can be predicted from the developed theories, and particular attention is given to the verification of the parabolic equation.

3. Synthesis of a portion of the arterial tree of a dog, where attention is directed to the prediction of pressures and flows for various outflow conditions.

In the appendices one will find the numerical methods necessary to solve the hyperbolic and parabolic forms of the momentum and continuity relations.

II. ANALYTICAL FRAMEWORK

This chapter is devoted to a theoretical consideration of flows, both steady and unsteady, in a fluid line experiencing distributed outflow. The general equations of momentum and continuity including a leakage term are presented. Relations are developed for flow in a manifold, both for a line possessing a number of discrete orifices, and for a line which contains a continuous orifice. By means of imposed limiting assumptions, the governing equations for the continuous-orifice system reduce to either hyperbolic or parabolic form. In addition, impedance relations which include leakage are given in a form applicable to a manifold system.

Throughout the remainder of this thesis, a manifold system refers to a tube with either one or a series of orifices distributed along its longitudinal axis, and the orifice may be circular or a continuous slot.

2.1. Equations of Motion and Continuity for a Tube Including Distributed Outflow

The general momentum and continuity relations including leakage have recently been presented by Rudinger,[17] whose basic equations appear in Chapter I. He does not take into account the possibility that the leaking fluid may possess a component of axial momentum. Earlier, Streeter et al.[20] accounted for this by assuming that the fluid leaving through the walls has its axial momentum reduced by contact with the lateral tube which branches from the main conduit. These authors were concerned with highly distensible tubing in which the fluid medium could be considered incompressible.

For the continuity and momentum balances, one can follow the normal procedure in water-hammer analysis where the pressure is assumed to be transversely uniform and to vary only along the longitudinal axis of a conduit. In a like manner the mean cross-sectional velocity is employed. Consider a horizontal, elastic tube containing a compressible fluid. The system is experiencing lateral outflow per unit length, designated as q, which is leaving a control volume with an axial velocity component v, and at an angle θ to the horizontal, Figure 1. After neglecting the differential terms of higher order, the equation of motion in the axial, or x-direction for one-dimensional flow is

$$-A \frac{\partial p}{\partial x} \delta x - \tau_0 \pi D \delta x = \frac{\partial}{\partial x} (\rho A V^2) \delta x + \frac{\partial}{\partial t} (\rho A V \delta x)$$
$$+ C_\beta \rho q V \delta x ,$$

(1)

in which A is the cross-sectional area, p the piezometric pressure, τ_0 the wall shear stress, D the inside tube diameter, ρ the fluid density, and V is the mean fluid velocity. The time and distance parameters are t and x, respectively.

It is assumed that the axial component of velocity of the outflow can be expressed as $v = C_\beta V$, where C_β is defined as a momentum coefficient. Since, in the manifold, the outflow is drawn off from the fluid within the boundary layer, the magnitude of C_β will depend upon the shape of the velocity profile in addition to the geometry of the outflow mechanism. Under steady-state conditions, various authors[7,13] have assumed $C_\beta = 1$ for orifice outflow, and for outflow which leaves through lateral branches normal to the manifold, they assumed $C_\beta = 0$. The assumption can be validated by experimental

$P \frac{\partial A}{\partial X} \delta X$

$\tau_o \pi D \delta X$

PA

$PA + \frac{\partial}{\partial X}(PA)\delta X$

(a)

$\rho V A \delta t$

$\left[\rho V A + \frac{\partial}{\partial X}(\rho V A)\delta X \right]\delta t$

$\rho q \delta X \delta t$
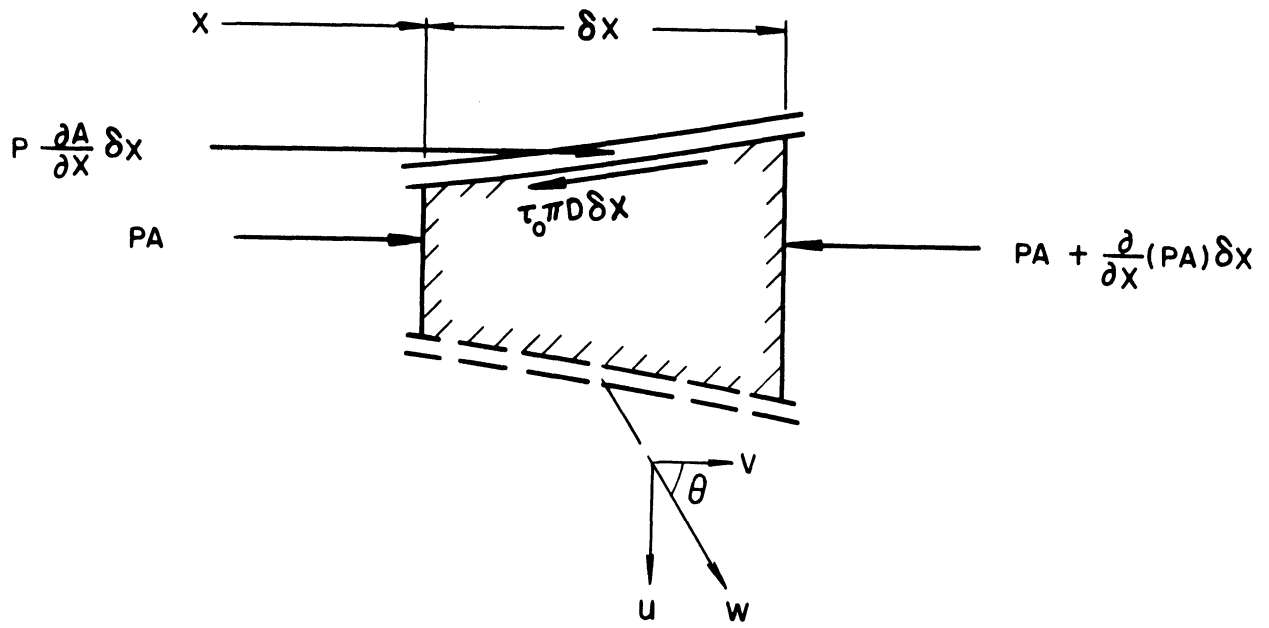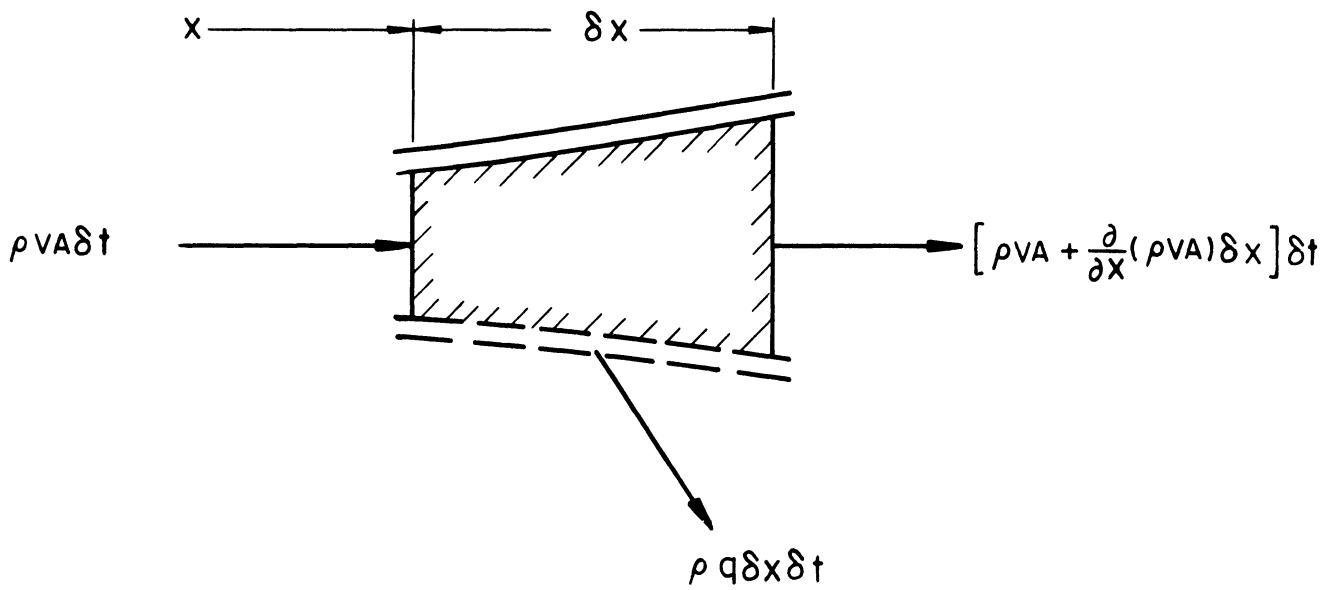
(b)

Figure 1.   (a) Forces Acting on Segment of Fluid. (b) Continuity
Balance on Segment of Fluid.

investigation, but due to its detailed nature, such a study is not considered here. For the systems which are analyzed in the following chapters, the effects of lateral axial momentum are minor.

The continuity balance, Figure 1, is expressed by the equation

$$- \frac{\partial}{\partial x} (\rho AV) \delta x - \rho q \delta x = \frac{\partial}{\partial t} (\rho A \delta x) . \qquad (2)$$

Equations (1) and (2) are basically those given by Streeter et al.,[20] where they assumed $C_\beta = 1$. The significance of C_β will be demonstrated in Chapter III.

2.2. Flow in a Manifold System

A restriction is now imposed on the distributed-outflow parameter, namely that consideration be given only to an orifice type of lateral outflow. This restriction will be eliminated in Chapter VI.

The study of unsteady flows in a manifold is a logical approach to the general analysis of distributed outflow. If one employs a smooth, stiff, cylindrical manifold the outflow parameter is somewhat isolated, and the use of an orifice as the outflow mechanism affords a reasonably well-defined head-flow relationship. There is a degree of similarity between a manifold system and a fluid line which possesses multiple lateral tubes; in either case one must study the momentum and energy relations of the dividing flow and account for these in the main conduit. Differences arise in the description of the outflow parameter, q , and in the limiting assumptions imposed upon the momentum and continuity relations.

Consider a manifold under steady-flow conditions; the lateral outflow can be related to the piezometric head, H , by the simplified Bernoulli relation

$$q = B \sqrt{H} , \qquad\qquad (3)$$

in which B will dictate whether the orifice is finite or continuous. For a single orifice, $q_O = C_d A_O \sqrt{2gH}$, in which C_d is the discharge coefficient and A_O is the orifice area. Any attempt to improve Equation (3) by including additional terms would distract from the ensuing analyses, and in the manifolds which are analyzed, including the experimental models, it will be seen that it is sufficient. The reader is directed to the references cited in Chapter I for detailed considerations dealing with the nature of orifice outflow.

In addition, it is assumed that Equation (3) is valid for any time at any given location in an unsteady flow situation. If we take the flow in the orifice to behave in a quasi-steady manner, Equations (1) through (3) can be combined to yield succinct, meaningful solutions.

2.2.1. Line Possessing a Finite Number of Orifices

In an actual physical situation lateral outflow might occur at discrete points along a manifold axis. However, if one can assume that the number of orifices in a given length is of sufficient size, then as a limiting condition, the manifold can be regarded as a homogeneous system consisting of a main tube with a longitudinal slot. Acrivos et al.[1] relate such criteria for steady flow conditions. Thus it seems appropriate to compare unsteady flows in a finite-orifice system with an equivalent continuously-slotted manifold.

Consider a cylindrical fluid line possessing 1, 2, ..., N orifices, Figure 2. Assume that across one orifice the magnitudes of the time rate-of-change of momentum and losses are small and can be neglected. Then the momentum and continuity balances across one orifice are,

$$H_2 - H_1 = \frac{1}{g}(V_1^2 - V_2^2) - \frac{C_\beta\, q_o\, V_1}{Ag} \,, \qquad (4)$$

$$V_2 - V_1 = -\frac{C_d\, A_o}{A}\sqrt{g(H_1 + H_2)} \,. \qquad (5)$$

It is assumed that from one orifice the outflow is

$$q_o = C_d\, A_o\, \sqrt{g(H_1 + H_2)} \,. \qquad (3a)$$

For the steady-state solution one can progress in the $+ x$ direction; in Figure 2 at point i , V_{1_i} and H_{1_i} are known, and a simultaneous solution of Equations (4) and (5) will give V_{2_i} and H_{2_i} . If $K_1 = (C_d A_o/A)^2$, then

$$V_{2_i} = \frac{1}{2(1+K_1)}\left[V_{1_i}(2 + C_\beta K_1) \right.$$

$$\left. - \sqrt{V_{1_i}^2(2+C_\beta K_1)^2 + 4K_1(1+K_1)[2gH_{1_i}+(1-C_\beta-1/K_1)V_{1_i}^2]} \right], \quad (6a)$$

$$H_{2_i} = \frac{1}{gK_1}(V_{2_i} - V_{1_i})^2 - H_{1_i} \,. \qquad (6b)$$

Furthermore,

$$V_{1_{i+1}} = V_{2_i} \,, \qquad (6c)$$

$$H_{1_{i+1}} = H_{2_i} - h_f(V_{2_i}) \,. \qquad (6d)$$

$H_o + \triangle H \sin(\omega t)$

H_o

R

1   2   3   i-1   i   i+1   N   S

X

O

ℓ

DISCRETE   MANIFOLD

H_1

V_1 H_2

V_2

q
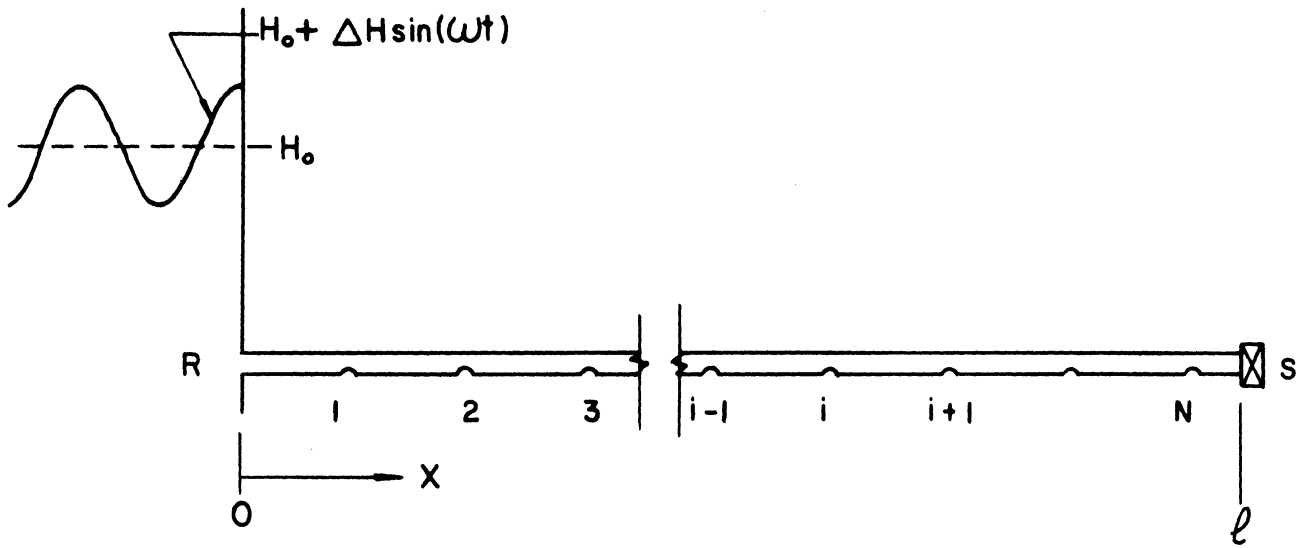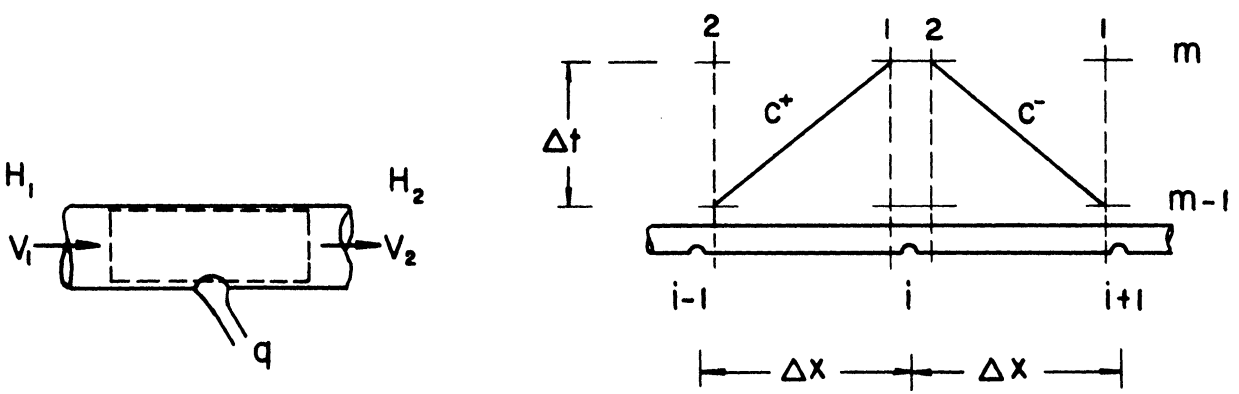
**DETAIL AT
ONE ORIFICE**

2   1 2   1   m

$\triangle t$

c^+ c^-

m-1

i-1   i   i+1

$\triangle x$ $\triangle x$

FINITE – DIFFERENCE   SCHEME

Figure 2.   Manifold Possessing a Finite Number of Orifices.

In Equation (6d), $h_f(V_{2_i})$ is the frictional head loss in the closed tube between orifices. Normally for fully developed flow,

$$h_f(V_{2_i}) = f \frac{\Delta x}{D} \frac{V_{2_i}^2}{2g} ,$$

in which f is the Darcy-Weisbach friction factor.

Unsteady flows are handled in the following manner. Assume values of H and V at points $i-1$ and $i+1$ to be known at time $m-1$. To compute the four unknowns at point i, time m, two relations in addition to Equations (4) and (5) are required: referring to Figure 2, these are the algebraic form of the wave equations[19] in the closed tube on either side of the orifice at i,

$$V_{1_{i,m}} = C_1 - C_2 H_{1_{i,m}} , \tag{7a}$$

$$V_{2_{i,m}} = C_3 + C_4 H_{2_{i,m}} , \tag{7b}$$

$$\left.\begin{aligned}
C_1 &= \frac{g}{a} H_{2_{i-1,m-1}} + V_{2_{i-1,m-1}} - \frac{g}{a} h_f(V_{2_{i-1,m-1}}) , \\
C_2 &= C_4 = g/a , \\
C_3 &= -\frac{g}{a} H_{1_{i+1,m-1}} + V_{1_{i+1,m-1}} - \frac{g}{a} h_f(V_{1_{i+1,m-1}}) .
\end{aligned}\right\} \tag{7c}$$

In these equations one assumes the frictional head loss to be lumped at one end of the segment Δx where the velocity is known at time $m-1$. The time increment, Δt, is $\Delta x/a$, in which a is the pressure-pulse wave speed. In addition, it is assumed that the frictional losses behave in a quasi-steady manner, e.g.,

$$h_f(V) = f \frac{\Delta x}{D} \frac{V|V|}{2g} ,$$

a method which has commonly been used by previous investigators.

The simultaneous solution of Equations (4), (5), (7a), and (7b) is simplified by letting $L_1 = H_1 + H_2$ and $L_2 = H_2 - H_1$:

$$L_1 = \frac{1}{2C_2^2} \left[[K_2^2 - 2C_2(C_3 - C_1)] \right.$$

$$\left. - \sqrt{[K_2^2 - 2C_2(C_3 - C_1)]^2 - 4C_2^2(C_3 - C_1)^2} \right] , \qquad (8a)$$

$$V_{1_{i,m}} = \frac{K_2^2 L_1 - g/C_2 [K_2\sqrt{L_1} + (C_3 + C_1)]}{K_2 \sqrt{L_1} (2-C_\beta) - 2g/C_2} , \qquad (8b)$$

$$V_{2_{i,m}} = V_{1_{i,m}} - K_2 \sqrt{L_1} , \qquad (8c)$$

$$L_2 = \frac{1}{C_2} [V_{2_{i,m}} + V_{1_{i,m}} - (C_3 + C_1)] , \qquad (8d)$$

$$H_{1_{i,m}} = \frac{1}{2} (L_1 - L_2) , \qquad (8e)$$

$$H_{2_{i,m}} = \frac{1}{2} (L_1 + L_2) . \qquad (8f)$$

In these equations $K_2 = C_d A_o \sqrt{g}/A$.

One can now proceed to evaluate system variables on a time-distance grid. At time zero, Equations (6a) through (6d) will yield the steady-state values of H_1 , V_1 , H_2 , V_2 , and q_o at discrete points i . At any time greater than zero, Equations (8a) through (8f) will evaluate the heads and velocities on either side of a lateral orifice, and the flow out of the orifice. The time-variable boundary conditions will complete the solution; if either head or velocity is known at the boundary, then the other can be computed. As illustration, in Figure 2, the upstream head is given by

$$H = H_o + \Delta H \sin(\omega t) ,$$

in which H_O, ΔH and ω are known. Then substituting into Equation (7b), V can be determined. It is assumed that no orifice exists at the upstream end of the manifold. The downstream boundary condition is handled in a similar manner; if a valve is located at $x = \ell$, a gate equation can be combined with Equation (7a) to yield H and V at that point. If one encounters a dead end at $x = \ell$, then $V = 0$ and the head can be determined from Equation (7a).

In the use of Equations (8a) through (8f) it is convenient to have equal time steps at each point i . Since $\Delta t = \Delta x/a$, and a is assumed to be constant, the segment Δx must be of the same length between each orifice and at each end of the manifold.

Equations (6a) through (6d) and (8a) through (8f) comprise a set of nonlinear difference equations from which heads and flows in a discrete-orifice manifold can be computed. In the following three sections the limiting case as the distances between orifices approach zero is considered. The resulting equations are simplified in the sense that they become differential equations.

2.2.2. The Steady-State Solution

Attention is now directed to the continuous manifold, Figure 3. Assume the walls of the conduit very rigid and the fluid incompressible. Then for a cylindrical tube $\frac{\partial}{\partial x} (\rho A)$ and $\frac{\partial}{\partial t} (\rho A \delta x)$ are zero, and Equations (1) and (2) combine in the manner

$$\frac{1}{\rho} \frac{\partial p}{\partial x} + \frac{4\tau_O}{\rho D} + (2-C_\beta) V \frac{\partial V}{\partial x} + \frac{\partial V}{\partial t} = 0 . \qquad (9)$$

$$H_o + \Delta H Sin (\omega t)$$

$$H_o$$

R
S

i-1   i   i+1

X

ΔX ΔX

O

ℓ

CONTINUOUS MANIFOLD

b
V
q
θ

A

δX

X

DETAIL OF CONTINUOUS ORIFICE
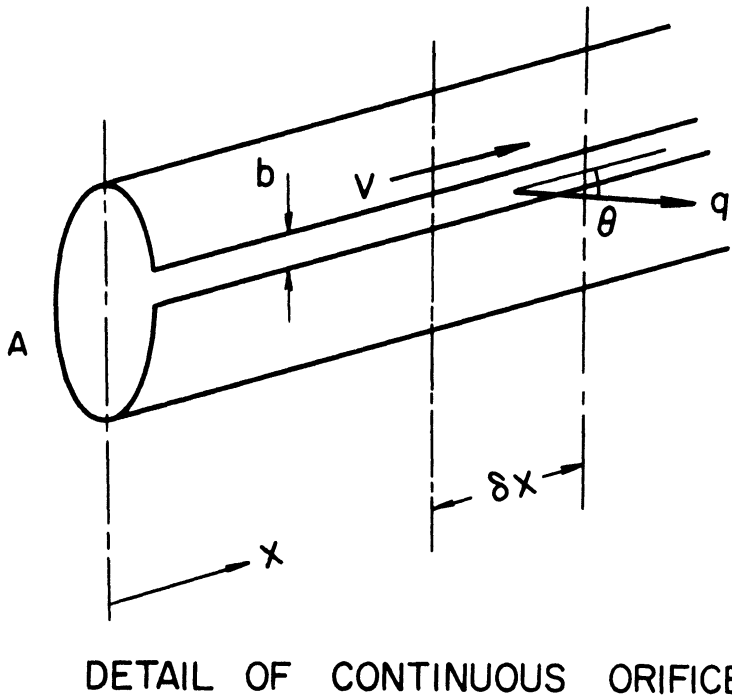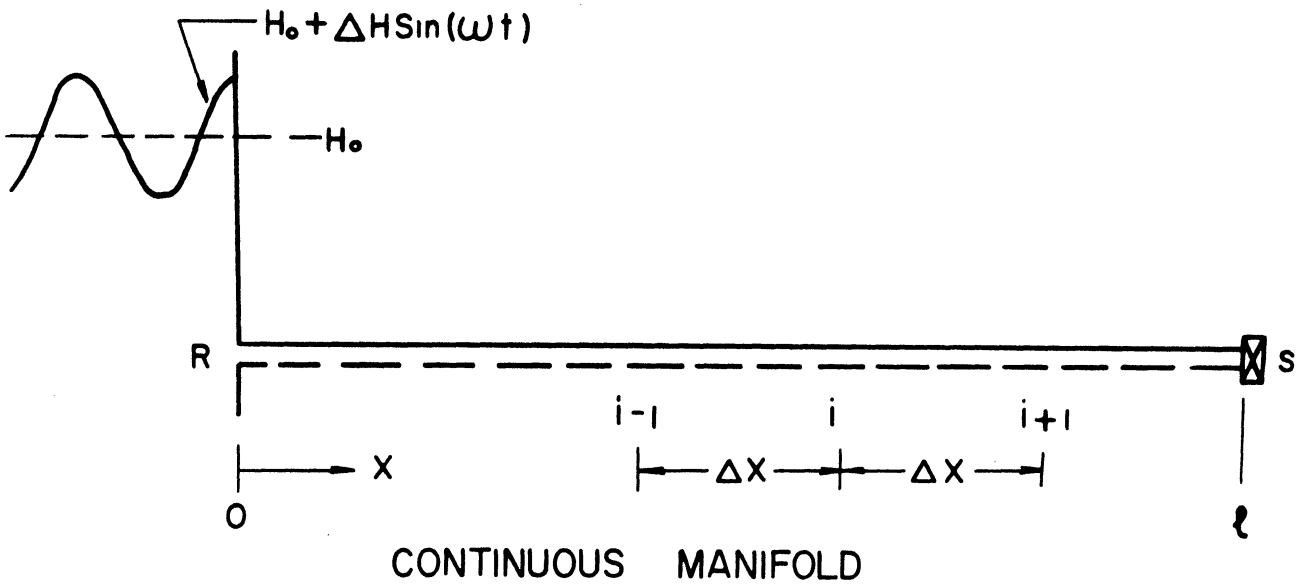
Figure 3. Manifold Possessing a Continuous Orifice.

For steady flows $\partial V/\partial t = 0$, and one can substitute for p the term $\rho g H$. The frictional-loss term can be given as

$$4\tau_o/\rho D = g\, h_f'(V) \ ,$$

in which

$$h_f'(V) = fV^2/2gD$$

is the head loss per unit length due to friction.

In the detail of Figure 3, the manifold contains a continuous orifice; for such a type of lateral outflow Equation (3) can be used,

$$q = C_d\, b\sqrt{2gH} \ , \qquad (3b)$$

where in Equation (3), $B = C_d b \sqrt{2g}$. The dimensions of q are volume rate per unit length. The discharge coefficient is C_d and b is the width of the slot. When one combines Equations (9) and (3b) with the reduced continuity relation, i.e.,

$$\frac{\partial V}{\partial x} = -\frac{q}{A} \ , \qquad (2a)$$

then H is eliminated, and since only one independent variable, x , is encountered the partial derivatives become total. The result is a non-linear, second-order differential equation:

$$\frac{d^2V}{dx^2} + K_1 V + K_2\, \frac{h_f'(V)}{\dfrac{dV}{dx}} = 0 \ , \qquad (10)$$

in which $K_1 = (C_d b/A)^2 (2-C_\beta)$ and $K_2 = (C_d b/A)^2 g$. If $Z_1 = V$ and $Z_2 = dV/dx$, then Equation (10) can be rewritten as two first-order differential equations,

$$\frac{dZ_1}{dx} = Z_2 \ ,$$

$$\frac{dZ_2}{dx} = -K_1 Z_1 - K_2\, \frac{h_f'(Z_1)}{Z_2} \ . \qquad (10a)$$

These can readily be solved simultaneously on a computer by utilizing a Runge-Kutta procedure.[2] This method is used to predict initial steady-state conditions in the unsteady flow situations encountered in Chapter III. Once V has been determined, H can be evaluated by combining Equations (2a) and (3b).

When the Darcy-Weisbach equation for the frictional head loss is used, i.e., $h_f^!(V) = fV^2/2gD$, it is possible to allow the friction factor, f , to vary in a prescribed manner. For example, consider a smooth manifold in which the flow is turbulent; for a Reynolds number up to 100,000 the Blasius formula can be used, where $f = .316\ Re^{-.25}$. If the flow were laminar, $f = 64/Re$. It is tacitly assumed that the velocity profile in the manifold is fully developed, and is akin to that in a closed tube. This is reasonably valid for a finite-orifice manifold which is approximated by a continuous orifice one. In the case that additional losses would occur due to flow separation, a modified loss term could be used in place of the Darcy-Weisbach relation.

With the steady-state equation for distributed outflow in a continuous manifold now formulated, the next two sections relate analytic framework necessary for the calculation of unsteady flows.

2.2.3. Parabolic Equation

If one considers unsteady flow in a fluid line with a continuous orifice, and assumes under specified conditions the system to be inelastic, Equations (9), (3b) and (2a) of Section 2.2.2 remain valid. Dividing Equation (3b) by A and equating with Equation (2a), one gets

$$\frac{\partial V}{\partial x} = -\frac{C_d b}{A}\sqrt{2gH} \ .$$

Differentiating with respect to x leads to

$$\frac{\partial^2 V}{\partial x^2} = - \frac{C_d b}{A} \sqrt{2g/H} \; \frac{1}{2} \; \frac{\partial H}{\partial x} = \left(\frac{C_d b}{A}\right)^2 g \; \frac{\frac{\partial H}{\partial x}}{\frac{\partial V}{\partial x}} \; ,$$

hence

$$g \; \frac{\partial H}{\partial x} = \left(\frac{A}{C_d b}\right)^2 \left(\frac{\partial V}{\partial x}\right)\left(\frac{\partial^2 V}{\partial x^2}\right) \; .$$

Substituting this relation into Equation (9), noting that $p = \rho g H$,
one obtains

$$\frac{\partial V}{\partial t} + \left(\frac{A}{C_d b}\right)^2 \left(\frac{\partial V}{\partial x}\right)\left(\frac{\partial^2 V}{\partial x^2}\right) + (2 - C_\beta) \; V \; \frac{\partial V}{\partial x} + g h_f'(V) = 0 \; . \quad (11)$$

Equation (11) can be classified as a nonlinear parabolic partial differ-
ential equation[5] with $V = V(x,t)$ as the dependent variable. A closed
analytic solution is not available; it is possible, however, to formulate
a finite-difference technique which will provide a numerical solution.
The method of solution is based on using the Crank-Nicolson approximation
of $\partial^2 V/\partial x^2$ combined with the Gauss-Seidel iteration within one time
step. Development of the implicit finite-difference equations corres-
ponding to the system of differential equations, and a discussion of
the convergence of the numerical solution will be found in Appendix A.

In a manner similar to the steady-state analysis of Section
2.2.2, we assume the frictional head loss in the manifold to be nearly
the same as that of a closed tube; if we further allow this head loss
to behave in a quasi-steady manner, the term $4 \, \tau_0/\rho D$ in Equation (9),
or identically $g h_f'(V)$ in Equation (11) becomes

$$g h_f'(V) = f \; \frac{V \, |V|}{2D} \; . \qquad (12)$$

Again it may be desirable to have f vary as a function of the Reynolds number.

The problem encountered in Equation (11) is one of mass transfer; since the walls of the manifold are assumed to be inelastic and the fluid incompressible, there will be no storage of energy in the system.

The nature of the unsteady flow in the system is analogous to the dissipation of heat by conduction in a rod of finite length, or a plate of finite width.[15] If T represents temperature and D_t thermal diffusivity, the temperature balance for such thermal conduction is

$$\frac{\partial T}{\partial t} = D_t \frac{\partial^2 T}{\partial x^2} \ .$$

This equation is linear and of parabolic form; it should be compared with Equation (11).

The boundary-value problem associated with the nonlinear parabolic equation requires $V(x,t)$ to be determined in the interior region by solving Equation (11). Equations (2a) and (3b) evaluate outflow and heads, respectively, and the solution of Equation (10) yields time-zero values of velocity. At the boundaries, the continuity balance, Equation (2a), provides time-variable relations which are known, since q is a function of H , related by Equation (3b), and H is an assumed known function of time. If a dead end exists at the downstream end of the system, the boundary condition is zero velocity. The boundary-value problem is summarized:

Variable	Relation to be Solved
$V(x,t)$	Equation (11)
$V(x,0)$	Equation (10)
$V(0,t)$	$\dfrac{\partial V}{\partial x} = -\dfrac{B}{A}\sqrt{H(0,t)}$
$V(\ell,t)$	$\dfrac{\partial V}{\partial x} = -\dfrac{B}{A}\sqrt{H(\ell,t)}$, or $V = 0$

The finite-difference solution to this system of equations is given in Appendix A.

2.2.4. Hyperbolic Equations

Equation (11) can be regarded as the limit of a hyperbolic equation which has the lines $t = $ constant as characteristics.[5] In order for Equations (1) and (2) to reduce to hyperbolic form, elasticity of the fluid and/or the tube must be taken into account. This means that in general, $\dfrac{\partial}{\partial x}(\rho A)$ and $\dfrac{\partial}{\partial t}(\rho A \delta x)$ are not equal to zero. For a stiff, elastic system one can relate the cross-sectional area and the density to the pressure head by the relation[21]

$$\frac{1}{\rho A \delta x}\ \frac{d}{dt}(\rho A \delta x) = \frac{g}{a^2}\ \frac{dH}{dt}\ , \tag{13}$$

in which a is the pressure-pulse wave speed. As an example, consider a manifold of length ℓ with $1, 2, \ldots, N$ evenly distributed orifices, each of area A_o . The distributed outflow can be expressed as

$$q = \frac{C_d A_o N}{\ell}\sqrt{2gH}\ . \tag{3c}$$

If the total area of the orifices, $A_o N$, is small, then the capacitance, or elasticity of the system will be close to that of a closed tube, and

it seems plausible that for such a system the pressure-pulse wave speed
can be approximated by $a = \sqrt{K/\rho}$, K being the system bulk modulus of
an equivalent closed tube.

When Equation (13) is combined with the momentum and continuity
relations, Equations (1) and (2) reduce to hyperbolic form, viz.,

$$g \frac{\partial H}{\partial x} + V \frac{\partial V}{\partial x} + \frac{\partial V}{\partial t} + gh_f'(V) + (C_\beta - 1) V \frac{q}{A} = 0 , \tag{14}$$

$$\frac{\partial V}{\partial x} + \frac{g}{a^2} \left(V \frac{\partial H}{\partial x} + \frac{\partial H}{\partial t} \right) + \frac{q}{A} = 0 . \tag{15}$$

Note that when $q = B \sqrt{H}$, these equations minus the second term in the
continuity balance are identical to Equation (11).

The characteristic equations corresponding to Equations (14)
and (15) are

$$\pm \frac{g}{a} \frac{dH}{dt} + \frac{dV}{dt} + \xi + \eta \pm \alpha = 0 , \tag{16}$$

$$\frac{dx}{dt} - (V \pm a) = 0 , \tag{17}$$

in which

$$\begin{rcases} \xi = gh_f'(V) , \\[2mm] \eta = (C_\beta - 1) V \frac{q}{A} , \\[2mm] \alpha = a \frac{q}{A} . \end{rcases} \tag{18}$$

Well known finite-difference methods have been established for their
solution.[5,9] It is necessary to integrate along two characteristic
lines simultaneously, and it is usually sufficient to make a first-order
approximation of the coefficients in the characteristic equations to do
so. However, the innocuous appearing term α in Equation (16) may be

of the same order of magnitude as either of the first two terms, $\frac{g}{a}\frac{dH}{dt}$
or $\frac{dV}{dt}$, and when an attempt to use a first-order approximation is made,
the solution becomes unstable. Lister[9] has presented a second-order
approximation to the coefficients, and Gray[6] has discussed the merits
of such an approximation used in conjunction with water-hammer problems.
When this method is applied, stable solutions can successfully be obtained.
Appendix B details the finite-difference methods used to solve Equations
(16) and (17). For a manifold $q = B\sqrt{H}$, and upon subsequent substitution
into Equation (16) and formulation of the finite-difference equations,
V can be eliminated and H is found by solving a quadratic equation.

The boundary-value problem relating to the hyperbolic equations
consists of solving Equations (16) and (17) in the interior region coupled
with the orifice-outflow relation $q = B\sqrt{H}$. The initial velocity dis-
tribution is afforded by the solution of Equation (10). At the boundaries,
if the head or velocity is a known function of time, then the other can
be computed by appropriately utilizing the characteristic equations.
Specific boundary conditions are presented in Appendix B.

2.3. <u>Impedance Relations Including Leakage</u>

In the previous section is was seen that for unsteady flows,
the momentum and continuity relations for a continuous manifold reduce
to one of two forms dependent upon assumed elastic properties of the
system. If one considers the manifold to be inelastic the governing re-
lations reduce to a parabolic equation; however, if one assumes some de-
gree of elasticity, either a compressible fluid or non-rigid walls, or
both, the equations become hyperbolic with the introduction of a pressure-
pulse wave speed. The elasticity of the system serves as the energy-storage

mechanism, and the distributed orifice along with frictional shear stresses tend to dissipate flow energy.

It would be desirable to have an analytic solution of Equations (1) and (2) to show in what measure friction, lateral outflow, elastic properties, and acceleration of fluid individually contribute to a distributed-outflow system such as a manifold. Such an analytic solution is obtainable only by eliminating or approximating the nonlinear terms in the governing equations. In this section impedance solutions are presented and a discussion is included which shows the range of applicability of the parabolic equation.

Impedance relations including leakage can be directly paralleled to those used in electric transmission-line theory.[15] Streeter and Wylie[21] have derived impedance equations for closed fluid lines. Their results are used herein, with the inclusion of a linearized leakage term.

Briefly, the differential equations, Equations (1) and (2), or alternatively, Equations (14) and (15) are taken in simplified form and averaged flow quantities are removed. The friction and distributed outflow terms are linearized, and the equations are solved for a sinusoidal disturbance imposed upon the system. The terms $V \frac{\partial H}{\partial x}$ and $V \frac{\partial V}{\partial x}$ are neglected; for large lateral outflow this may introduce a small error. With $C_\beta = 1$, a reasonable assumption for orifice outflow, Equations (14) and (15) are rewritten with head and flow as the dependent variables:

$$\frac{\partial H}{\partial x} + \frac{1}{gA} \frac{\partial Q}{\partial t} + h'_f(Q) = 0 , \qquad (14a)$$

$$\frac{\partial Q}{\partial x} + \frac{gA}{a^2} \frac{\partial H}{\partial t} + \tilde{q} = 0 , \qquad (15a)$$

in which $\tilde{q}$ is now the leakage term in place of q . Introducing the substitutions $H = \bar{H} + h'$ and $Q = \bar{Q} + q'$, in which $\bar{H}$, $\bar{Q}$ are mean values, and h' and q' are sinusoidal perturbations, $h_f'(Q)$ and $\tilde{q}$ can be linearized:

$$h_f'(Q) = \tilde{C} \, Q^n = \tilde{C} \, \bar{Q}^n + n \, \tilde{C} \, \bar{Q}^{n-1} \, q' + \ldots \, ,$$

$$\tilde{q} = BH^m = B\bar{H}^m + mB\bar{H}^{m-1} \, h' + \ldots \, .$$

Here frictional losses are assumed to be proportional to a power law of flow, (e.g., $\tilde{C} = f/(2gDA^n)$) and similarly, the leakage is proportional to some power of the pressure head. The first two terms of the expansions are retained (they are convergent for $q'^n < \bar{Q}^n$ and $h'^m < \bar{H}^m$), and the perturbations are substituted into Equations (14a) and (15a) resulting in

$$\frac{\partial h'}{\partial x} + L \frac{\partial q'}{\partial t} + Rq' = 0 \, , \qquad (14b)$$

$$\frac{\partial q'}{\partial x} + C \frac{\partial h'}{\partial t} + Gh' = 0 \, , \qquad (15b)$$

in which

$$L = \frac{1}{gA} \, , \qquad (19)$$

$$C = \frac{gA}{a^2} \, , \qquad (20)$$

$$R = n \, \tilde{C} \, \bar{Q}^{n-1} \, , \qquad (21)$$

$$G = mB\bar{H}^{m-1} \, , \qquad (22)$$

and are respectively termed inertance, capacitance, resistance and conductance. For orifice outflow, $m = 1/2$. If the leakage is large it would be more appropriate to base the resistance on an averaged mean flow, e.g., $R \approx n \, \tilde{C} \, (\bar{Q}/2)^{n-1}$.

The solutions of Equations (14b) and (15b) for steady periodic flows are,

$$h'(x,t) = (C_1 e^{-\gamma x} + C_2 e^{\gamma x}) e^{i\omega t} , \qquad (23)$$

$$q'(x,t) = \frac{1}{Z_c} (C_1 e^{-\gamma x} - C_2 e^{\gamma x}) e^{i\omega t} , \qquad (24)$$

$$\gamma = \sqrt{(G + i\omega C)(R + i\omega L)} , \qquad (25)$$

$$Z_c = \sqrt{(R + i\omega L)/(G + i\omega C)} . \qquad (26)$$

The complex propagation constant in γ and Z_c is termed the characteristic impedance. The real part of h' and q' represent the solution. In Equations (23) and (24), C_1 and C_2 are integration constants and depend upon boundary conditions. Consider the manifold of Figure 3; for an oscillating head input at the upstream end R , and a dead end downstream at S , the boundary conditions are

$$h'(0,t) = H(0) e^{i\omega t} , \text{ and } q'(\ell,t) = 0 .$$

H(0) is a known complex constant. With the values of C_1 and C_2 inserted, Equations (23) and (24) become

$$h'(x,t) = H(0)\frac{\cosh[\gamma(\ell-x)]}{\cosh(\gamma\ell)} e^{i\omega t} , \qquad (23a)$$

$$q'(x,t) = \frac{H(0) \sinh[\gamma(\ell-x)]}{Z_c \cosh(\gamma\ell)} e^{i\omega t} . \qquad (24a)$$

Furthermore the input impedance is

$$ZR = \frac{h'(0,t)}{q'(0,t)} = \frac{Z_c}{\tanh(\gamma\ell)} , \qquad (27)$$

and the pressure-head transfer function is given as

$$HR = \frac{h'(\ell,t)}{h'(0,t)} = \frac{1}{\cosh(\gamma\ell)} . \tag{28}$$

In Chapter III, Figures 13 and 14 show the input impedance and the trans-fer function, respectively, versus frequency, ω . It can be seen that leakage greatly affects the frequency-response patterns (the parameter ϕ corresponds to the magnitude of leakage). Particularly, a high leak-age can completely obliterate any response due to capacitance at a res-onating frequency.

It can be shown[15] that the analytical solution of the lin-earized form of Equation (11), the parabolic relation, is exactly given by Equation (24) or (24a) if capacitance, C , is neglected. Equations (14a) and (15a) are applicable to any transient-flow situation, whereas the use of the continuity balance leading to the parabolic equation, viz., $\frac{\partial V}{\partial x} + \frac{q}{A} = 0$, is restrictive, and implies that the middle term in Equation (15a) is minor compared to the remaining terms and hence can be neglected.

A term-by-term comparison of the continuity relation would prove beneficial in understanding the contribution of each one under given conditions. Thus in Equation (15a) one can compare the three terms $\left|\frac{\partial Q}{\partial x}\right|$, $\left|C\frac{\partial H}{\partial t}\right|$, and $\left|\tilde{q}\right|$, or alternatively in Equation (15b), $\left|\frac{\partial q'}{\partial x}\right|$, $\left|C\frac{\partial h'}{\partial t}\right|$, and $\left|Gh'\right|$. Differentiating Equations (23) and (24) where appropriate and substituting into Equation (15b), one gets

$$- \frac{\gamma}{Z_c} + i\omega C + G = 0 .$$

Hence the problem is reduced to examining the terms $\left|\dfrac{\gamma}{Z_c}\right|$, $\left|i\omega c\right|$, and $\left|G\right|$. In Equations (25) and (26) it is seen that

$$\left|\frac{\gamma}{Z_c}\right| = \left|G + i\omega C\right| = \sqrt{G^2 + \omega^2 C^2}.$$

In addition,

$$\left|G\right| = G \text{ , and } \left|i\omega C\right| = \omega C \text{ .}$$

These terms can be interpreted in the following manner: in Equation (15a), $\dfrac{\partial Q}{\partial x}$, represented by $\left|\dfrac{\gamma}{Z_c}\right|$, is composed of contributions from elastic properties, $C\,\dfrac{\partial H}{\partial t}$, and leakage, $\tilde{q}$, represented by $\left|i\omega C\right|$ and $\left|G\right|$, respectively. This is shown graphically in Figure 4. For small values of ω the leakage is the predominant term; as the frequency increases, capacitance effects become larger and eventually may be equal to or greater than the leakage effect.

It is now apparent where one can apply the parabolic equation —— when the outflow parameter is of such magnitude that the capacitance, or elasticity of the system can be neglected in comparison. Thus it is possible in a given system to have no resonance at a supposed resonating frequency. Again refer to Chapter III, Figures 13 and 14.

2.4. Chapter Summary

A set of difference equations have been developed which will allow the comparison of unsteady and steady flows in a discrete manifold with those in an equivalent continuous one.

Further, unsteady flows in a continuous manifold can be treated in several ways. If the leakage parameter is large with respect to capacitance effects, the continuity and momentum relations reduce to a
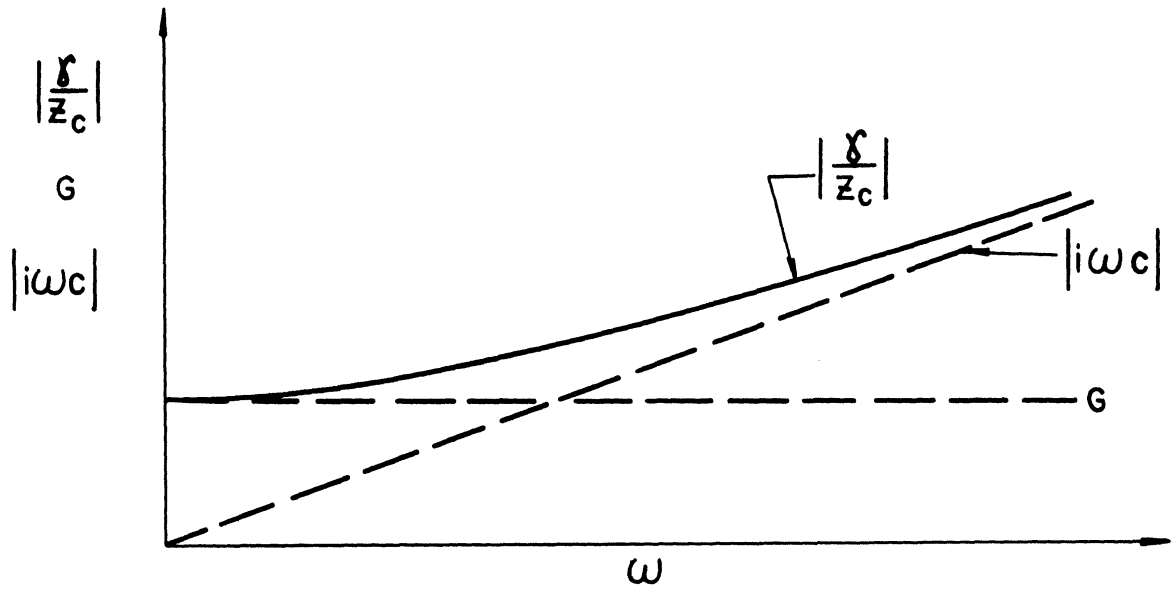
Figure 4. Graphical Representation of Terms Contributing
to Continuity Balance in Impedance Relations.

parabolic equation; if the converse is true, the governing equations are hyperbolic, and true water-hammer surges may exist. These two reduced forms (parabolic and hyperbolic) can be analytically solved via impedance methods once they have been linearized.

Intuitively, it should be possible to deal with any type of manifold problem using the hyperbolic equations, Equations (14) and (15), which can be solved using the parabolic relation, Equation (11).

III. COMPUTER ANALYSIS OF DISTRIBUTED OUTFLOW IN A MANIFOLD

Attention is now focused upon the computer analysis of flows in idealized manifold systems such as the two pictured in Figures 2 and 3. Emphasis is given to the solutions of the wave equations for the discrete manifold, Equations (8a) through (8f), and the hyperbolic equations and the impedance relations for the continuous manifold. In particular, consideration is given to the simple manifold of Figure 6; more complicated fluid systems, such as series or parallel pipes including a manifold section, can easily be analyzed once a basic understanding of the transients in the manifold has been attained.

3.1. Line With a Single Orifice

The highly dissipative nature of a tube with leakage can readily be understood by considering a simple closed line containing a centrally-located orifice, Figure 5. V_O and V_2 are initial steady-state velocities, H_O the reservoir head, a the pressure-pulse wave speed, A_O the orifice area, and A the area of the tube. The steady-state outflow through the orifice is q_O, and Q_O is the initial flow input at the reservoir. The dimensionless parameters ζ and ϕ indicate the magnitudes of the lateral outflow relative to the inflow and the effective orifice area relative to the tube area, respectively. The line is assumed frictionless and the relations developed in Section 2.2.1 are used to evaluate system parameters.

The initial conditions are such that when the valve is suddenly shut at the downstream end, a dimensionless pressure rise of magnitude $\beta = \dfrac{aV_2}{gH_O}$ will begin to propagate upsteam. As the pulse reaches the
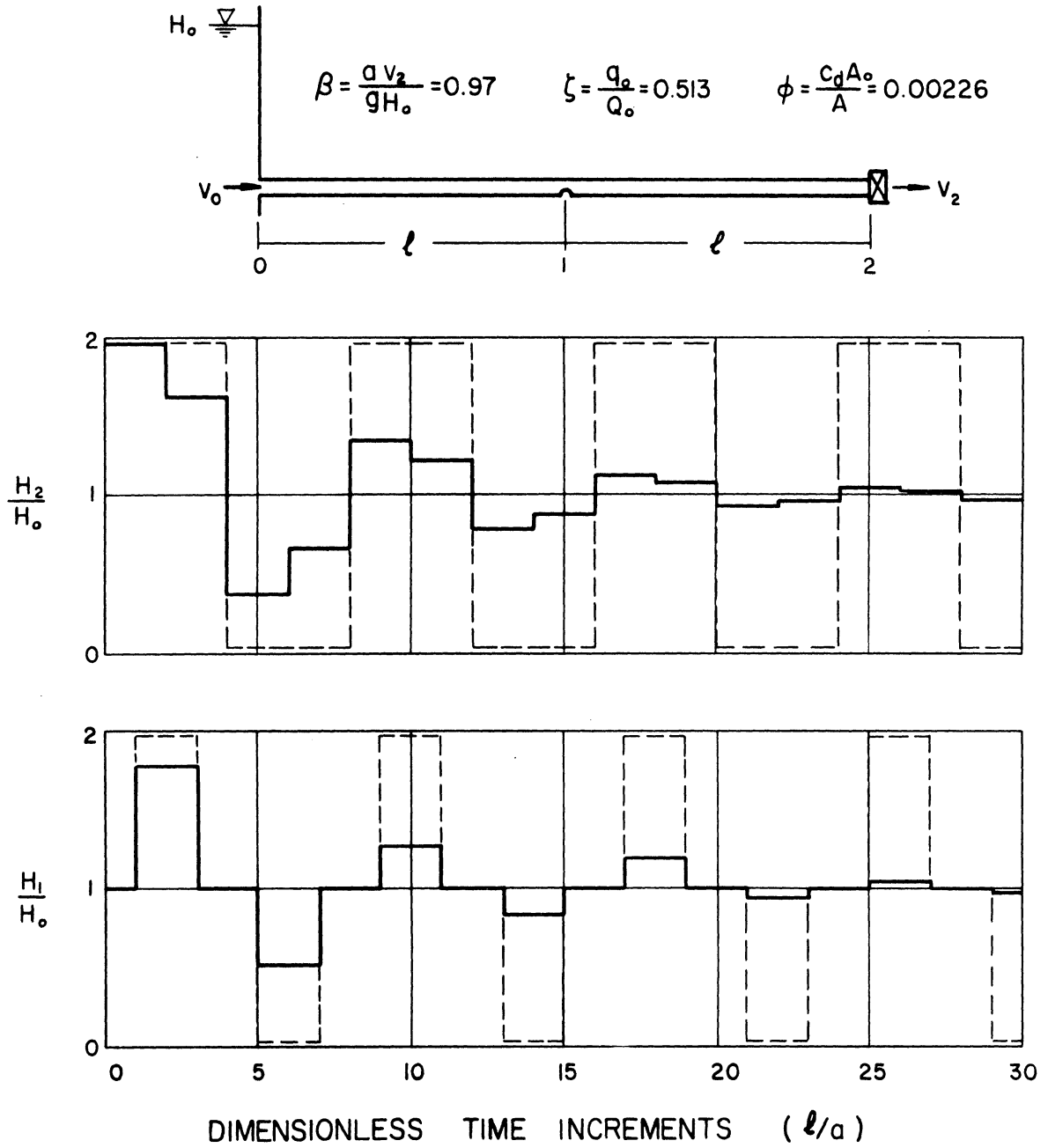
Figure 5. Water Hammer in a Frictionless Fluid Line Which Possesses Centrally-Located Orifice. H_1 is the Head at the Orifice, and H_2 the Head at the Valve. The Dashed Line is the Solution for an Equivalent Closed System.

orifice, immediate relief of pressure is afforded, and an attenuated wave continues to travel upstream, while a negative wave travels downstream to the closed valve. Since reflections occur at the boundaries, wave action will continue until new steady-state conditions are attained. Figure 5 shows the pressure variations at the valve and at midpoint for $\beta = 0.97$, $\zeta = 0.513$, and $\phi = 0.00226$. Friction effects are neglected, so that the attenuation of the heads is due only to the dissipative nature of the orifice. The dashed lines are the heads in an equivalent closed, frictionless tube. If the orifice area were smaller the head fluctuations would take longer to dampen out.

3.2. Comparison of a Discrete Manifold with a Continuous Manifold

In place of a single orifice as shown in Figure 5, suppose that a tube now contains 1, 2, ..., N orifices. Furthermore, assume the number and geometry of the orifices are such that one can replace the discrete manifold with an equivalent continuous one. To show the validity of this assumption, let us proceed to compare various flow situations in such systems.

3.2.1. Steady-State Conditions

The steady-state analysis of a manifold with a finite number of orifices approximated by a continuous slot has been achieved.[1,7,13] It is included here to provide a complete picture of unsteady flow in manifolds, inasmuch as the initial conditions on such a system are usually steady-state in nature.

Suppose that a discrete manifold contains nine orifices and that a continuous manifold is made equivalent by matching ζ and ϕ

for the two systems. Now ζ becomes the ratio of total lateral outflow to inflow under steady-state conditions, and ϕ is the ratio of total effective orifice area to the area of the manifold, Figure 6.

Figure 7 shows dimensionless head and velocity distributions along the manifolds for $\phi = .113$ and $\zeta = 1.0$. H_0 and V_0 are the head and velocity, respectively, at the upstream ends. The variables are computed from Equations (6a) through (6d), Section 2.2.1, for the case of the discrete manifold, and from Equation (10), Section 2.2.2 for the continuous manifold. In one case a frictionless system is assumed, and in the other the head loss due to friction is included, making use of the Darcy-Weisbach relation and assuming the Blasius formula for f . For either case the resulting velocity distribution is identical; the head distribution is altered when friction is taken into account. For manifold systems one can assume that the axial component of momentum leaving via the orifices possesses a velocity approximately equal to the mainstream velocity; thus $C_\beta = 1$ in Equations (6a) and (10). It is seen that the continuous manifold approximates the discrete one to a fair degree. The value of .113 for the parameter ϕ is the largest which is used in ensuing analyses. As ϕ is reduced, the steady- state solutions of the discrete and continuous systems tend to converge.

3.2.2. Unsteady Flow Considerations

Consider the manifold of Figure 6 experiencing steady flow with the downstream gate remaining open. Now $\zeta < 1$, and if the gate is suddenly shut at time zero, transient pressure and velocity waves will be initiated, and their durations and magnitudes will depend upon the parameters β , ζ , and ϕ , provided that friction is neg- lected.

$$\beta = \frac{aV_2}{gH_o} \qquad \zeta = \frac{V_0 - V_2}{V_0} \qquad \phi = \frac{NC_dA_0}{A}$$
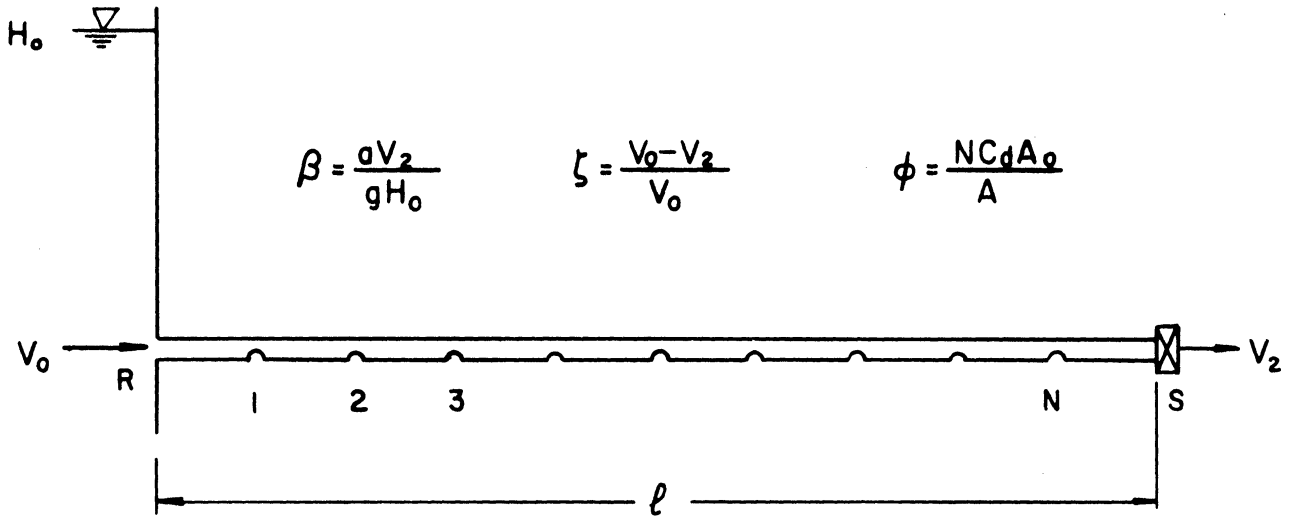
$$q_o = C_d A_0 \sqrt{2gH} \qquad - \text{DISCRETE CASE}$$

$$q = C_d A_o \frac{N}{\ell} \sqrt{2gH} \qquad - \text{CONTINUOUS CASE}$$

$\ell = 100 \text{ cm}$ $\qquad A = 1.0 \text{ cm}^2$ $\qquad H_o = 100 \text{ cm } H_2O$

$a = 1 \times 10^5 \text{ cm/sec}$ $\qquad \rho = 1.0 \text{ gm/cm}^3$ $\qquad g = 980 \text{ cm/sec}^2$

Figure 6. Idealized Manifold.
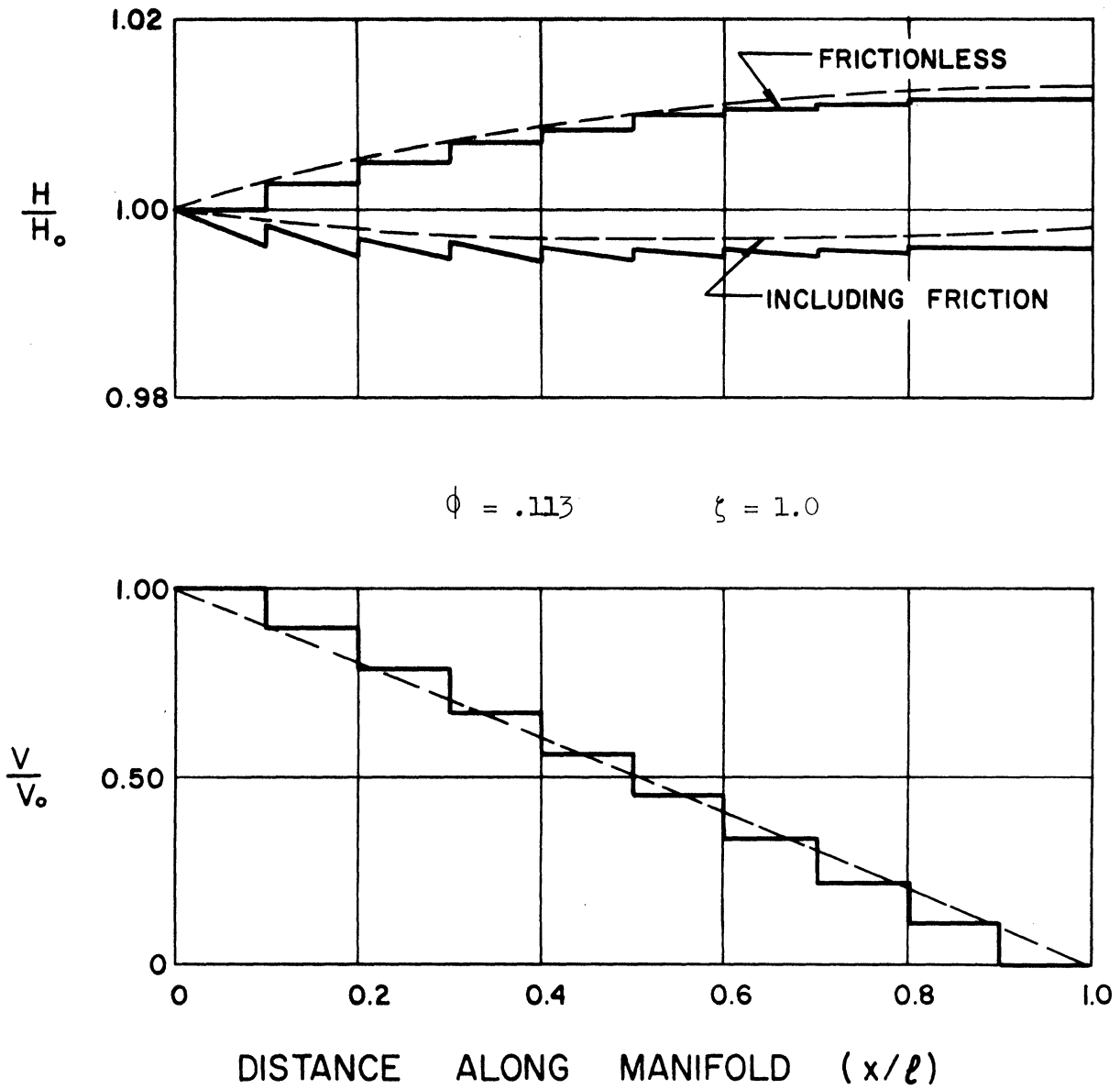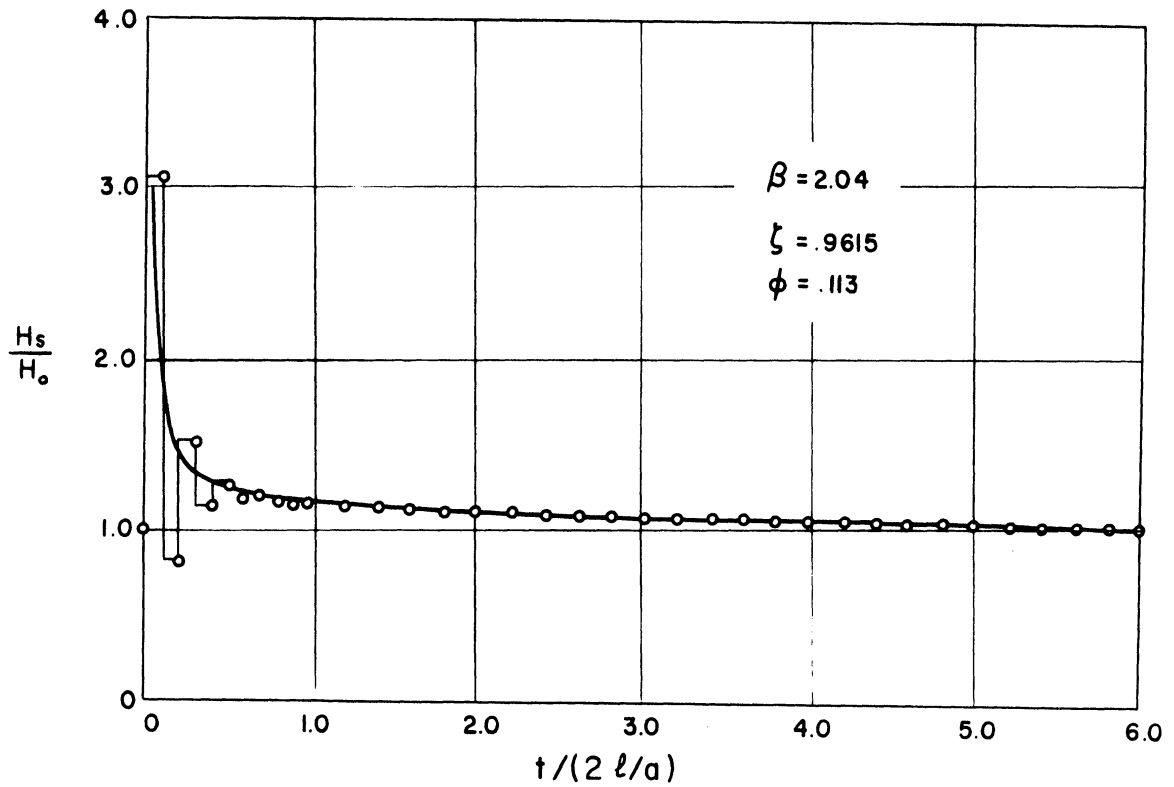
$$\phi = .113 \qquad \zeta = 1.0$$

Figure 7. Steady-State Solutions of System Variables. The Solid Line Refers to the Discrete System, and the Dashed Line Refers to the Equivalent Continuous One.

Figure 8 shows head at the valve versus time for three sets of values of β , ζ , and ϕ . The system variables are solved using Equations (8a) through (8f) for the discrete manifold, and Equations (3c), (16) and (17) for the continuous system (see Appendix B). The discrete manifold possesses nine orifices; hence for the equivalent continuous one, $b = .09$ C_d A_o in Equation (3c). For $\phi = .113$, the pressure transient is rapidly attenuated; the intermediate figure, when $\phi = .0113$, shows some water-hammer effect, and for $\phi = .00226$, a true water-hammer response is discernable.
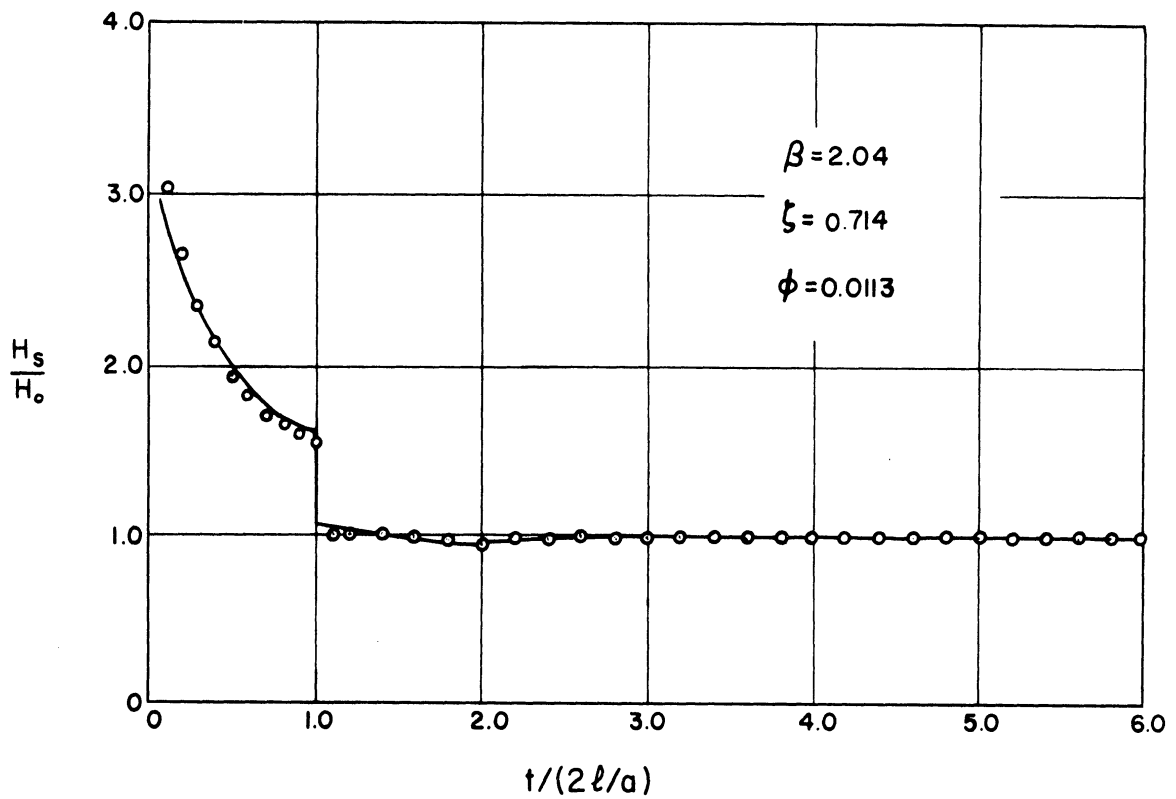
Some discrepancy between the discrete and continuous systems is seen for early time in the case where $\phi = .113$. In the discrete manifold water hammer is taking place in the closed line between the last orifice and the closed valve; however, the two solutions quickly converge. For the remaining two cases of Figure 8 there is good agreement between the two systems.

In the second situation, Figure 9, the downstream boundary condition is a dead end so that $\zeta = 1.0$ and at time zero, a step-head input with a dimensionless value of 0.2 is imposed upstream. Again, for the smaller value of ϕ , the dispersive effect of the orifice outflow becomes less pronounced, and the water-hammer effects take precedence.

In addition to the responses of step-input functions, it would be of value to visualize the response patterns of an oscillating-input function, shown in Figures 10 and 11, where the idealized manifold now possesses a dead end and is excited at the upstream end by a forced sinusoidal-head variation. Figures 2 and 3 show the upstream boundary condition $H_R = H_O + \Delta H \sin (\omega t)$.

$\beta = 2.04$

$\zeta = .9615$

$\phi = .113$

$\dfrac{Hs}{H_o}$

$t/(2\,\ell/a)$

(a)

$\beta = 2.04$

$\zeta = 0.714$

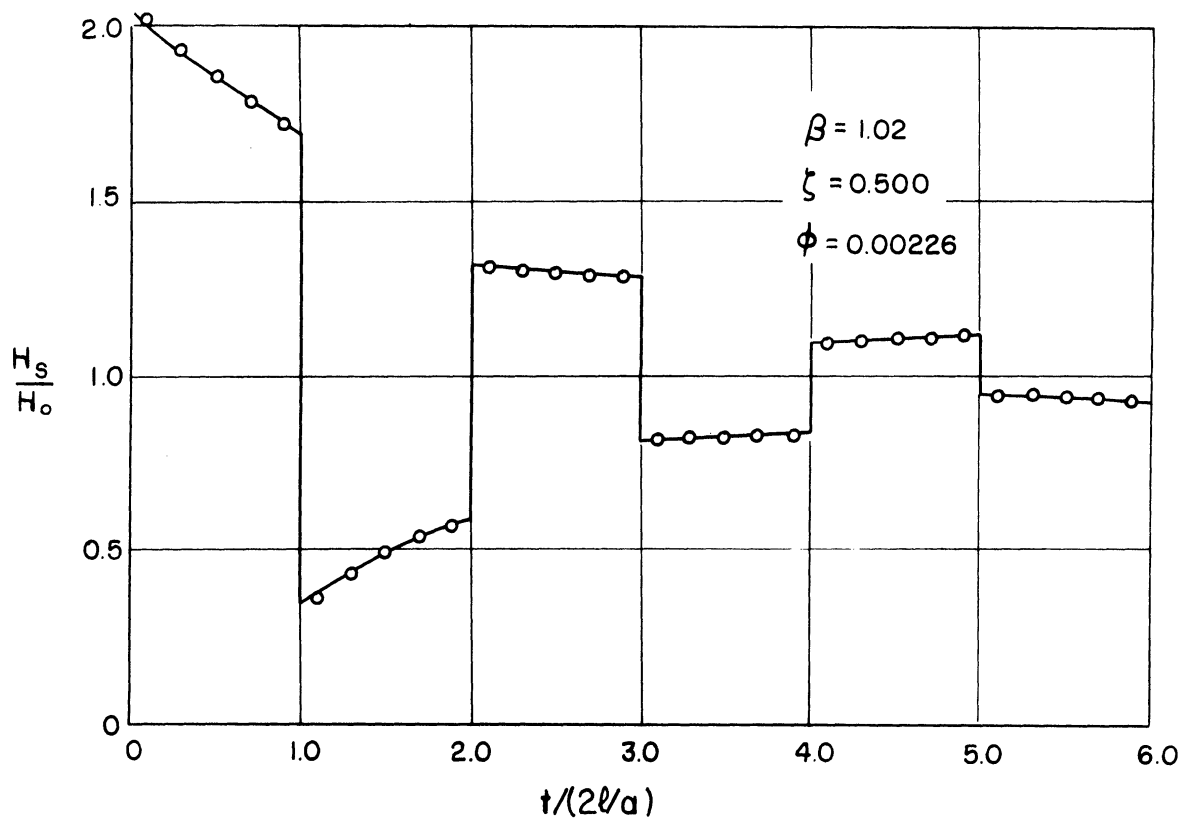$\phi = 0.0113$

$\dfrac{H_s}{H_o}$

$t/(2\ell/a)$

(b)

Figure 8.   Head at Valve versus Time for Sudden Closure.   The Circles
are the Solution of the Discrete-System Equations, and the
Solid Lines are the Solution of the Continuous-System Equa-
tions.

$\beta = 1.02$

$\zeta = 0.500$

$\phi = 0.00226$

(c)

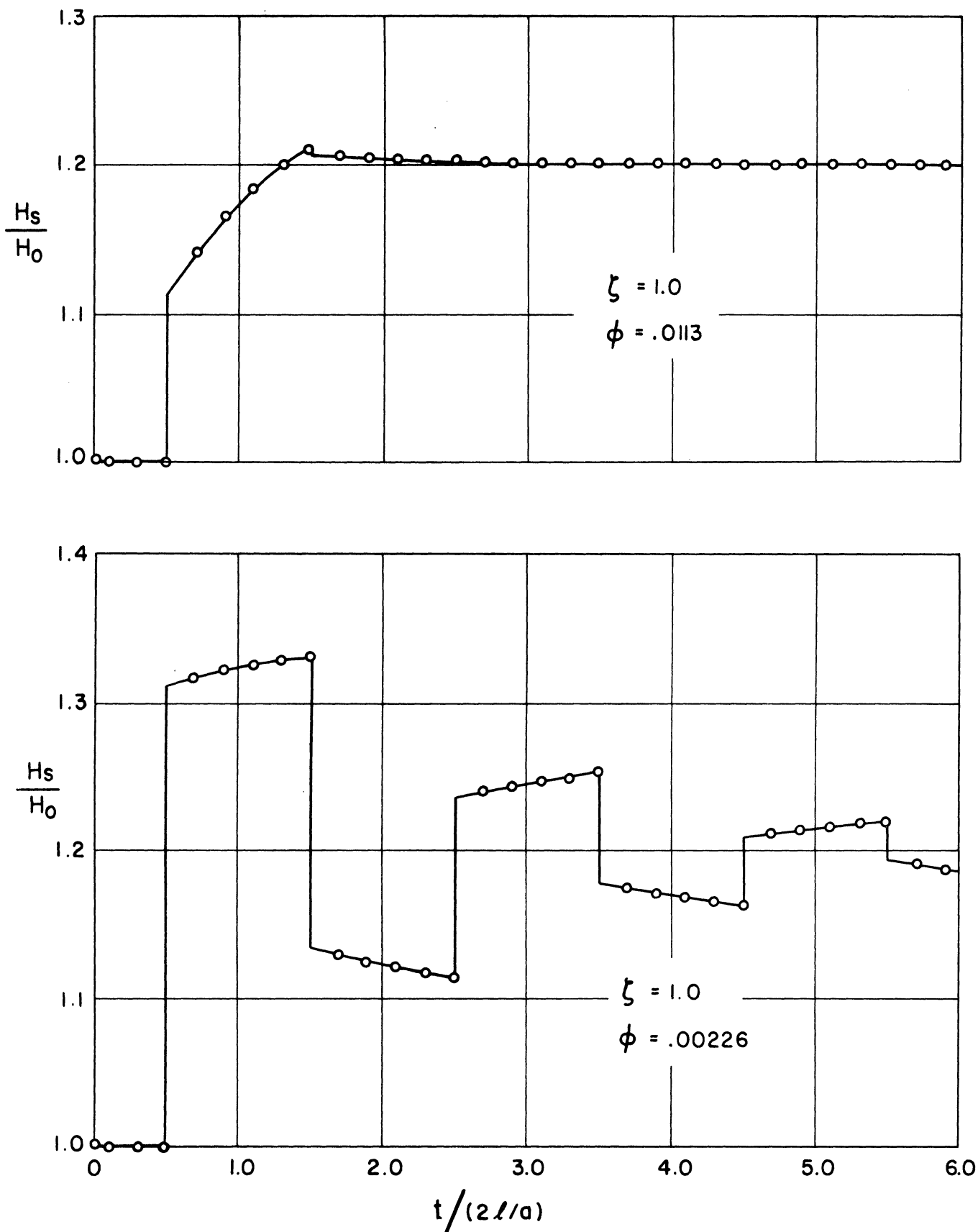Figure 8. (Cont'd)

Figure 9.   Head at Dead End versus Time for Step-Head Input. The
            Circles are the Solution of the Discrete-System Equations,
            and the Solid Lines are the Solution of the Continuous-
            System Equations.

Figure 10. Head at Dead End versus Time for Oscillating-Head Input with a Period of $4\ell/a$. H_R is the Head Input at the Upstream End. The Circles are the Solution of the Discrete-System Equations, and the Corresponding Solid Lines are the Solution of the Continuous-System Equations.
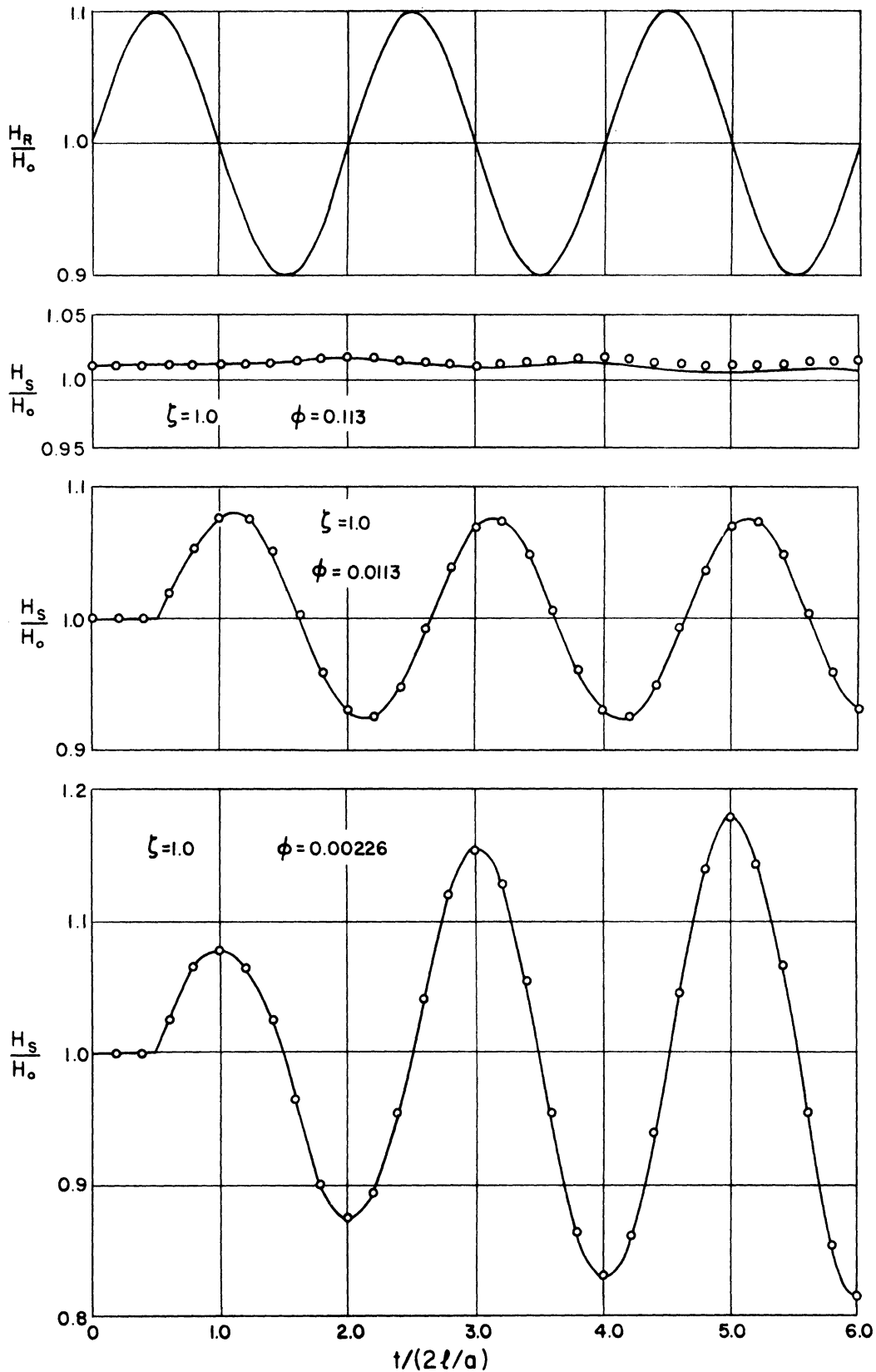
Figure 11. Head at Dead End versus Time for Oscillating-Head Input with a Period of $40\ell/a$. H_R is the Head Input at the Upstream End. The Circles are the Solution of the Discrete-System Equations, and the Corresponding Solid Lines are the Solution of the Continuous-System Equations.
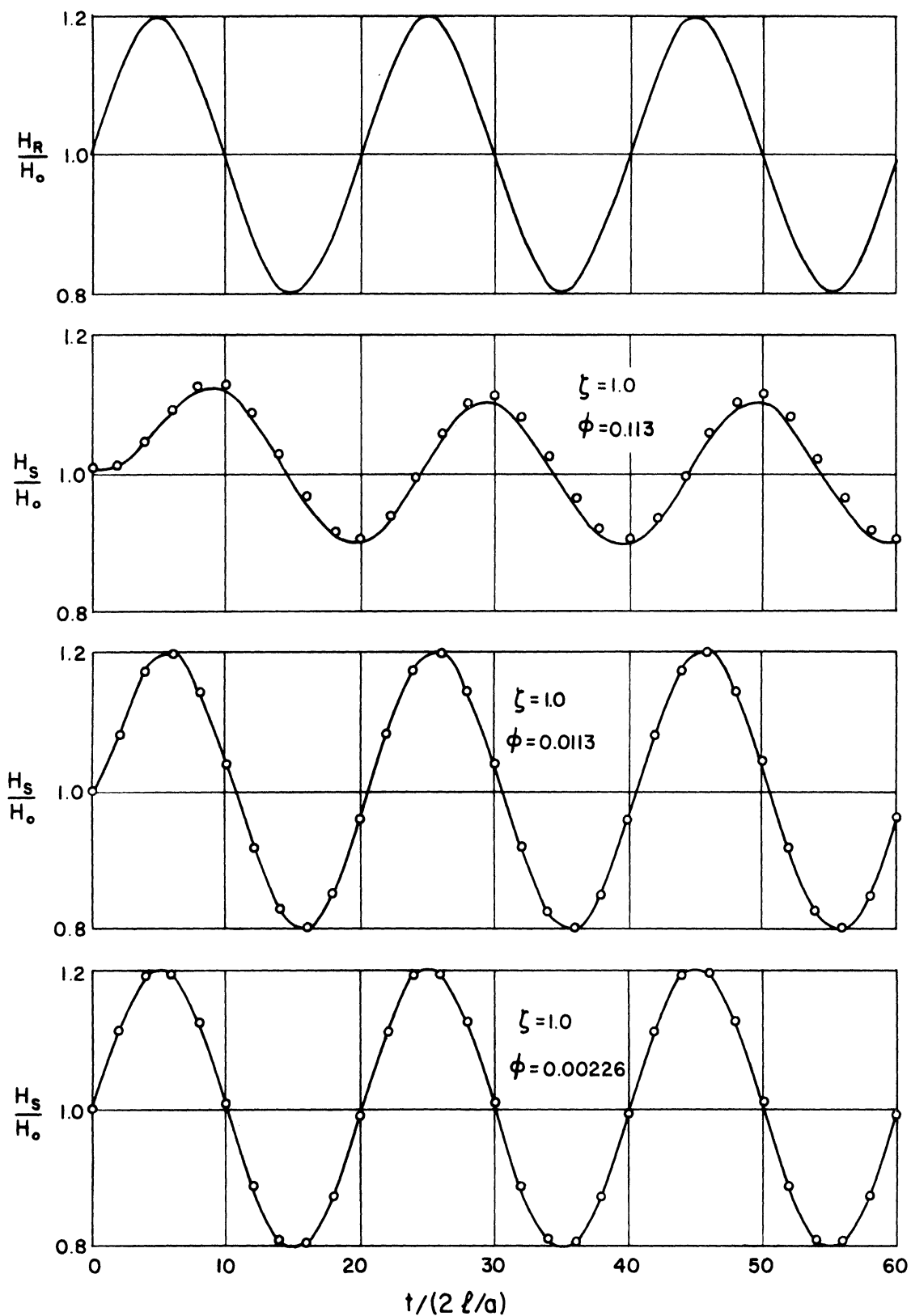
In Figure 10, $\Delta H = 0.1\ H_0$, and the period of the head input is $4\ell/a = .004$ sec.; this is the frequency at which resonance should occur. Several interesting observations can be made. When $\phi = .113$ there is very little head response at the dead end. For $\phi = .0113$, a steady-oscillating response is quickly attained, and a phase shift with respect to the upstream head is evident. If no lateral outflow were present, the downstream head would lag the input by $t/(2\ell/a) = 0.5$, i.e., the phase shift would be 90 degrees. The additional lag in response is due to the leakage. Furthermore, the outflow tends to attenuate the amplitude of the response for this value of ϕ . In contrast, if $\phi = .00226$, the system is in resonance -- the amplitude of the downstream head is increased and the phase lag is nearly 90 degrees. Hence it can be stated that for certain values of ϕ the dissipative effects of the lateral outflow may be of such magnitude that no storage of energy is possible; however, when ϕ becomes sufficiently small, the capacitance effects become significant and resonance occurs.

Head-input oscillations of a lower frequency are shown in Figure 11. In this situation the period of oscillation is $40\ell/a = .04$ sec., and $\Delta H = 0.2H_0$. For the largest value of ϕ a pronounced phase lag between the upstream and downstream heads exist, and the dead-end head fluctuation is attenuated. For the intermediate and smallest values of ϕ the pressure amplitudes are transmitted to the downstream end with no attenuation, but for $\phi = .0113$ a phase shift occurs. For a closed tube the phase shift would be neglibible, and for the manifold with a very small orifice area, i.e., $\phi = .00226$, this is also true.

Generally, Figures 8 through 11 show that the continuous manifold is an adequate representation of the discrete one for ϕ = .0113 and .00226. In Figures 10 and 11, when ϕ = .113 , the solutions for the two types of manifold differ by deviations in the base lines. This may be due in part to the limiting assumptions imposed upon the corresponding governing equations presented in Chapter II; in addition, in the solution for the continuous system, the characteristic equations are approximated by finite-difference relations which may introduce some error. It should also be noted that this value of ϕ may be close to an upper limit for matching the two systems, beyond which the manifold could be treated only as a discrete one.

The effect of varying the momentum coefficient is shown in Figure 12, in which the solution for the continuous system, ϕ = .113 of Figure 11, is reproduced. In this chapter it is assumed that $C_\beta = 1$. If $C_\beta = 0$ the solution is essentially the same except that there is a base-line shift. For the two smaller values of ϕ the effect of varying C_β is negligible, which implies that the axial momentum leaving the manifold laterally is quite small, and can be neglected.

The heads in Figures 8 through 11 have been computed under frictionless conditions. The fluid medium is water, and for the manifolds described herein it is relatively inviscid. If one assumes a quasi-steady head loss, $h_f^\prime(V) = f\,V|V|/2gD$, it can be shown that friction effects are negligible for values of ϕ = .0113 and .00226 . Only in the case of large lateral outflow is friction significant. This is shown in Figure 12, where for oscillating flows, its effect is to lower the base line of the downstream head oscillation. If the fluid
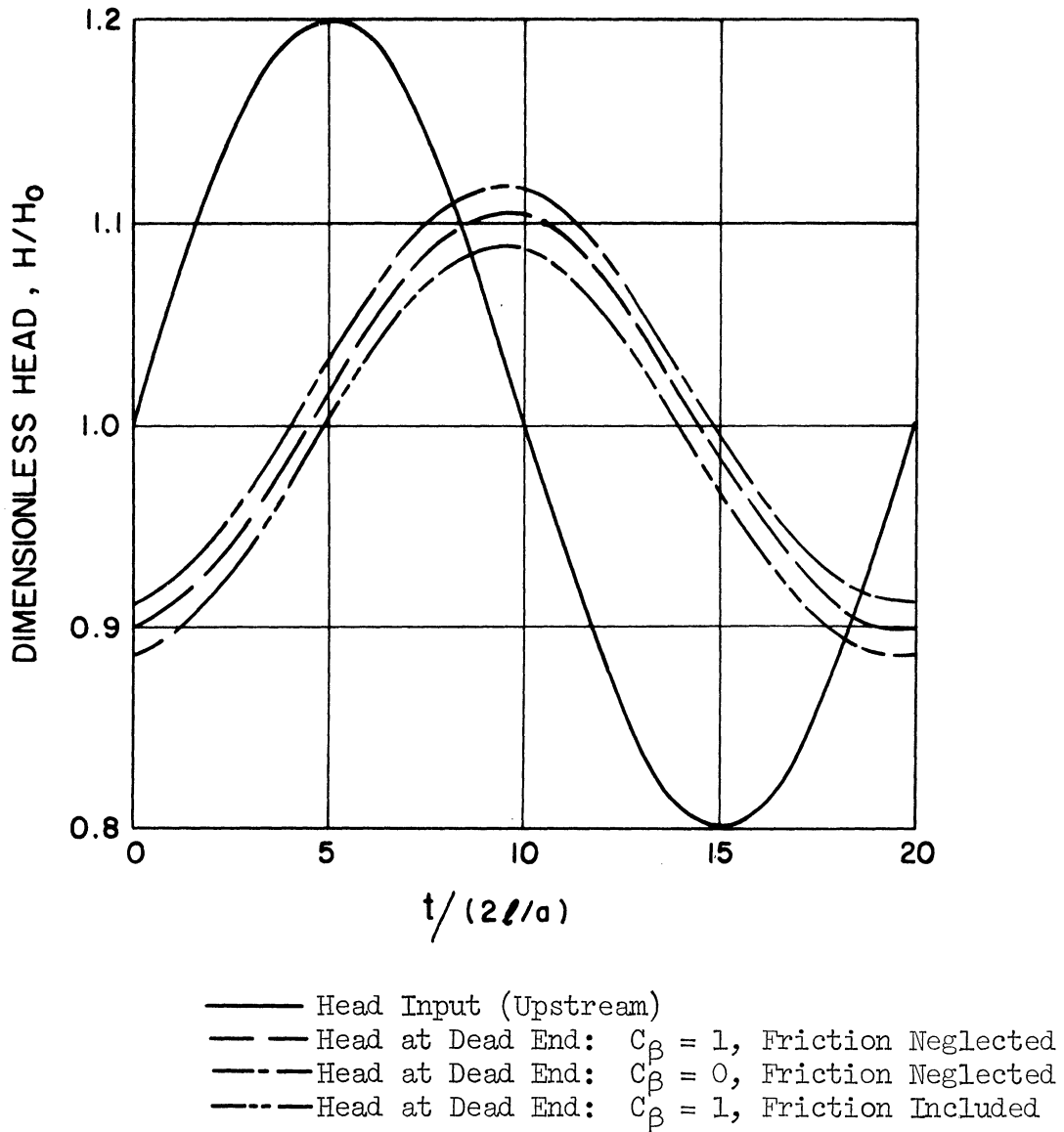
Figure 12. Head at Dead End versus Time for Oscillating-Head Input, Showing Effects of Including Friction and Varying C_β. ϕ = .113.

medium is relatively viscous, frictional losses will become significant, and if the flow is laminar, they will have a dispersive effect upon the predicted response patterns.[25]

3.3. Impedance Solutions

A broader picture of oscillating flows in a manifold system can be provided by utilizing impedance relations. Equations (27) and (28) give the input impedance and the pressure-head transfer function, respectively, of a dead-end continuous manifold with a forced, oscillating head input:

$$ZR = \frac{Z_c}{\tanh(\gamma \ell)} \, , \tag{27}$$

$$HR = \frac{1}{\cosh(\gamma \ell)} \, . \tag{28}$$

These functions are shown for various values of ϕ in Figures 13 and 14. Again the idealized manifold of Figure 6 is used as the representative system. $|ZR|$ and ψ_{ZR} are the amplitude and phase of the input impedance, respectively; in a similar manner $|HR|$ and ψ_{HR} are the amplitude and phase of the transfer function. Even though they are a manifestation of the linearized wave equations, the results agree quite well with the solutions of the nonlinear equations shown in Figures 10 and 11.

As an example, consider the oscillations in Figure 10, where $\phi = .0113$ and $\omega = 1571$ radians per second. The upstream and downstream head oscillations are replotted in Figure 15 along with the upstream flow. With $Q_0 = 5.0$ ml/sec, and $H_0 = 100$ cm , it is seen that $\psi_{ZR} \approx 40°$, $|ZR| \approx 60$ sec/cm^2 , $\psi_{HR} \approx - 115°$, and $|HR| \approx .75$. These values are in agreement with those of Figures 13 and 14 for the same system.
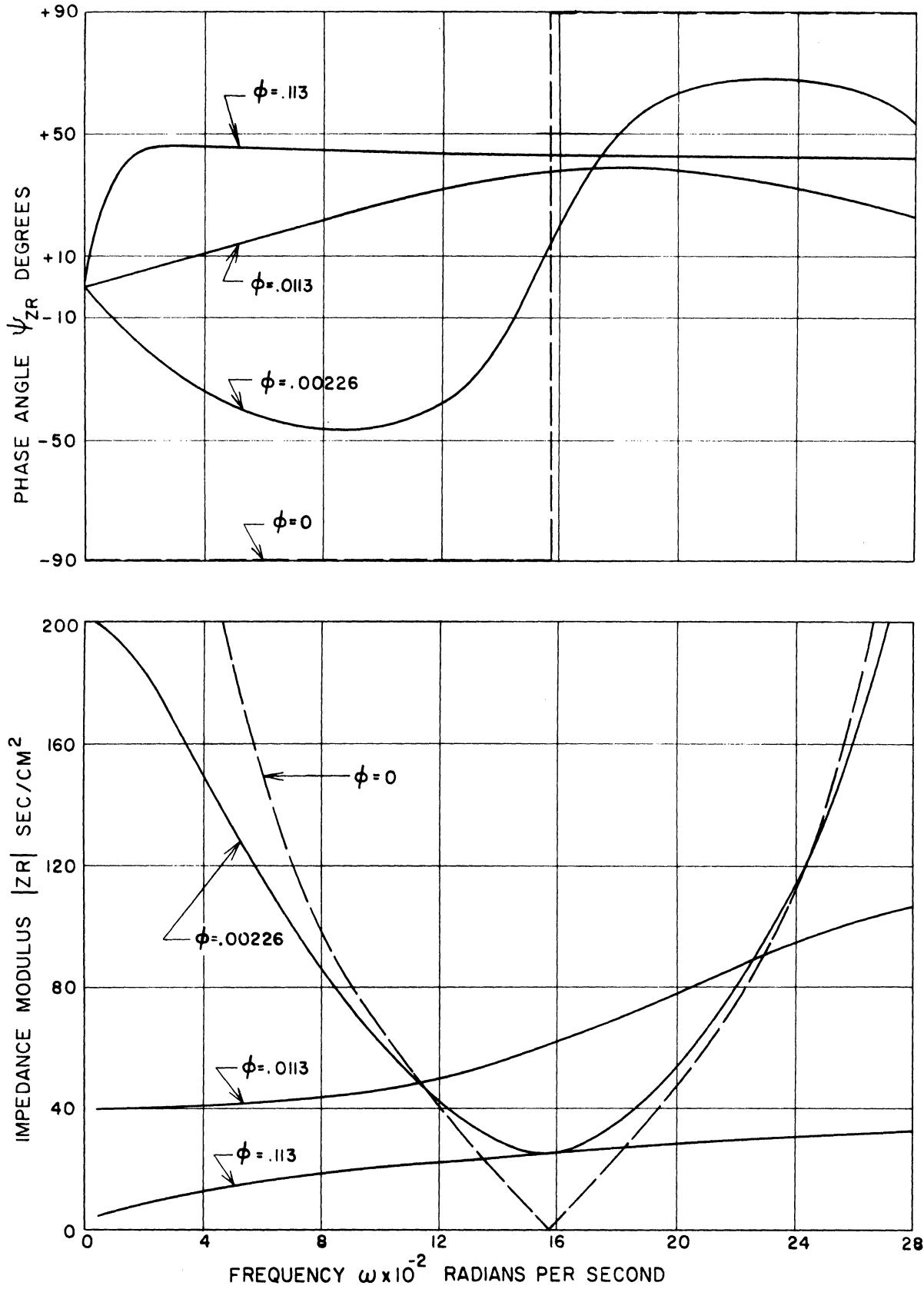
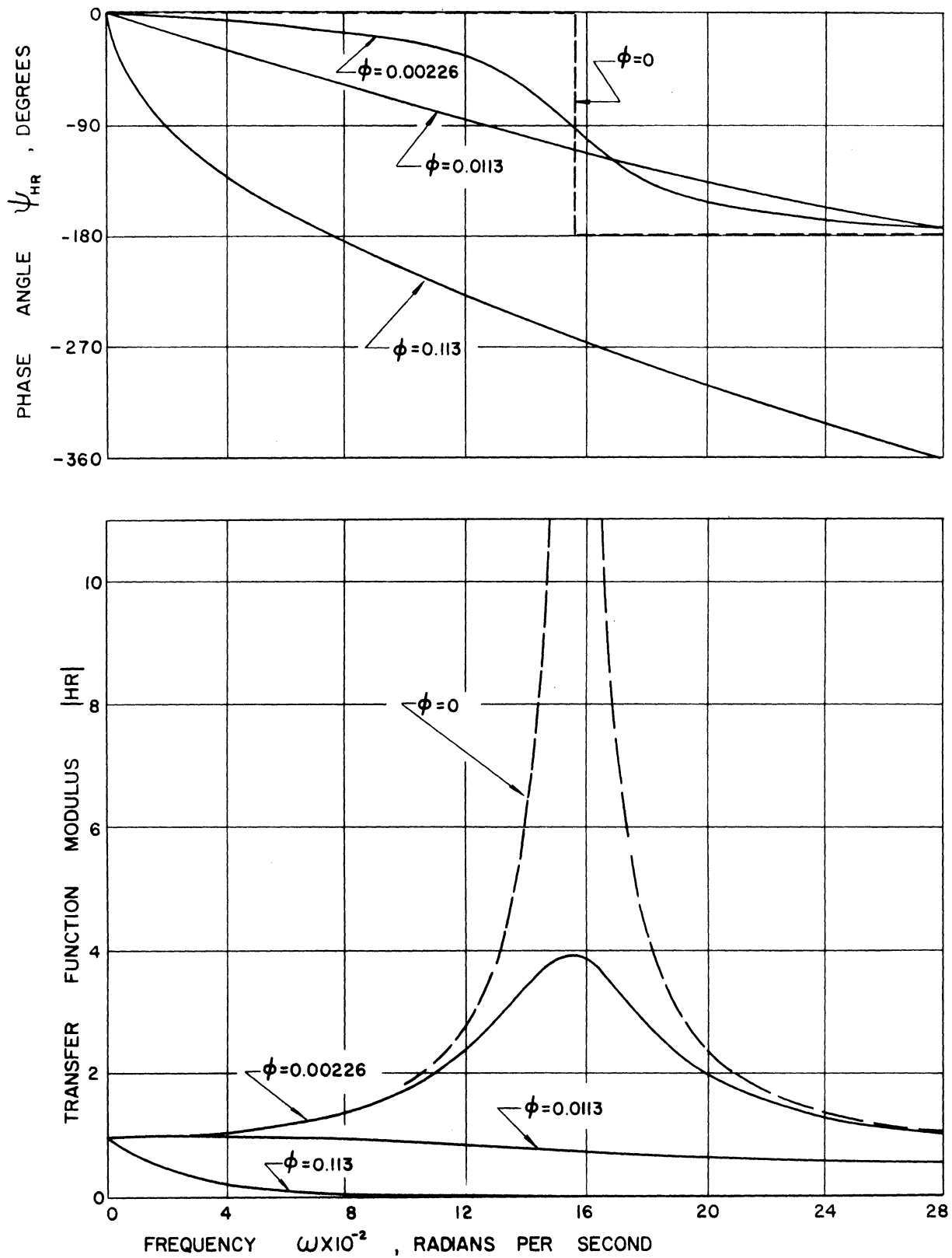Figure 13. Frequency Response of Input Impedance for a Dead-End Manifold.

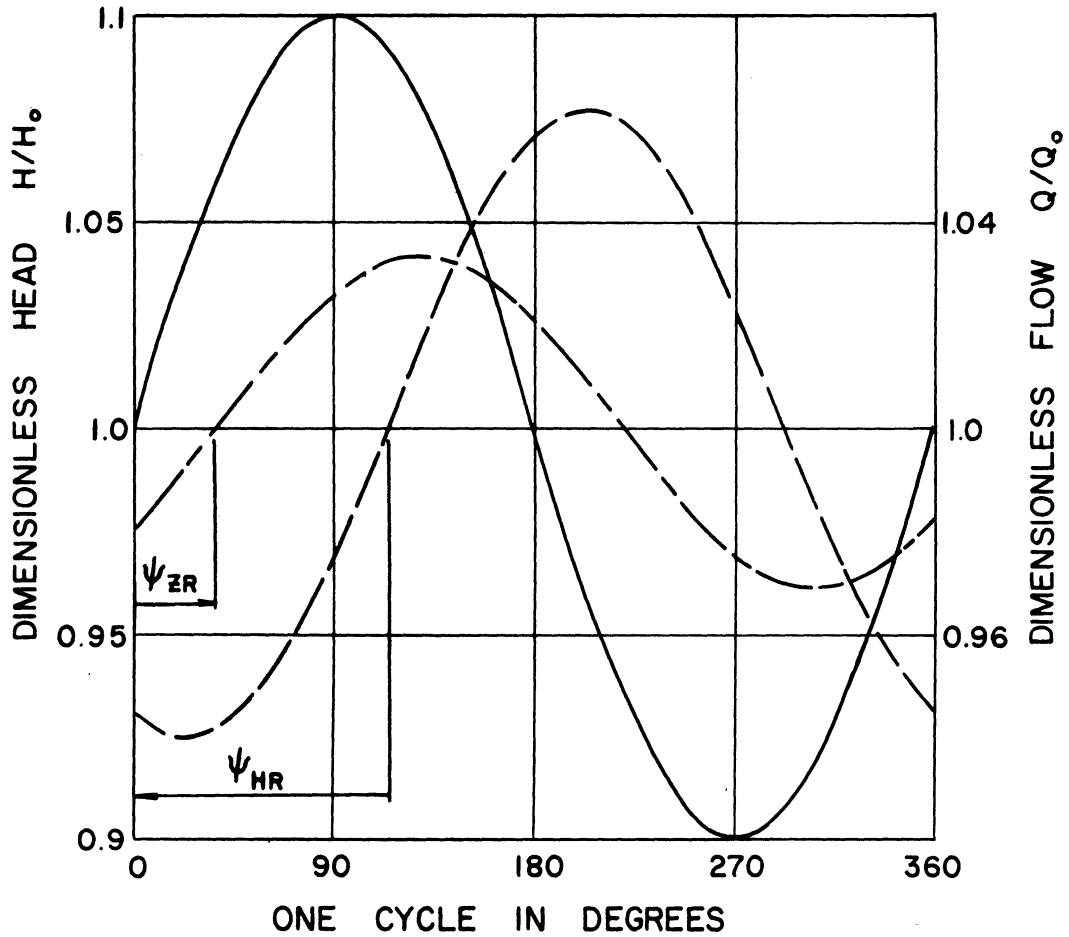Figure 14. Frequency Response of the Pressure-Head Transfer Function for a Dead-End Manifold.

Figure 15. System Variables versus Time for Oscillating Flow. ϕ = .0113.

The impedance and transfer function diagrams show the spectrum of phase and attenuations when a leakage term is included in a closed-end fluid line. If the leakage term is of sufficient size, capacitance effects seem to have little or no impact, and no resonance occurs at the supposed resonating frequency, in this case 1571 radians per second. As ϕ decreases, the capacitance terms come into play, and the response curves approach those of a closed system, where $\phi = 0$.

If a friction term is included in the impedance analysis, it will affect only the response of the manifold when $\phi = .113$, and at small frequencies, since the mean flow input is quite large (about 55 ml/sec). The frictional effects for smaller values of ϕ are negligible for the system of Figure 6.

It is material to further discuss the frequency response curves for the case of $\phi = .113$, since this system is very much like the manifolds whose experimental data is discussed in Chapter V.

The pronounced phase lags at low frequencies for both the input impedance and transfer function are due to inertial effects coupled with distributed outflow. The physical situation which is taking place can be explained in a fundamental manner by referring to the fluid line with one orifice shown in Figure 5, Section 3.1. Suppose that initial steady-state conditions exist and the downstream gate is always closed; at time zero a small step head is imposed at the upstream end. When the pressure wave reaches the midpoint, immediate relief is afforded by the orifice; the flow out of the orifice is increased and the head at that point is suddenly reduced*. This will create a gradient which will

---

* A small velocity perturbation will accompany the step head; it is assumed that this increase is small, and hence the orifice will remain "starved".

accelerate the flow in an attempt to reach new steady-state momentum and continuity balances. However, a finite amount of time is required to accelerate the plug of fluid between the upstream end and the orifice, and if after a small time increment, the upstream head is again increased, the response at the orifice will be such that it is constantly attempting to equilibrate with the upstream conditions. This same situation is true for a manifold, either discrete or continuous, and takes place in a less interrupted manner.

Thus in Figure 9, when $\phi = .0113$, the downstream pressure response to a step-head input does not immediately balance when the pressure wave reaches the dead end, but attains equilibrium when the fluid has accelerated sufficiently to compensate for the increased outflow required by the higher head. And in Figure 14 a pronounced phase lag and attenuation exist due to this phenomenon.

Another way which transients in leaking lines can be visualized is to recognize the existence of traveling waves.[15] First consider oscillating flows so that the impedance relations can be utilized. The propagation constant, γ , was shown in Chapter II to be

$$\gamma = \sqrt{(R + i\omega L)(G + i\omega C)}.$$ (25)

The coefficient of the imaginary part of γ is termed the phase constant. In turn, the phase velocity or velocity of propagation, v_p , is defined as the frequency of oscillation, ω , divided by the phase constant; it is the velocity with which one must move along the manifold to observe a stationary head or velocity.

If, for a given frequency, the leakage is sufficiently large and frictional losses are minor, i.e., $G >> \omega C$ and $\omega L >> R$,

$$\gamma \approx \sqrt{i \omega LG} = \sqrt{\frac{\omega LG}{2}}\ (1 + i)\ , \qquad (25a)$$

and the phase velocity becomes

$$v_p = \sqrt{\frac{2\omega}{LG}}\ . \qquad (29)$$

These conditions are valid at low frequencies for the idealized manifold where $\phi = .113$. (In contrast, the phase velocity for a frictionless, closed fluid line is merely the pressure-pulse wave speed.) An interesting result is that v_p is frequency dependent.

Consider the idealized dead-end system in which flow is oscillating with a frequency $\omega = 157$ rad/sec . If $\phi = .113$, from Figure 14 the phase lag between upstream and downstream pressure fluctuations is $\psi_{HR} \approx -80°$. If the period of oscillation is .04 seconds, and $\ell = 100$ cm , then the velocity of propagation is 112 m/sec. This condition is shown in Figure 11. In comparison, v_p can be computed from Equation (29). Here, $L = 1.02 \times 10^{-3}$ sec^2/cm^3 , and $G = 2.5 \times 10^{-3}$ cm/sec (recall $G = m\ B\ \bar{H}^{m-1}$), and consequently, $v_p = 111$ m/sec .

Such traveling waves exist because of the large amount of energy input required to "feed" the orifices. It is of interest to note that the input impedance for $\phi = .113$ in Figure 13 is nearly identical to the characteristic impedance of the system except for very low frequencies.

If a step-input function is imposed on a manifold system, the wave becomes highly distorted and its corresponding front is difficult to define. This is illustrated in Figure 16 which shows a spatial
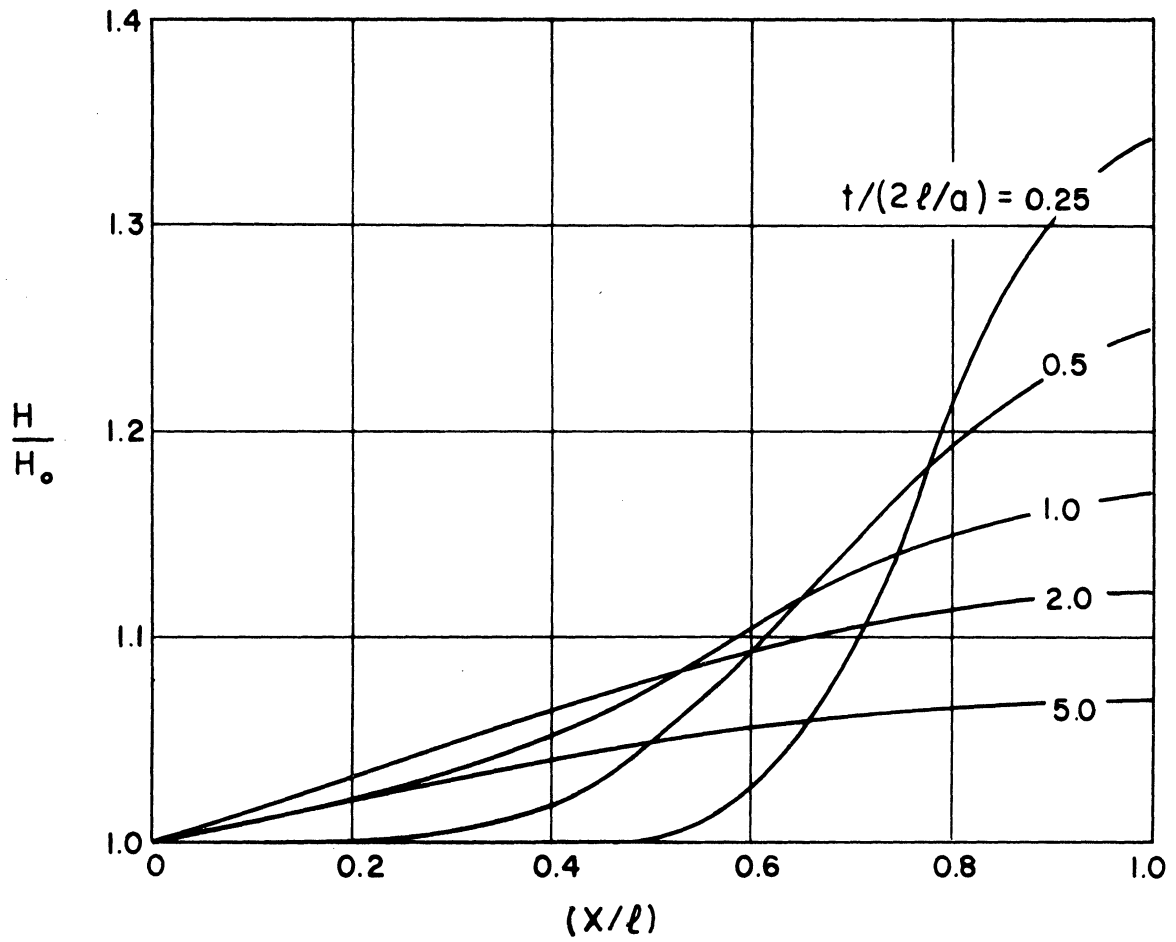
Figure 16. Head Distribution at Various Times for Sudden
Closure. ϕ = .113 .

distribution of heads for various time when $\phi = .113$. This figure

should be compared with its corresponding head-versus-time curve in

Figure 8. This type of wave response is similar to those found in tran-

sient diffusion problems.[15]

IV.   EXPERIMENTAL STUDY OF A MANIFOLD SYSTEM

Chapter II relates several analytical methods which are available for predicting unsteady heads and flows in a manifold.   In Chapter III it is seen that if a manifold is experiencing oscillating flows, the leakage parameter strongly dictates the nature of the flow.   A laboratory investigation was initiated to analyze such a system in which high leakage and low frequencies were exhibited.   The motivation was twofold: verification of the theory for a continuous manifold was in order, and furthermore, it was hoped that by observing such a system, one would come closer to understanding the nature of flows in more complicated systems such as a branching arterial tree.

4.1.   Mechanical Arrangement

A schematic of the experimental arrangement is shown in Figure 17.   A continuous flow supply is provided by the head difference between the upstream and donwstream constant-head reservoirs, while the fluid oscillator induces a sinusoidal component to the flow as it enters the upstream end of the manifold.   The downstream gate valve may be open or closed.   A trough returns the spent fluid to a sump, and a small centrifugal pump lifts the fluid to the upstream reservoir to complete the cycle.   A portion of the system is shown in Plate I.   Tygon* and rubber tubing serve as supply and drainage lines.   System variables are recorded at three locations: flow and head at the upstream end of the manifold, head at the midpoint, and head at the downstream end.

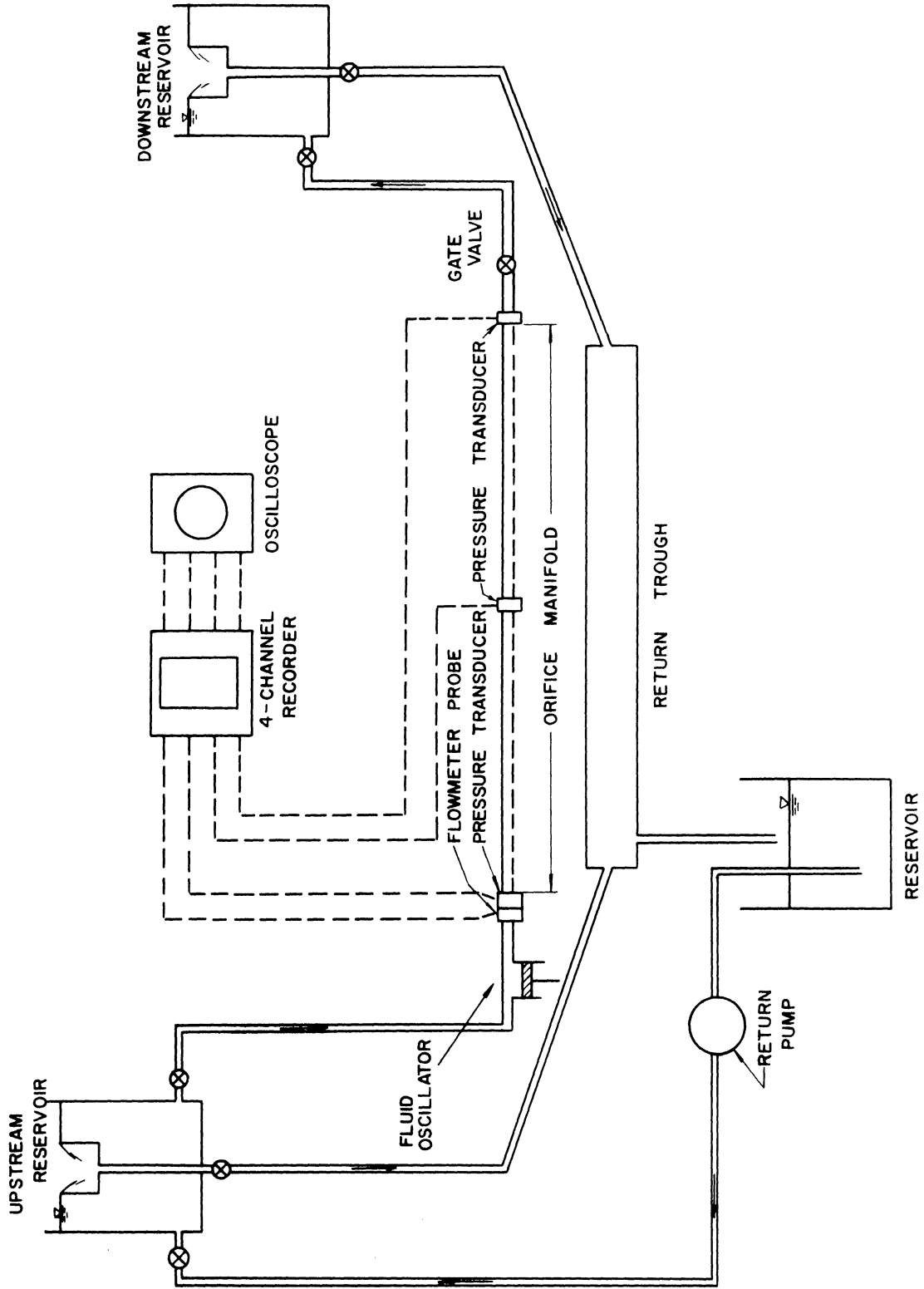
* A trademark of U. S. Stoneware, Akron, Ohio.

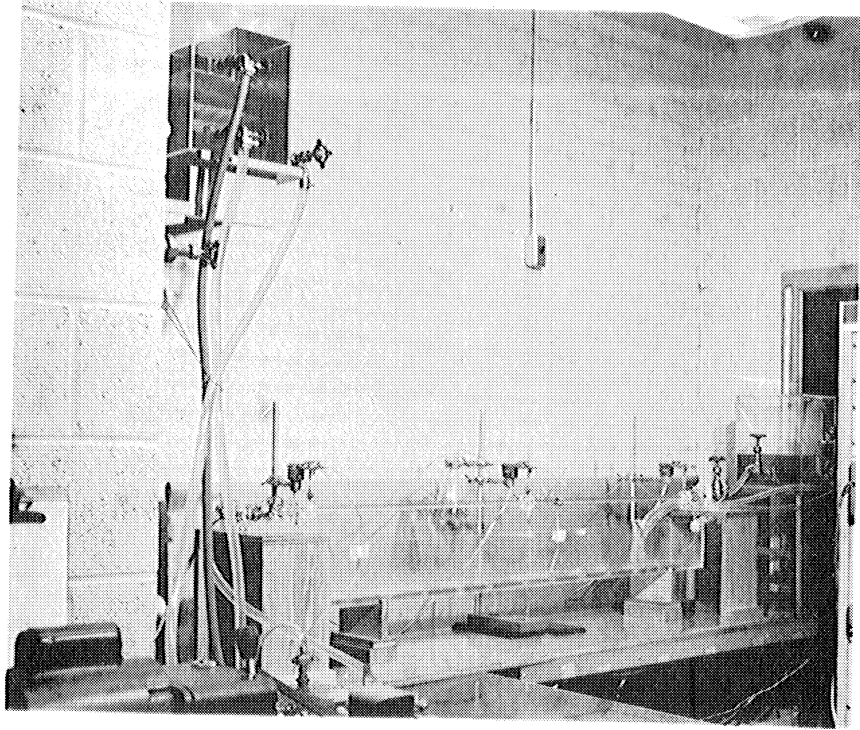Figure 17. Schematic of Experimental System.
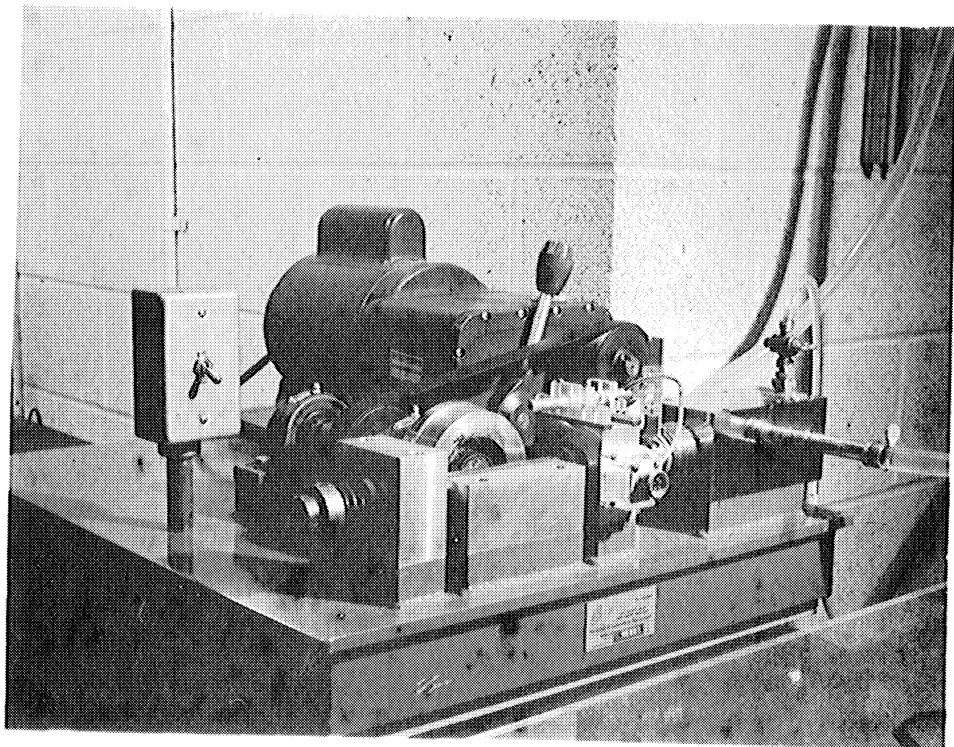
Plate I. Experimental System.

Plate II. Fluid Oscillator.

The fluid oscillator is shown in Plate II. It is essentially a cam-driven piston oscillating in a fluid chamber. The piston diameter is 2.0 in., and its stroke is approximately 0.216 in. The range of oscillation varies from 0 to about 9 cps.

Two test manifolds were used; their characteristics are given in Table I. They were fabricated from extruded acrylic tubes, approximately 1/2 in. inside diameter by 1/16 in. thickness by 6 ft. length. Sharp-edged orifices were machined along the axis of the tube. Extreme care was taken so that tolerances were minimized and no burrs remained on the interior surfaces.

The system was constructed in such a manner that the manifolds could be interchanged; a flange containing an "O" ring seal at each end of a manifold can be secured to an upstream or downstream acrylic block. The flowmeter probe is adjacent to the upstream block, and the gate valve is fastened to the downstream block.

Piezometer rings were fused to the manifolds, and to the rings, pressure transducers were connected, Plate III. Four radial holes of 1/32 in. diameter were drilled symmetrically about the tube circumference. The ring was slipped in place and welded to the tube.

The flow capability of the system is such that mean Reynolds numbers range from 0 to 15,000 for a closed tube. Tap water was used as the fluid medium; enough electrolytes were present so that the flowmeter could be calibrated. Throughout the experiment, the density of the water was assumed to be 1.0 gm/cm^3.

TABLE I

EXPERIMENTAL MANIFOLDS
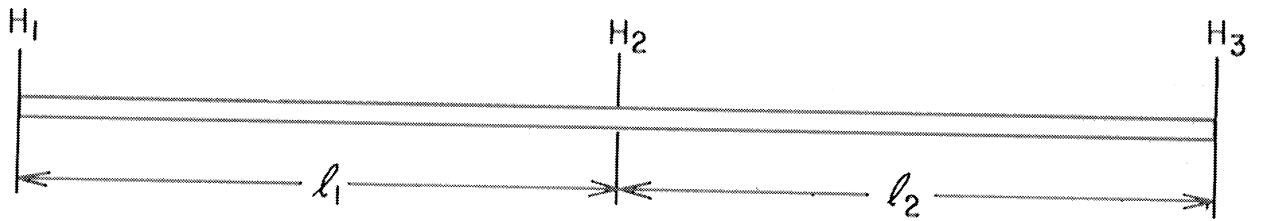
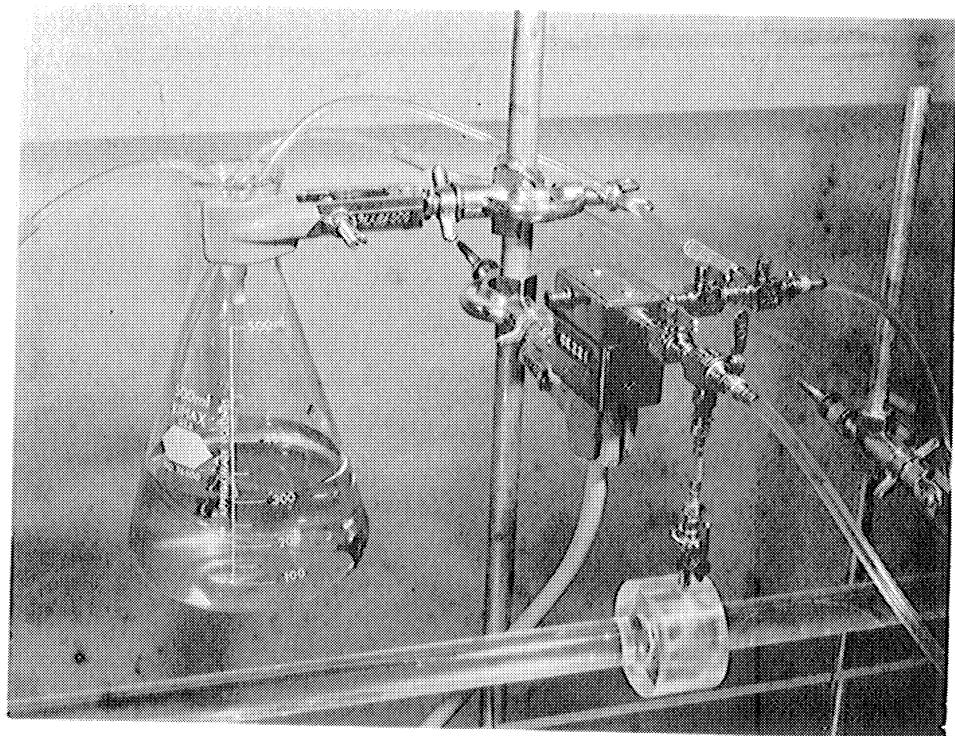| Manifold	No. of Orifices	ℓ_1 (cm)	ℓ_2 (cm)	Ave. A_o (cm^2)	Ave. A (cm^2)
M1	18	77.15	77.15	.0227	1.321
M2	12	76.10	76.10	.0227	1.291

Plate III.   Detail of Pressure Pickup.

4.2. Recording of Data

Electronic instrumentation was used to record the data. Piezometric heads were monitored with Sanborn Model 267B Physiological Pressure Transducers, and a Model 201 Square-Wave Flowmeter (Carolina Medical Electronics) measured flows. Pressure-time and flow-time curves were recorded on a Sanborn 7714A Oscillographic Recording System. A four-channel oscilloscope was used for monitoring purposes.

The pressure transducers were statically calibrated in two ways: first by a known voltage supplied by the recording system, which in turn was verified by loading the transducers with actual static pressures. The calibration factors remained quite stable; however, some base-line shift was discernable. The flowmeter was calibrated by passing known volume rates through the probe and recording the corresponding voltage outputs. The probe was quite sensitive to thermodynamic changes, and hence, shifting of the calibration factor and base line were noticed. A discussion of the pressure transducer and flowmeter frequency responses are reserved for Section 5.2 of the next chapter.

Plate IV shows a typical data run recorded on the oscillograph. Q_1 is the upstream flow, and H_1 , H_2 , and H_3 are the upstream, midstream, and downstream heads, respectively, in the experimental manifold. Preceeding the run, care was taken to purge the entire system of air bubbles, and calibration and base-line checks were made before and after each series of runs.

Two properties of a closed tube were also evaluated. The system bulk modulus for a closed tube was determined by measuring the change
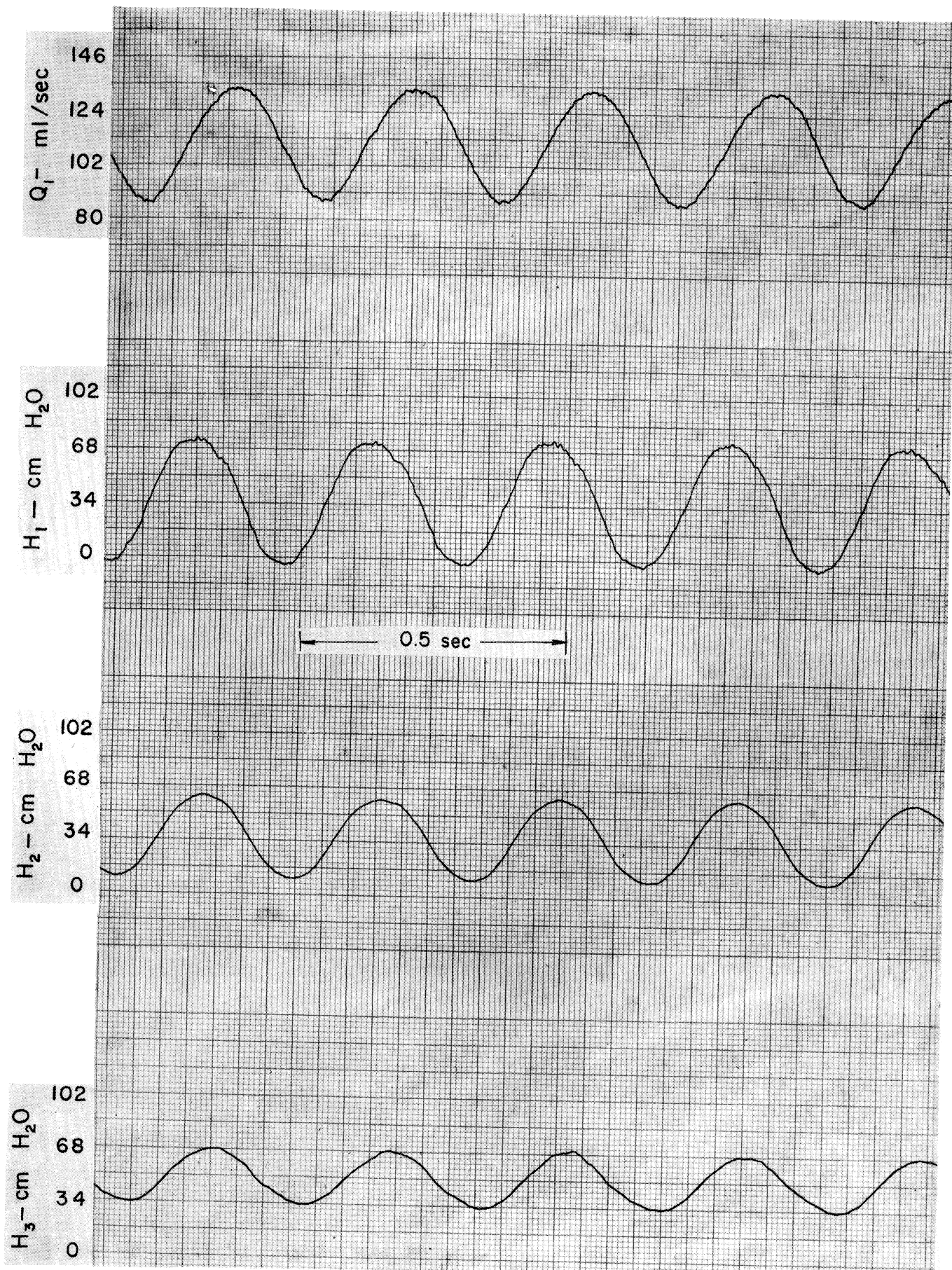
Plate IV. Experimental Data. Run M1-0-5.

in pressure for a corresponding change in volume; a small syringe injected fluid into the tube. Steady-state frictional head-loss-versus-flow data was also recorded. Figures 18 and 19 in Chapter V show the data for the determination of K and h_f, respectively.

V. ANALYSIS OF EXPERIMENTAL DATA

The preceeding chapter described experimental equipment and procedures which were used to obtain oscillating pressures and flows in a manifold system. Attention is now drawn to the analysis of the data.

5.1. Properties of a Closed Tube

For the solution of the hyperbolic equations, it is necessary to define a pressure-pulse wave speed. It was proposed in Chapter II, that if the capacitance effects of a manifold were similar to those of a closed tube, then the wave speed, a , is given by $\sqrt{K/\rho}$, K being defined as the system bulk modulus of elasticity. In Chapter III this assumption was utilized, and it was seen that the hyperbolic equations would predict flows in a manifold even if elastic effects were minor.

The determination of K for an acrylic closed tube similar to those from which the experimental manifolds were fabricated is shown in Figure 18. It is about twenty-five per cent lower than the theoretically computed value. The discrepancy may be due to small air bubbles entrapped in the tube. No refinement was attempted, since the knowledge of an accurate wave speed is not critical -- recall that the analysis is mainly one of surging flows and capacitance effects are minor. In Figure 18, K = 1.505 x 10^9 dyn/cm^2 , and if ρ = 1.0 gm/cm^3 , the corresponding value of the wave speed is a = 388 m/sec.

The steady-state frictional head loss in the manifolds is likened to that of a closed tube; this enables the determination of an empirical head-loss-versus-flow relation, Figure 19. The manifolds were designed so that the effects of friction would be minimized, and as a result it was difficult to obtain accurate data.
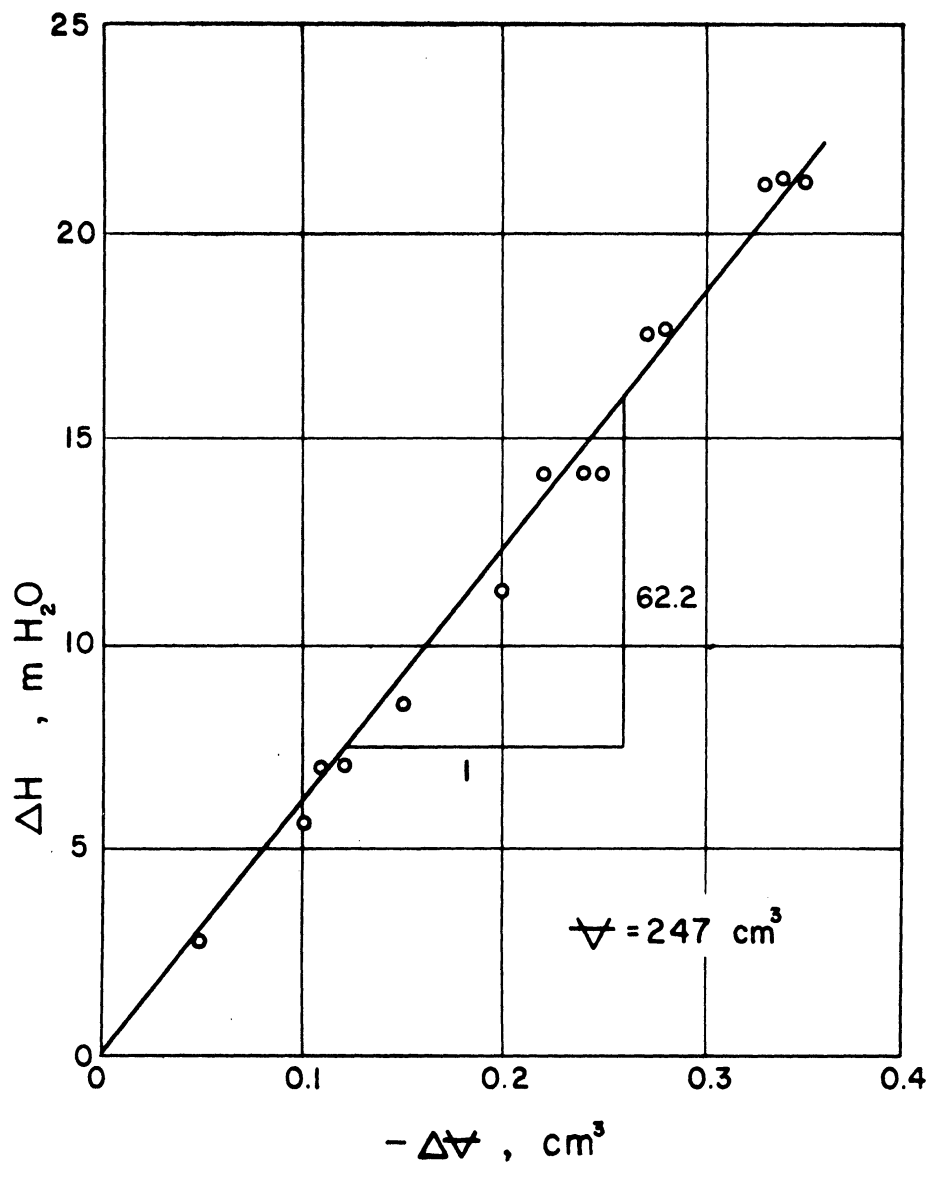
$$K = -\frac{(\rho g \Delta H)}{\Delta V / V} = 1.505 \times 10^{9} \ dyn/cm^{2}$$

Figure 18. Determination of Bulk Modulus of
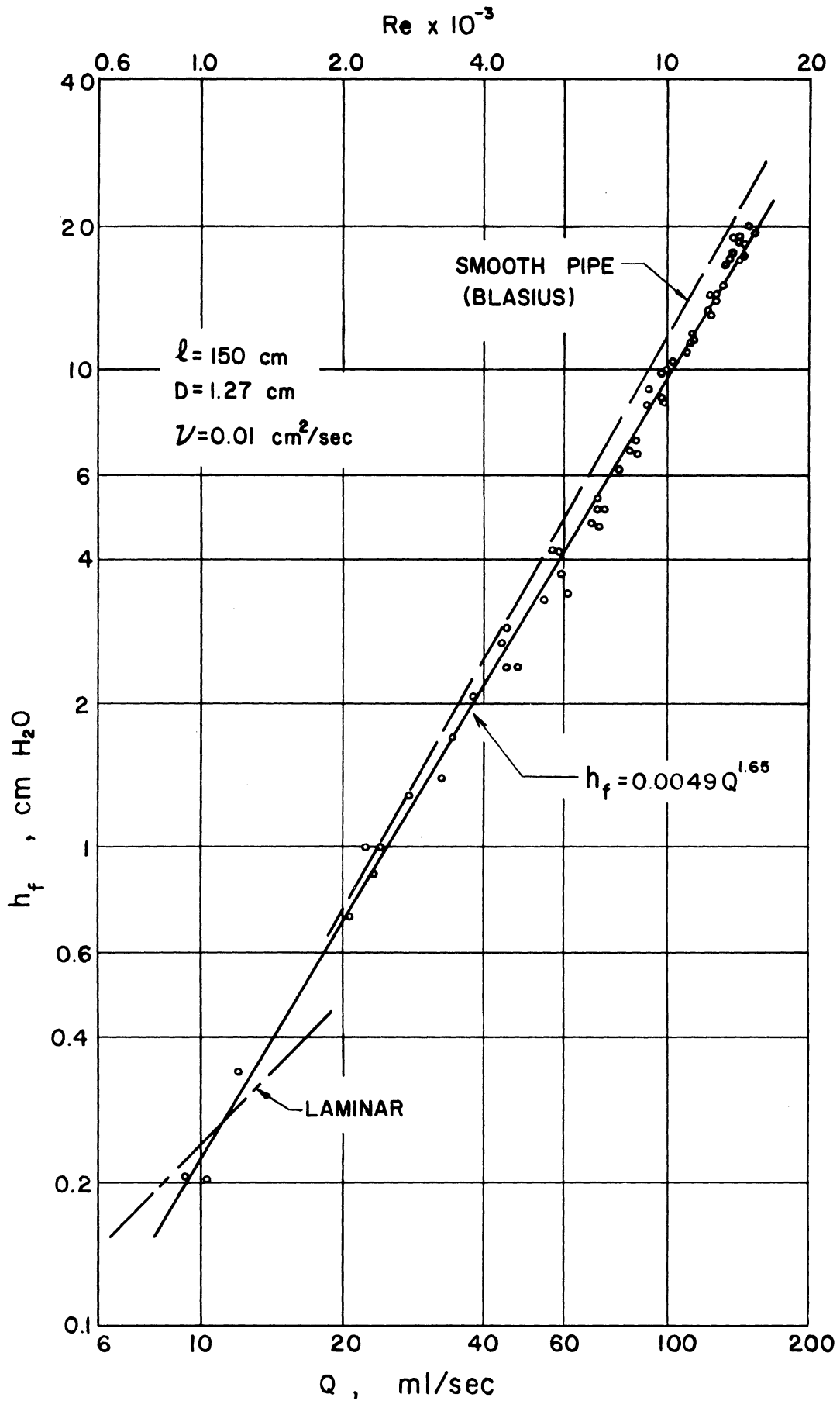Elasticity for a Closed Tube.

Figure 19. Steady-State Head Loss versus Flow for a Closed Tube.

The scattering of the data may be due to several causes: (1) the relatively short length of tube (150 cm) between pressure measurements, (2) neglection of inlet conditions, (3) inaccurate recording of the small head gradients, and (4) transition effects at low Reynolds numbers. A least-squares analysis of the data determined the constants for the head-loss relation. The maximum flows encountered in the experiment were about 150 ml/sec, and the corresponding head loss per unit length is 0.127 cm/cm.

5.2. Frequency-Response Analysis

So that an accurate description of the experimental pressures and flows can be obtained, it is necessary to know instrumentation frequency response. In the process of recording data, the pressure transducers contain a finite amount of fluid which possesses inertia, and the flowmeter has response lag due to its electronic filtering circuits.

A representative pressure transducer was calibrated, and the frequency-response analysis described by McDonald[10] was performed, Figure 20. The transducer is underdamped (damping factor = .04), and at 25 cycles per second the response is flat. The natural resonating frequency is approximately 149 cycles per second, a frequency well above those of significance in this study.

Frequency-response curves of the flowmeter were obtained by employing a dummy-probe input modulated by an electronic sine-wave oscillator. The results in Figure 21 show that the amplitude begins to drop immediately and the phase is highly nonlinear. It is evident that the various harmonics of a given flow pattern will be distorted unless the data is adjusted. This can be accomplished by subjecting
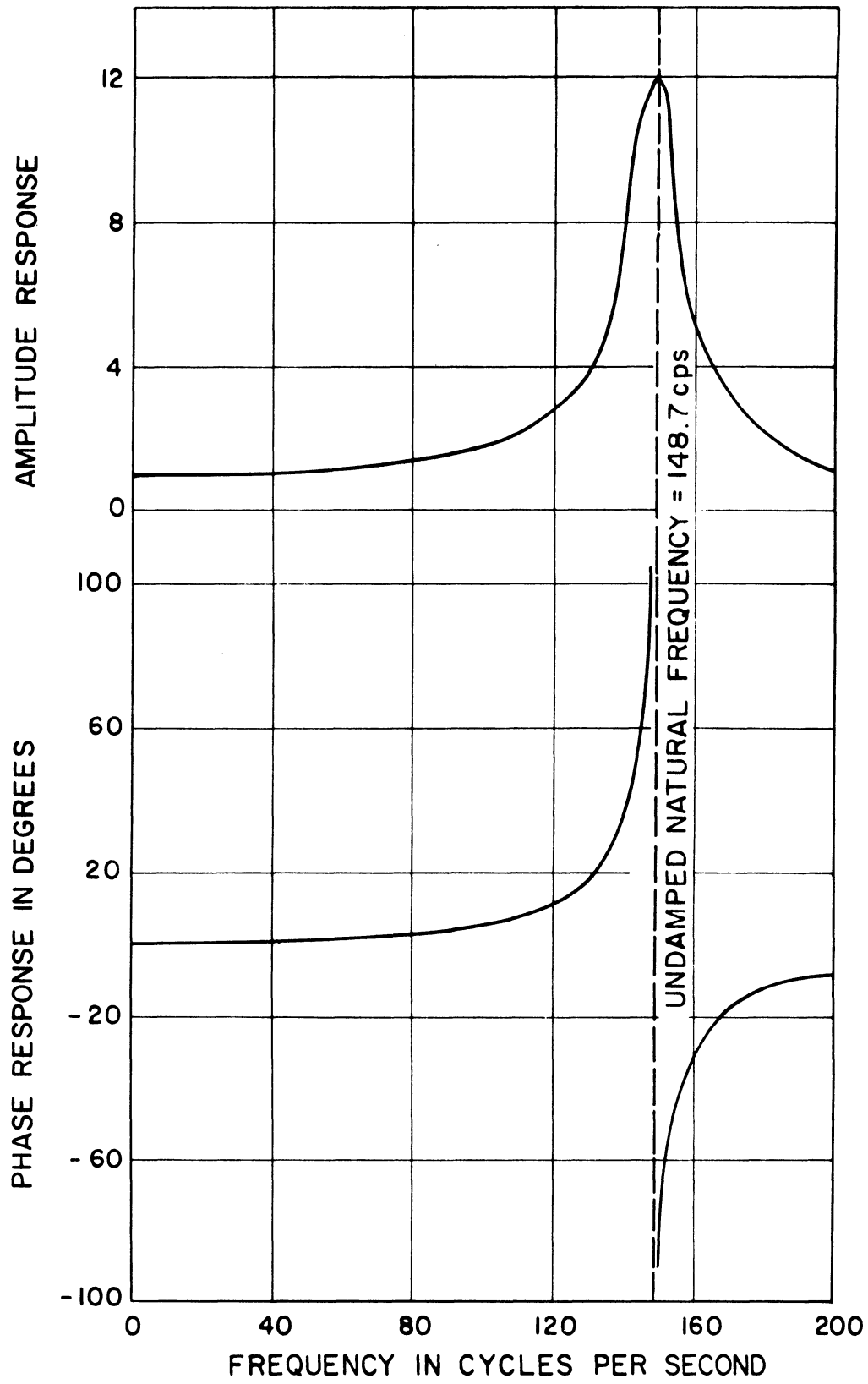
Figure 20. Frequency Response of Pressure Transducer.
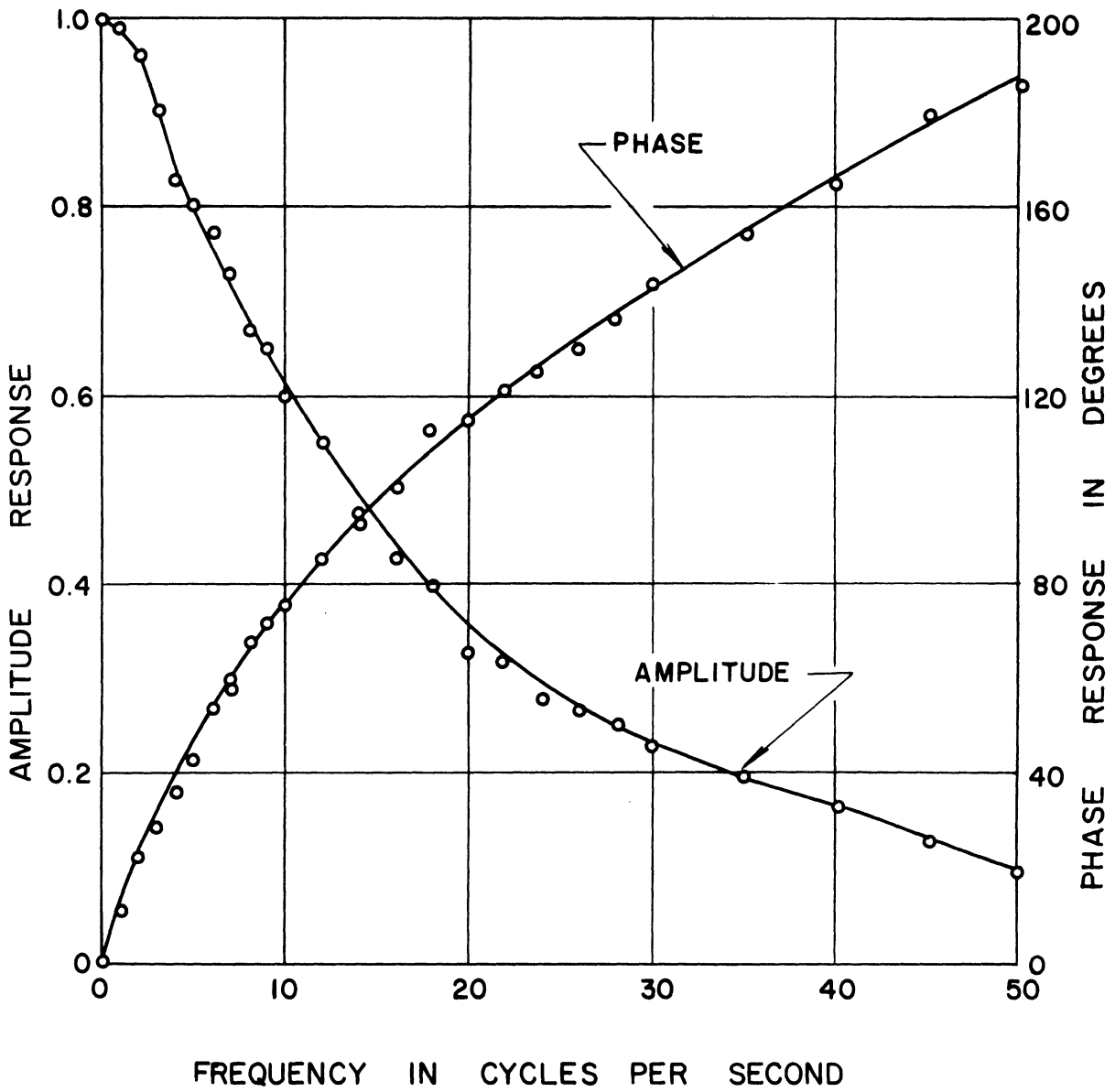
Figure 21. Frequency Response of Square-Wave Flowmeter.

the flow curve to a Fourier analysis and modifying each component for phase and amplitude error.[22,23] The procedure can be performed on a digital computer and is outlined below:

1. Data points of the flow curve are read and subjected to a Fourier-analysis subroutine. If there are n points and kk is the desired number of harmonics, then for the ith data point

$$Q_i = A_o + \sum_{k=1}^{kk} [A_k \cos(ky) + B_k \sin(ky)] \ ,$$
$$y = 2\pi \ i/n \ , \ i = 0,1,...,n \ . \tag{30}$$

A and B are Fourier coefficients. The flow curve is re-constituted by means of Equation (30) to assure that the designated number of harmonics is sufficient to describe the curve accurately.

2. Data points of the flowmeter frequency-response curves are read in, and at each harmonic, a parabolic interpolation[19] is used to evaluate the phase and amplitude corrections, respectively designated as PH_k and AMP_k .

3. The flow curve is then corrected by adjusting the amplitude and phase of each harmonic, resulting in Q'_i , the corrected flow:

$$Q'_i = A_o + \sum_{k=1}^{kk} [\frac{A_k}{AMP_k} \cos(ky + PH_k) + \frac{B_k}{AMP_k} \sin(ky + PH_k)]. \tag{31}$$

The result of such an analysis is shown in Figure 25. Throughout the analysis of the experimental data it was found sufficient to let kk = 6 .

5.3. Analytical Verification of System Variables

How well the theory presented in Chapter II relates to actual physical situations can best be demonstrated by a direct comparison of predicted and observed parameters. It was seen earlier that a discrete manifold can be approximated by a continuous one for a wide range of orifice geometry. In this section attention is given only to the relations pertaining to continuous manifolds.

Four sets of data are used for analysis; some pertinent parameters are related in Table II.

TABLE II

RESUME OF EXPERIMENTAL DATA

Run No.	Freq. (cps)	ϕ	ζ
M2-C-11	2.64	0.213	1.0
M2-C-12	3.34	0.213	1.0
M1-C-9	3.70	0.310	1.0
M1-O-5	3.03	0.310	0.603

The results of predicted heads and flows are compared with the experimental data in Figures 22 through 25. In all cases the upstream boundary condition for the computer solutions is taken as the experimental head-versus-time curve -- the data points were read into the computer and a Fourier analysis was performed to give a continuous time-variable curve. Six harmonics were found sufficient to describe the curve accurately (compare Figure 25 with Plate IV). The downstream boundary condition for runs M2-C-12, M2-C-11, and M1-C-9 is a dead end. During
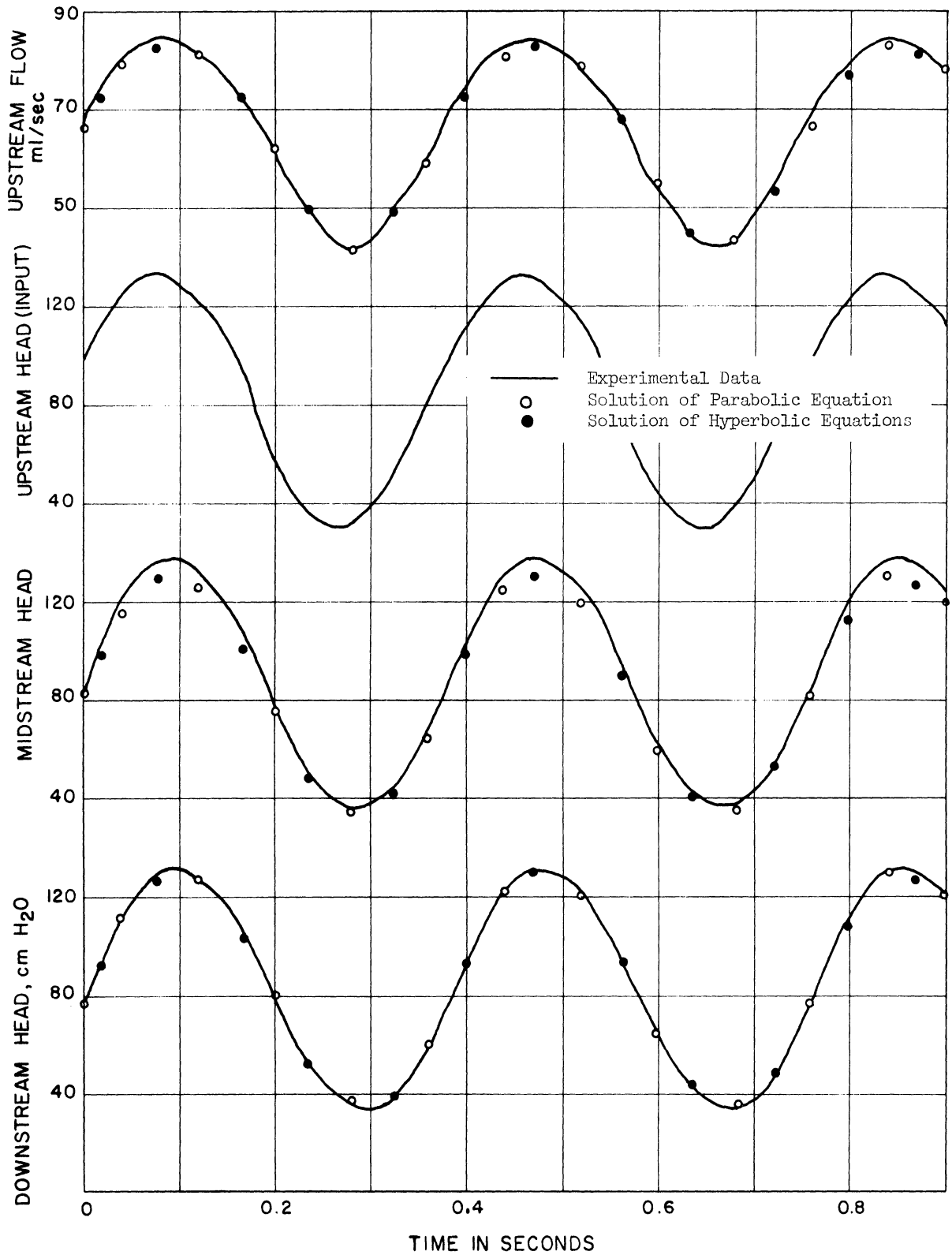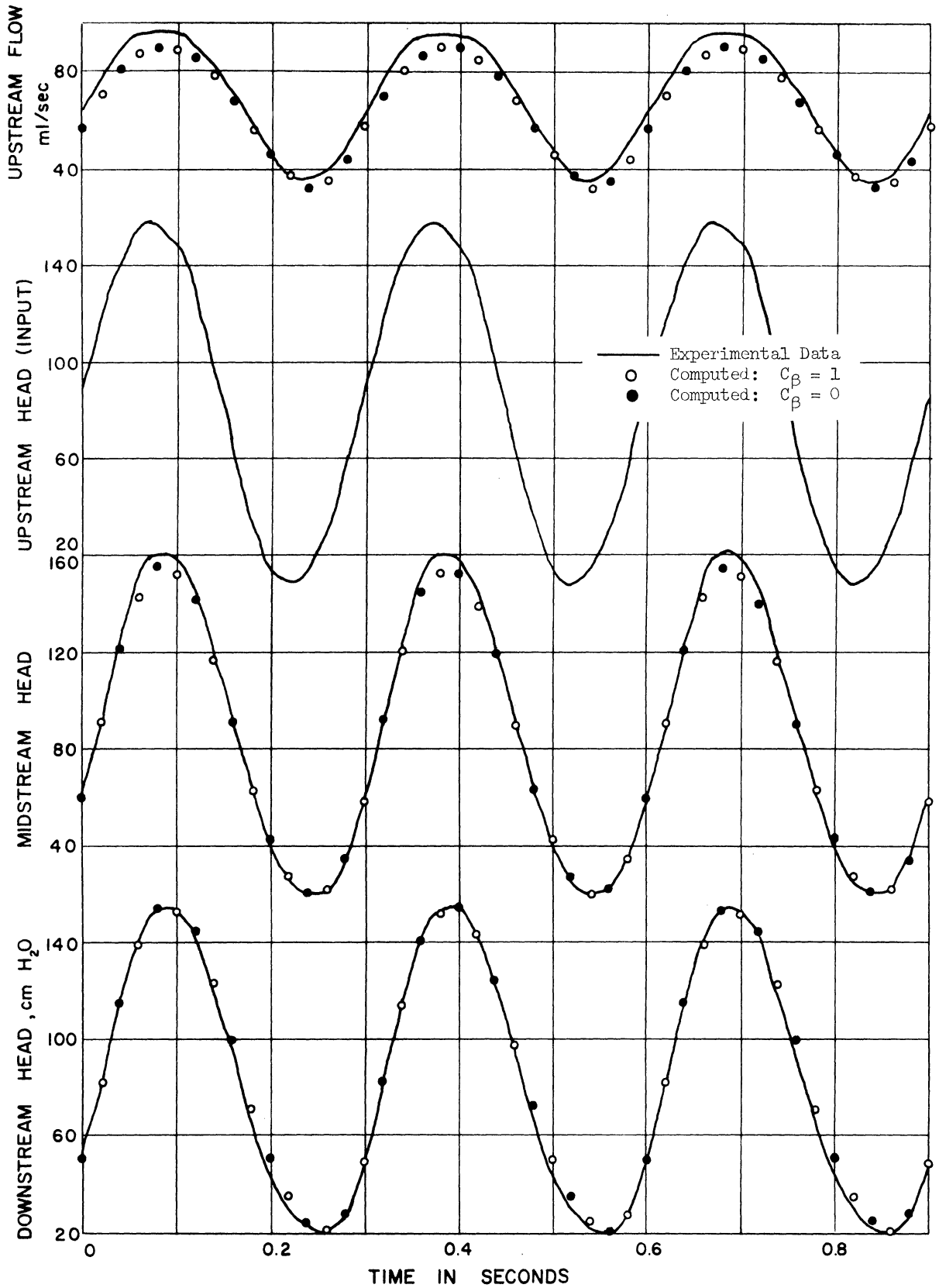
Figure 22. System Variables versus Time. Run M2-C-11.

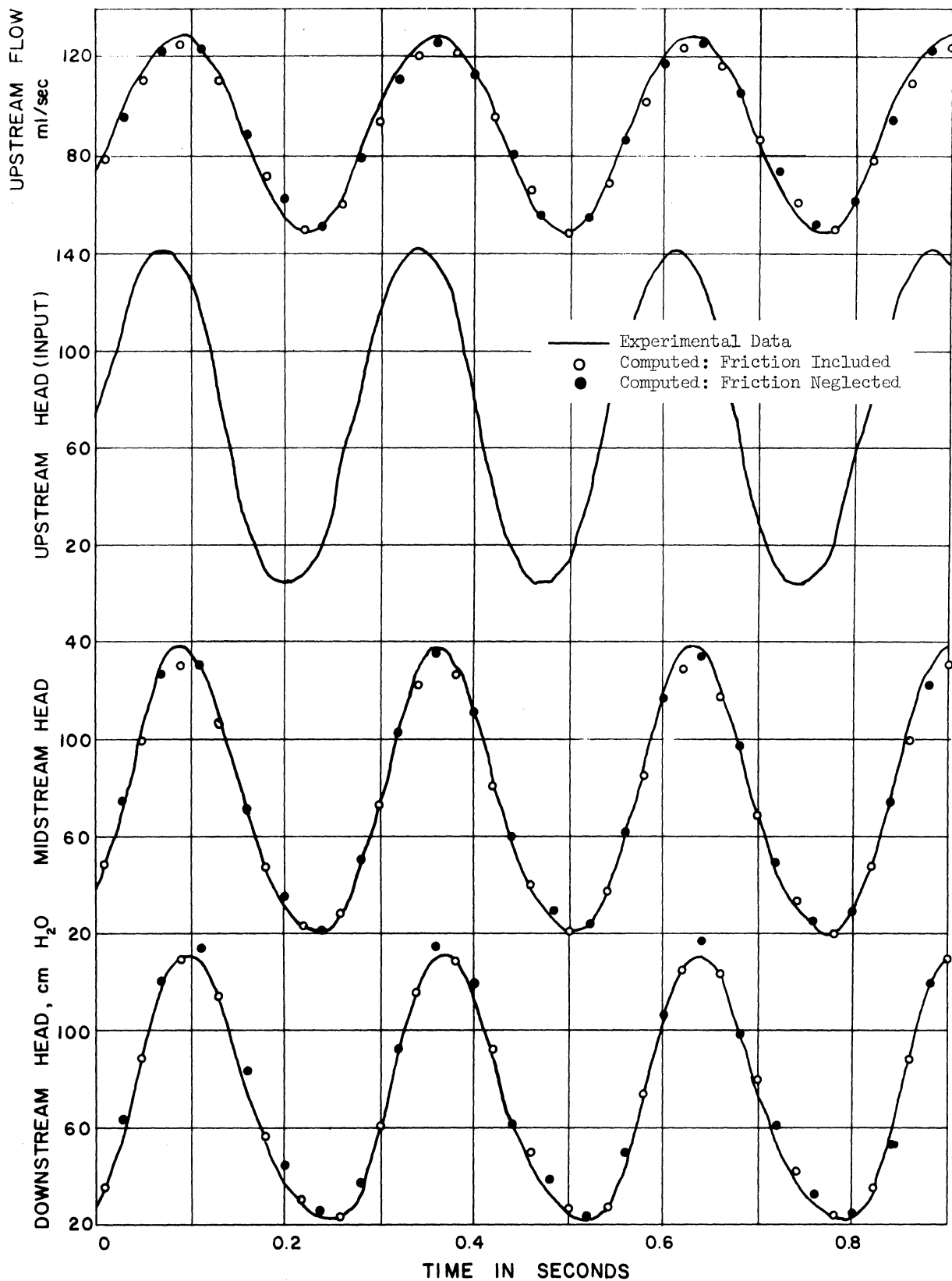Figure 23. System Variables versus Time. Run M2-C-12.

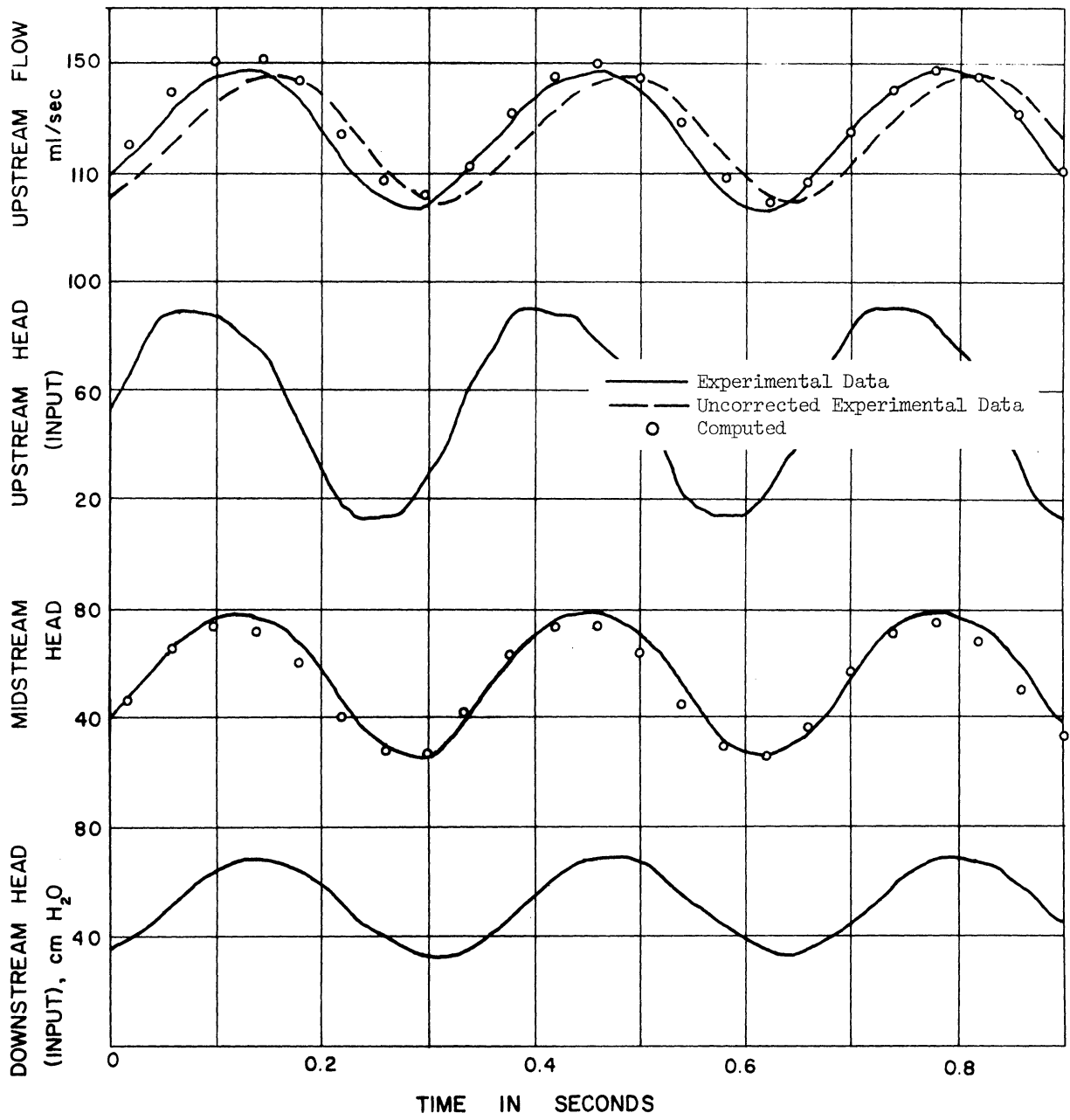Figure 24. System Variables versus Time. Run Ml-C-9.

Figure 25. System Variables versus Time. Run M1-0-5.

run M1-0-5, the downstream gate was open and the experimental head-versus-time curve was used as the boundary condition.

The experimental head-input pulses are essentially composed of one harmonic, and for the closed-end systems a qualitative reference can be made to the impedance relations shown in Figures 13 and 14 of Chapter III. In these figures, the system with ϕ = .113 is similar to the experimental manifolds. In the data, ω ranges from 16.6 to 23.2 radians per second. Since ϕ is large and the frequencies are small, capacitance effects are of minor importance. The momentum and continuity relations reduced to either parabolic or hyperbolic form can be used to predict system variables.

A digital computer was used to evaluate heads and flows on the time-distance grid. First, the Fourier analysis was performed on discrete boundary head data -- the upstream curve, and if necessary, the downstream one. At time zero, the initial distributions were computed by means of the Runge-Kutta solution of Equation (10). Then for times greater than zero, the solutions of either the parabolic or hyperbolic relations, Equations (11) or (16) and (17), were carried out, applying boundary conditions when appropriate. The finite-difference solutions of these equations are given in the appendices.

Computation was continued until steady-oscillatory conditions were attained -- three to four flow cycles were sufficient. Note in Figures 22 through 25 that the time scale is relative -- the variables are behaving in a steady-oscillating manner. A continuity check was made for the last computed flow cycle, and for all cases shown, the inflow minus the outflow agreed within $\pm$ 1/2 per cent.

System variables in the finite-difference scheme were computed and printed at quarter lengths along the tube axis. It is significant to note that only four sections were required. Figure 22 shows a comparison of computed and experimental system parameters -- heads at midpoint and the downstream end, and upstream flow. The predicted parameters result from a solution of either the parabolic or hyperbolic equations. Figures 23 through 25 show similar comparisons except that only the parabolic relation has been used.

Difficulty is encountered when attempting to predict a multiple number of parameters in a precise manner; several factors contributing to some discrepancies warrant mention.

First, instrumentation errors cause the data to be inaccurately recorded. Base-line shift can readily cause an error in a prescribed head gradient, which may be the case in Figure 25 where the flow has not stabilized, and the discrepancy in the midstream heads of all the runs may be due to such an error. The problem of accurately recording the flows has been discussed in Section 5.2. Secondly, the finite-difference methods used to solve the equations are only approximations, and some error is introduced when using them. Lastly, assumptions must be made regarding some system parameters; even though their effects may be small, they must be included in the list of uncertainties.

It is assumed that the axial component of momentum leaving through the orifices has the same velocity as the mainstream -- thus $C_\beta = 1$. The effects of letting $C_\beta = 0$ are minor, Figure 23. Generally, C_β may lie somewhere between these two extremes. An interesting qualitative picture of this outflow phenomenon can be seen in

Plate V, which shows a portion of a manifold under steady-flow conditions. In one case, the downstream gate is shut; the mainstream velocity is small, and consequently, the lateral outflow possesses a small axial component of momentum. However, when the downstream gate is open, the large mainstream velocity will substantially increase this axial component.

The orifice contraction coefficient, C_d , is based on a value theoretically predicted by McNown and Hsu.[12] For divided flows such as orifice outflow, the limiting value of C_d as the ratio of the orifice area to the main tube area approaches zero is 0.6. For the experimental manifolds, the magnitude of the area ratio is such that $C_d \approx 0.6$, an assumption which is used throughout the analysis and appears to be valid.

The frictional losses in the manifolds were assumed to be similar to steady-state losses in a closed tube, and the predetermined head-loss-versus-flow curve of Figure 19 was employed. The frictional effects of this particular experimental system are minor; in Figure 24 can be seen the results of neglecting the head-loss term.

Figure 25 describes the system variables when the downstream gate is open, so that all of the flow input does not leave the manifold laterally, but under steady-state conditions, $\zeta = 0.603$. The flow prediction is extremely sensitive to the head gradient.

Generally, the predicted curves are in agreement with the experimental data. Substantiation is given to the intuitive reasoning of Chapter II, namely, that the hyperbolic equations will handle flows under such conditions, but since capacitance effects are negligible, the parabolic relation serves equally well. Indeed, for such a class of flows,

(a)

(b)
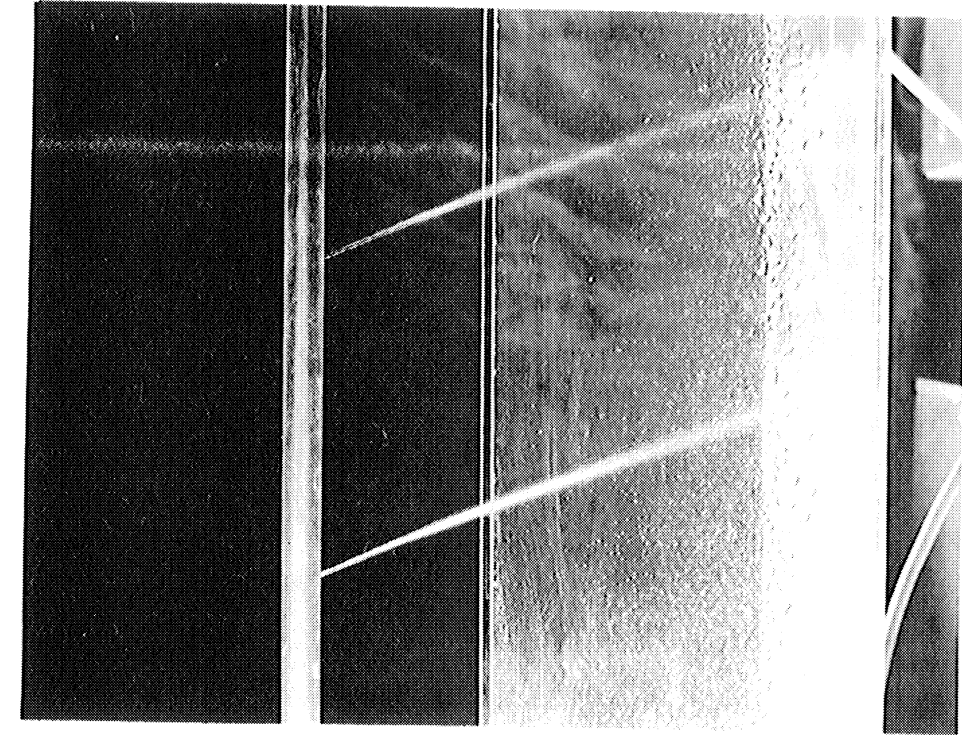
Plate V. Steady-State Lateral Outflow. (a) Downstream Valve Closed;
(b) Downstream Valve Open.
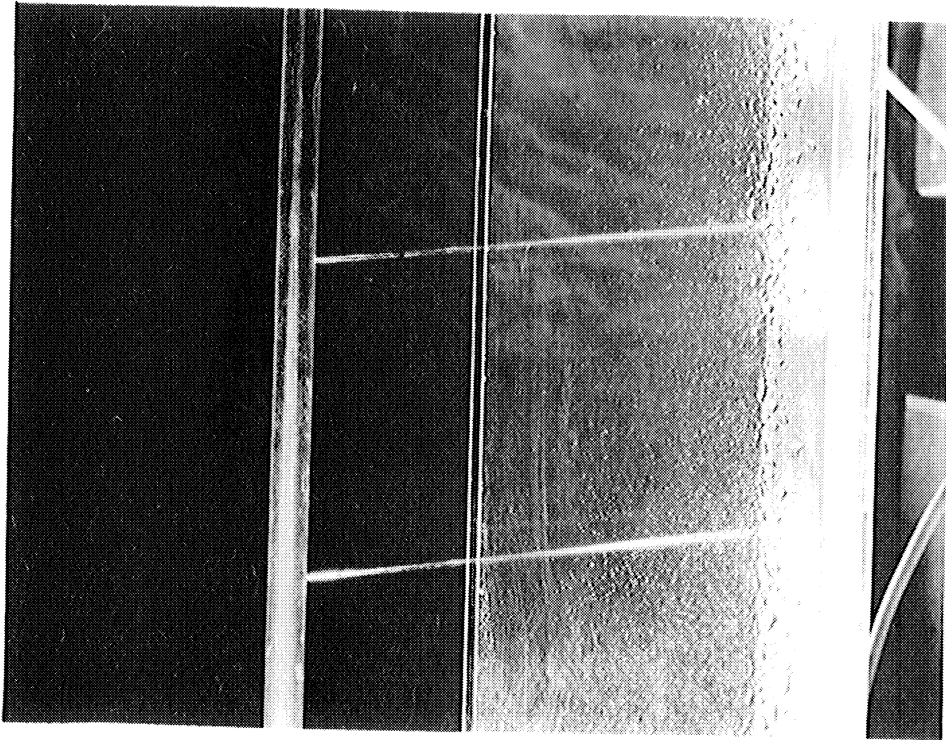
the hyperbolic equations seem awkward, and on the computer their solutions can be time consuming. The experimental curves exhibit the traveling-wave phenomena which was predicted in Chapter III. The evidence can be seen by observing the phase relationships between the head curves in any of the figures.

The approximate continuous manifold theory seems will suited to predict flows in such systems as described in this chapter.

VI. SIMULATION OF A BLOOD-FLOW SYSTEM

In the introductory chapter, mention was made of the manner
in which a portion of the arterial tree, namely the thoracic and ab-
dominal aorta, could be considered as a distributed-outflow system.
One application of the theory presented in Chapter II would be to pre-
dict and analyze pulsatile pressures and flows in this major artery.

The aorta is highly flexible -- hence capacitance effects
cannot be ignored. A convenient way to solve the governing equations
of motion and continuity is to reduce them to hyperbolic form, and
utilize characteristic methods to evaluate system variables.

6.1. Nature of the Lateral Outflow

Consider the idealized model of a dog aorta shown in Figure
26. It is basically a tapered, elastic tube and possesses a number of
lateral branches -- the intercostal arteries in the thoracic region,
and primarily the celiac, mesenteric, and renal arteries in the abdom-
inal region.[14] The length of the aorta in these areas is about 40 cm;
approximately two-thirds of it lies in the thorax. The total area of
the intercostal arteries is smaller than the area of the remaining
branches; the lateral outflow can be described to account for this.

Assume that the input impedance to the laterals is purely re-
sistive; this is tantamount to neglecting acceleration forces in them.
It may be valid for very small laterals which are highly resistive,
but will be in error for larger branches. (Experimental investigation
would help to clarify the assumption.) Let H_B be a constant bed
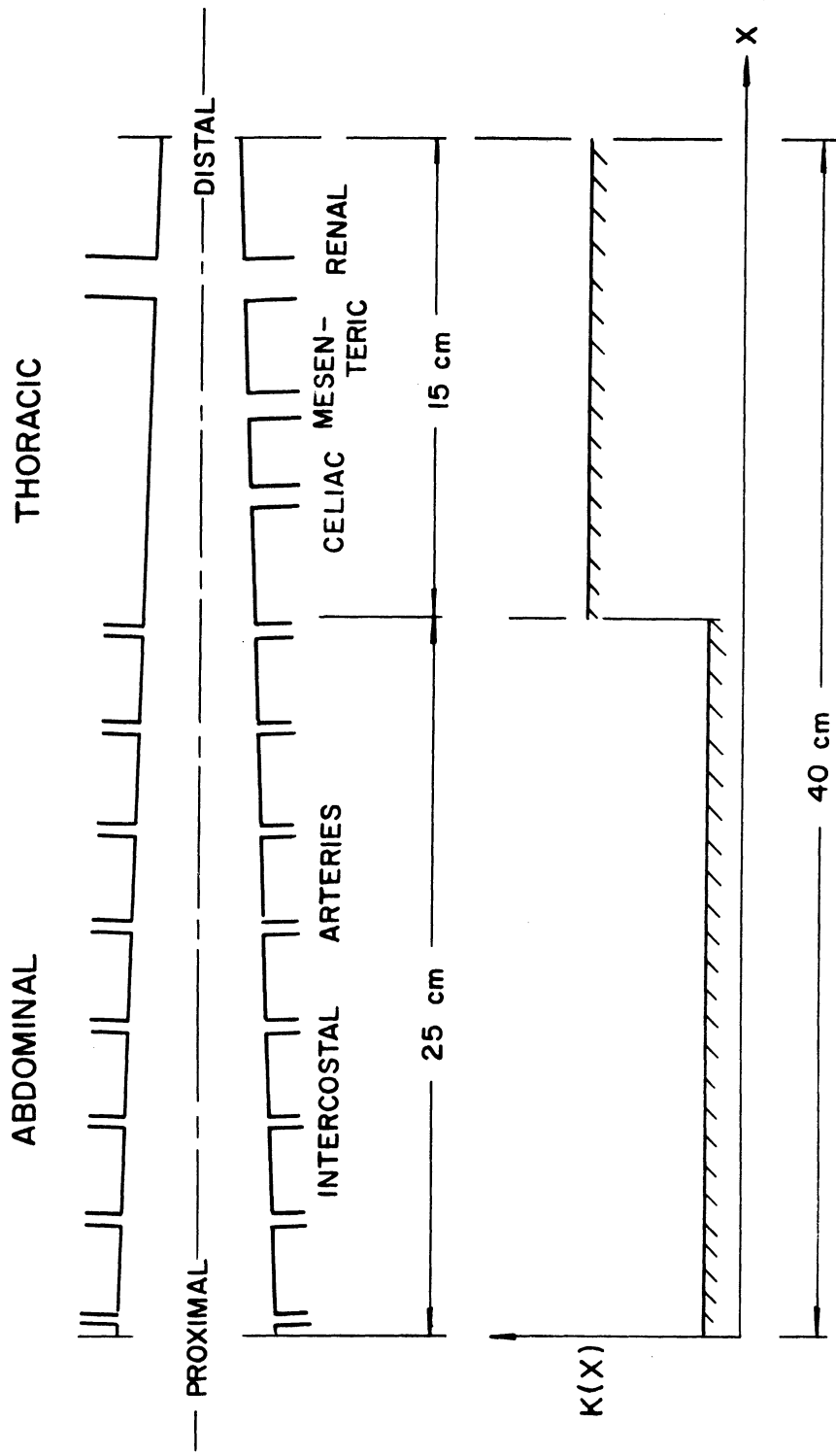
Figure 26. Idealized Model of Aorta.

pressure at some distance from the aorta. Then the flow into the branches, which is a summation of a mean plus a component due to pressure pulsations in the aorta, can be expressed as an outflow per unit length,

$$q = K(x)[H - H_B] , \qquad (32)$$

in which $K(x)$ is the outflow coefficient, and H the pressure head in the aorta. The coefficient accounts for the geometries and axial distribution of the laterals. The outflow is assumed to be laminar, and can be likened to flow between two parallel plates.

Equation (32) is the same which Streeter et al.[20] assumed in their study. Some typical lateral data are shown in Table III.

TABLE III

REPRESENTATIVE LATERAL DATA

Branches	Number	Diam. (cm)	Length (cm)
Intercostal	16	0.10	15
Celiac Mesenteric Renal	4	0.30	5

One way in which $K(x)$ can be distributed along the aorta is shown in Figure 26.

6.2. Method of Solution

Equations (1) and (2) of Chapter II -- the momentum and continuity relations -- are general, and describe the pressures and flows in a highly flexible and nonuniform vessel such as the canine aorta.

The following assumptions regarding the system of Figure 26 are made:

1. The aorta has a linearly tapering diameter.

2. The elastic relationship of the wall material is linear as described by Wylie,[24] and the blood is incompressible.

3. Flow is laminar, and the frictional losses are assumed to be quasi-steady in nature, i.e.,

$$h'_f(V) = 32\nu \, V/gD^2 \ . \tag{33}$$

With regard to the last assumption, it is possible to include a frequency-dependent friction term which has been shown to be a better approximation.[8,25] It is not used here due to resulting added computational procedures.

When the assumptions are introduced into Equations (1) and (2), they reduce to

$$g \frac{\partial H}{\partial x} + V \frac{\partial V}{\partial x} + \frac{\partial V}{\partial t} + \frac{32\nu}{D^2} V + (C_\beta - 1) V \frac{q}{A} = 0 \ , \tag{34}$$

$$\frac{\partial V}{\partial x} + \frac{g}{a^2} \left(V \frac{\partial H}{\partial x} + \frac{\partial H}{\partial t} \right) + 2 \frac{\alpha}{D_o} + \frac{q}{A} = 0 \ , \tag{35}$$

with the auxiliary equations

$$a^2 = a_{oo}^2 \left(\frac{D_o}{D} \right)^2 \left[1 - 2\ln\left(\frac{D}{D_o} \right) - g \frac{H_o}{a_{oo}^2} \right] \ , \tag{36}$$

$$\alpha = \frac{\partial D_o}{\partial x} \ , \tag{37}$$

wherein a_{oo} is the wave speed at zero pressure, D_o and H_o refer to initial conditions, and α is the rate of change of D_o per unit length. The diameter is related to the pressure head by the equation

$$H = \left(\frac{2a_{oo}^2}{g} \right) \left(\frac{D_o}{D} \right)^2 \left[\ln\left(\frac{D}{D_o} \right) + g \frac{H_o}{2a_{oo}^2} \right] \ . \tag{38}$$

Equations (34) and (35) are combined by a linear operator to form the characteristic equations

$$\pm \frac{g}{a} \frac{dH}{dt} + \frac{dV}{dt} + \left[\frac{32\nu}{D^2} V + (C_\beta - 1) V \frac{q}{A} \right] \pm a \left[\frac{q}{A} + 2 \frac{\alpha}{D_o} V \right] = 0 \ , \quad (39)$$

$$\frac{dx}{dt} - (V \pm a) = 0 \ . \qquad (40)$$

The finite-difference analogues of Equations (39) and (40) are formulated with a second-order approximation only for q in the last term of Equation (39), and the remaining coefficients are approximated by a first-order procedure. The details are not presented here -- they are similar to the methods given in Appendix B. Since a of Equation (36) may vary considerably, and may even be of the same order of magnitude as V , the characteristics grid solution of the equations is utilized.[9]

When the lateral outflow relation, Equation (32), is substituted into the finite-difference equations, V can be eliminated, and H is found by the solution of a linear equation. This manner of solving the characteristic equations is stable for the magnitudes of outflow which are investigated in the following section.

6.3. Evaluation of System Variables

It is difficult to obtain a complete and accurate set of in vivo data for the system which is being considered. However, by combining synthesized time-variable boundary conditions with the model aorta of Figure 26, one can, in a qualitative way, see how various assumed lateral outflow conditions will affect the predicted heads and flows.

The boundary-value problem is formulated in the following manner. At the proximal end of the aorta, the input flow pulse is assumed to be a rectified sine wave, shown in Figure 27. The amplitude of the pulse is 160 ml/sec, and its period is 0.4 second. At the distal end, the impedance can be matched with the characteristic impedance of an equivalent, frictionless, closed fluid line, $Z_c = a/gA$. This approximation has been previously employed;[24] with it, no significant pressure waves are reflected from the boundary. These boundary conditions in combination with the finite-difference analogues of the characteristic equations solve the system variables on a time-distance grid. The initial conditions can be handled by the method described in Chapter II.

Three variations of $K(x)$ are supposed; referring to Figure 26 they are:

	K(x), cm/sec	
	Thorax	Abdomen
(1)	0	0
(2)	0.0002	0.015
(3)	0.002	0.025

In the first case, there is no lateral outflow. Under the given steady-state conditions, about one-third of the mean inflow leaves laterally for case (2), and in case (3), approximately two-thirds. For the two conditions where $K(x)$ is greater than zero, most of the outflow will take place in the abdominal aorta. The intermediate case might be similar to an in vivo situation.

Figure 27 shows the steady-oscillatory solutions of heads and flows. The system variables are plotted at the proximal, center, and
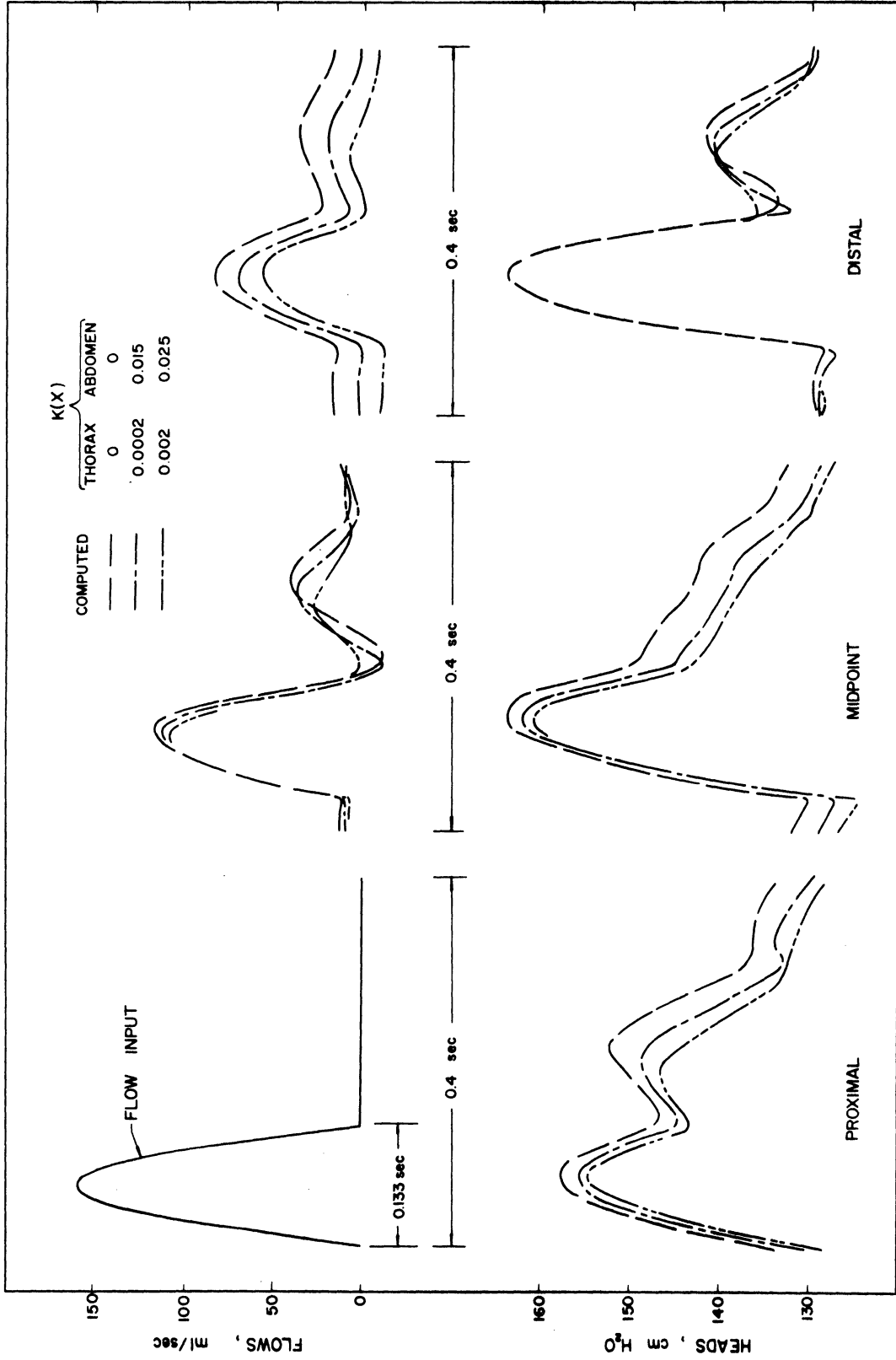
Figure 27. System Variables versus Time for a Simulated Flow Pulse.

distal points of the aorta for the three assumptions of $K(x)$. In the computer analysis, the aorta was divided into eight sections. For all cases, the input and initial conditions are:

$$a_{oo} = 600 \text{ cm/sec,} \qquad Q_o = 34 \text{ ml/sec (proximal),}$$

$$H_o = 141 \text{ cm } H_2O, \qquad H_B = 80 \text{ cm } H_2O,$$

$$D_o = 2.0 \text{ cm (proximal),} \qquad \alpha = -0.025 \text{ cm/cm,}$$

$$C_\beta = 1.0, \qquad \nu = 0.04 \text{ cm}^2/\text{sec.}$$

One cannot separate completely the effects of the imposed boundary conditions from those due to lateral outflow. However, since a major portion of the distal head curve is identical for all assumed outflow cases, the boundary condition seems to be well defined.

The variation of $K(x)$ is seen to affect the predicted para-meters in two distinct ways: (1) the baselines of the distal flow, and proximal and midpoint heads are lowered; (2) portions of some curves, such as the midpoint flow and proximal head, are attenuated. There is no appreciable phase shifting due to lateral outflow. Since the system is highly elastic, capacitance effects dominate the response patterns, and any consequences due to the outflow are minor in comparison.

It is assumed that the axial component of momentum leaving the aorta through the walls is reduced by contact with the branch, i.e., $C_\beta = 1$. If this momentum were destroyed before it left the main tube, then C_β would be zero. The same boundary value problem was solved for this latter condition, and the results were nearly identical to those of Figure 27.

The analysis of the variable, distributed outflow parameter described in this chapter provides further refinement to the complex

and intriguing problem of accurately predicting pressures and flows in arterial systems. The next vital step would be to obtain experimental data, and qualify some of the assumptions.

VII. SUMMARY AND CONCLUSIONS

The main purpose of this thesis is to analyze unsteady, non-uniform flows in pipelines which are experiencing leakage. Particular attention is given to the orifice manifold, since it provides a well-defined outflow relation, i.e., $q = B\sqrt{H}$, and can be applied to a wide range of practical problems.

Relations are developed for flows in both finite and continuous manifolds. For the finite system, the algebraic wave equations are coupled with momentum and continuity balances across the orifices, and thereby provide a set of nonlinear difference relations which allow the comparison of flows with those in an equivalent, continuous manifold.

Unsteady flows in the continuous manifold can be treated in several ways.

1. When the leakage parameter is of such magnitude that capacitance effects can be neglected, the continuity and momentum relations reduce to a nonlinear parabolic equation.

2. More generally, if the elasticity of the system is included, the governing equations become hyperbolic, and a pressure-pulse wave speed is introduced.

3. Impedance methods provide analytical solutions of the linearized equations for steady periodic flows, and encompass the two above-mentioned situations.

The elastic properties provide energy-storage mechanisms, and the orifice outflow together with frictional shear stresses tend to dissipate flow energy.

Numerical solutions of the nonlinear equations are based on the following techniques: (1) the Runge-Kutta method for steady flows, (2) the method of characteristics for the hyperbolic equations, and (3) for the parabolic relation, a finite-difference approximation based on relaxation methods.

Generally, the discrete manifold can be approximated by a continuous one for a wide range of orifice geometry. Several specific conclusions can be presented with regard to transient flows in manifolds, and are summarized.

1. The response to step-input functions is greatly affected by the magnitude of the lateral outflow. In the case of large outflow, the pressure transient is highly dissipated as it travels the length of the manifold: its corresponding wave front is distorted and propagates at an unsteady rate. This type of response is similar to those found in diffusion problems. As the outflow parameter, ϕ , is decreased, the dispersive effects become less pronounced; a condition is reached where water-hammer surges take precedence, and the pressure wave travels with the speed $a = \sqrt{K/\rho}$.

2. When a dead-end manifold is excited at a frequency of period $4\ell/a$, resonance will not necessarily occur. The criteria is set forth in the asymptotic solution of the linearized continuity relation, Figure 4 of Chapter II.

If, at a given resonating frequency, the leakage, repre-
sented by G , is the primary contributor. to the conti-
nuity balance, resonance will not take place. The dis-
sipative effects of the leakage are of such magnitude that
no accumulation. of energy is possible. Conversely, if the
geometry of the system is of such a size that the effect
of flow oscillation and capacitance, $i\omega C$, is the prime
element, flow energy accumulates in the manifold and res-
onance occurs.

3. If the dead-end system is excited at low frequencies, and
    $G \gg \omega C$, traveling waves are discernable, and the corres-
    ponding phase velocities are frequency dependent.

A laboratory investigation of low-frequency, oscillating flows
in a discrete manifold is included. The traveling-wave phenomenon can
readily be observed. For such a class of flows, the parabolic equation
is valid. The problem encountered is one of mass transfer; the nature
of the flow in the system is analogous to heat dissipation in a rod of
finite length, or a plate of finite width.

As an application of the theory, a portion of the main aorta
of a dog is synthesized as a nonuniform, distributed-outflow system.
Flows are assumed to be laminar, and if the input impedance to the
branches is resistive, the lateral outflow is given as $q = K(x)[H-H_B]$.
The governing equations reduce to hyperbolic form, and attention is
directed to the prediction of heads and flows for various assumed out-
flow conditions. Since the aorta is highly distensible, capacitance
effects dominate the response patterns.

The following items are recommended as areas for futher study:

1. An extension of the analysis described in Chapter III to include manifold systems which possess pronounced frictional losses.

2. In addition to the laboratory investigation described in Chapters IV and V, it would be desirable to study the response patterns in manifolds for a broader range of ϕ. Various boundary conditions, such as oscillating heads or sudden valve closure, could be imposed.

3. In the laboratory, model a highly elastic outflow system which would synthesize a complex arterial tree. The boundary conditions would be well defined, and the distributed outflow could be studied in detail. This would lead to an _in vivo_ investigation of an arterial system.

APPENDIX A

FINITE-DIFFERENCE APPROXIMATION OF PARABOLIC EQUATION

Equation (11) is a nonlinear parabolic partial differential equation with $V = V(x,t)$ as the dependent variable:

$$\frac{\partial V}{\partial t} + \left(\frac{A}{C_d b}\right)^2 \left(\frac{\partial V}{\partial x}\right)\left(\frac{\partial^2 V}{\partial x^2}\right) + (2 - C_\beta)\, V\frac{\partial V}{\partial x} + gh_f'(V) = 0. \quad (11)$$

Various finite-difference approximations to the derivatives can be made;[4,5,18] they have been shown to be convergent for linear parabolic equations. Little, however, is known concerning nonlinear ones.[5] One possible way to find a difference scheme which will ultimately yield a solution is by numerical experimentation.

In his review of numerical methods for parabolic differential equations, Douglas[4] has suggested the use of the Crank-Nicolson approximation to $\partial^2 V/\partial x^2$; it will be used here, coupled with the Gauss-Seidel iteration. Reference is made to the book of Smith[18] from which the following finite-difference schemes are obtained.

We choose approximations to Equation (11) which will readily yield an implicit difference equation whose solution can be obtained for any reasonable time step. Consider the x-t plane subdivided into rectangles with sides Δx and Δt as shown in Figure 1-A. Let the integers i and m refer to coordinates on the finite grid; m designates a new time and i distances along the space coordinate. The finite-difference approximations at an interior point are,

$$\frac{\partial V}{\partial t} = \frac{1}{\Delta t}\left(V_{i,m} - V_{i,m-1}\right), \quad (A-1)$$
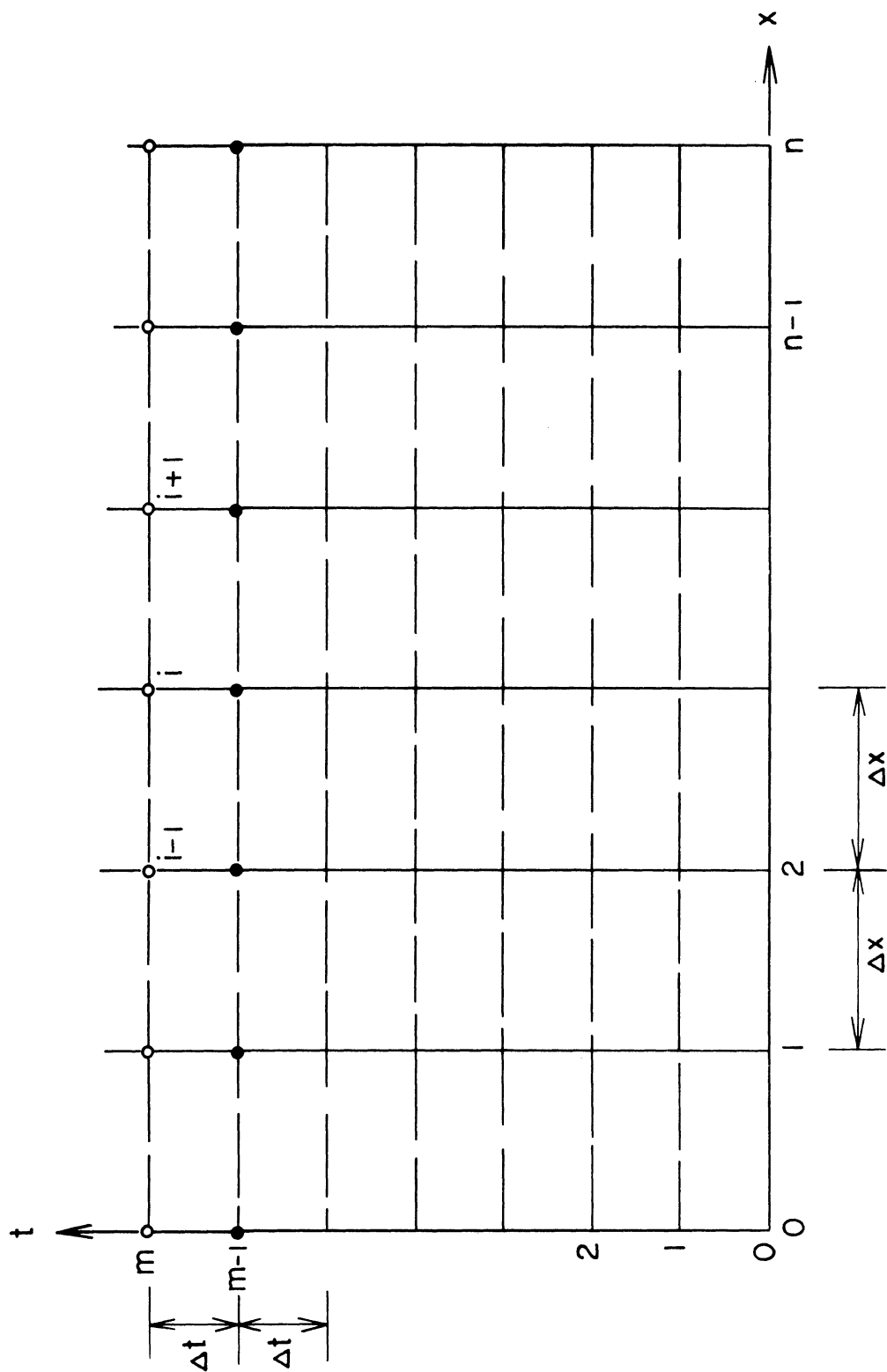
Figure 1-A.   Finite-Difference Grid for Solution of Parabolic
Difference Equation.

$$\frac{\partial V}{\partial x} = \frac{1}{2\Delta x} \left(V_{i+1,m} - V_{i-1,m} \right) , \qquad\qquad (A-2)$$

$$\frac{\partial^2 V}{\partial x^2} = \frac{1}{2(\Delta x)^2} \left(V_{i+1,m} - 2V_{i,m} + V_{i-1,m} + V_{i+1,m-1} - 2V_{i,m-1} + V_{i-1,m-1} \right).$$
$$(A-3)$$

The first two equations are derived by expanding V in a Taylor series about t and x. It is assumed that V and its derivatives are single-valued, finite, and continuous functions of x and t. The third equation is the Crank-Nicolson approximation of $\partial^2 V / \partial x^2$. Substituting these into Equation (11) yields the difference analogue of the parabolic equation:

$$\left. \begin{array}{l} \left(\dfrac{V_{i,m} - V_{i,m-1}}{\Delta t} \right) + \left(\dfrac{A}{C_d b} \right)^2 \left(\dfrac{V_{i+1,m} - V_{i-1,m}}{2\Delta x} \right) . \\[2em] \left(\dfrac{V_{i+1,m} - 2V_{i,m} + V_{i-1,m} + V_{i+1,m-1} - 2V_{i,m-1} + V_{i-1,m-1}}{2(\Delta x)^2} \right) \\[2em] + (2 - C_\beta)\, V_{i,m} \left(\dfrac{V_{i+1,m} - V_{i-1,m}}{2\Delta x} \right) + g h_f'(V_{i,m}) = 0. \end{array} \right\} \quad (A-4)$$

This relation is implicit, since it is necessary to simultaneously solve for V at every point i for a given new time m.

Since Equation (A-4) is nonlinear it is expedient to use an iterative point method as a means of solution. A systematic iteration which has been shown to converge rapidly to the exact solution for linear parabolic equations, termed the Gauss-Seidel iteration, can be used. Assume that V is known initially and has been computed through time $m - 1$ at the interior points and along the boundaries, Figure 1-A. Let the superscript j refer to the number of iterations within one

time step. Equation (A-4) can be rewritten to evaluate $V_{i,m}^{(j+1)}$ after j iterations:

$$V_{i,m}^{(j+1)} = \frac{V_{i,m-1} + C_1\lambda[V_{i-1,m}^{(j+1)} - V_{i+1,m}^{(j)}][V_{i-1,m}^{(j+1)} + V_{i+1,m}^{(j)} + U_i] - C_3 h_f(V_{i,m}^{(j)})}{1 + C_2[V_{i-1,m}^{(j+1)} - V_{i+1,m}^{(j)}]} \quad ,$$

(A-5)

in which

$$\lambda = \Delta t / (\Delta x)^2 \quad ,$$

$$C_1 = \left(\frac{A}{C_d b}\right)^2 \cdot \frac{1}{4\Delta x} \quad ,$$

$$C_2 = 2C_1\lambda - (2 - C_\beta) \, \Delta t / 2\Delta x \quad ,$$

$$C_3 = g\Delta t \quad ,$$

$$U_i = V_{i-1,m-1} - 2V_{i,m-1} + V_{i+1,m-1}$$

(A-6)

The iterative procedure can be executed on a digital computer and is stated in the following manner:

1. Of the terms on the right-hand side of Equation (A-5), only $V_{i,m-1}$ and U_i $(i = 0,1,...,n)$ are known at the outset; approximate the terms $V_{i-1,m}^{(1)}$, $V_{i,m}^{(1)}$, $V_{i+1,m}^{(1)}$ using the corresponding values at time m-1 .

2. Calculate a new $V_{i,m}^{(2)}$ for all i and store; with these new approximations, substitute into the right-hand side of the equation.

3. Repeat the above process j + 1 times for all $V_{i,m}$ until desired accuracy is obtained.

In particular, the iteration is terminated when $\epsilon \leq \epsilon_{max}$, where ϵ is defined as

$$\epsilon = \sum_{i=0}^{n} |V_{i,m}^{(j+1)} - V_{i,m}^{(j)}| \; . \tag{A-7}$$

Note that the most recent iterates are used as soon as they become available, i.e., $V_{i,m}^{(j)}$ is replaced by $V_{i,m}^{(j+1)}$ as it is computed.

The reduced continuity relation, viz., $\partial V / \partial x = - q/A$ provides a derivative boundary condition which is a time-variable known relation, since $q = C_d b \sqrt{2gH}$, and H is given. It is desirable to represent $\partial V / \partial x$ at $x = 0$ and $x = \ell$ in such manner as to be consistent in accuracy with Equations (A-1) through (A-3). Thus, to use a central-difference formula such as Equation (A-2) is necessary to imagine fictitious velocities $V_{-1,m}$ and $V_{n+1,m}$ by assuming the fluid line to be extended. Consider the left boundary condition:

$$\frac{V_{1,m} - V_{-1,m}}{2\Delta x} = - \frac{C_d b}{A} \sqrt{2gH_{o,m}} \; . \tag{A-8}$$

When this is combined with Equation (A-5), $V_{-1,m}$ can be eliminated and $V_{o,m}$ can be determined. In a similar manner, if $H_{n,m}$ is a known function of time, $V_{n,m}$ can be found. If the line possesses a dead end at n , then $V_{n,m} = 0$; assuming a mirror image, i.e., $V_{n+1,m} = - V_{n-1,m}$, then

$$- \frac{2V_{n-1,m}}{2\Delta x} = - \frac{C_d b}{A} \sqrt{2gH_{n,m}} \; ,$$

or
$$H_{n,m} = \left(\frac{A}{C_d b \Delta x}\right)^2 \frac{V_{n-1,m}^2}{2g} . \qquad \text{(A-9)}$$

Equations (A-5), (A-7), and the appropriate boundary conditions are used in Chapter V to predict the flows in the experimental manifolds. To compute the heads and lateral outflow at any point i, the orifice relation combined with the continuity equation in finite-difference form can be used once $V_{i,m}$ $(i = 0,1,\ldots,n)$ has been computed:

$$q_{i,m} = C_d b \sqrt{2g\,H_{i,m}} = -\frac{A}{2\Delta x} (V_{i+1,m} - V_{i-1,m}) . \qquad \text{(A-10)}$$

The most important property required of a difference analogue of a differential equation is that under certain conditions its solution converges to that of the differential equation as Δx and Δt approach zero. In a system such as the nonlinear one described herein, it is difficult to isolate the errors due to inconsistency (discretization errors) and those due to rounding off (instability). Generally, stability and consistency imply convergence. The best argument that the finite-difference approximations we are considering here are appropriate analogues of their corresponding differential equations is verification with the experimental data presented in Chapter V. To further substantiate this we can demonstrate what type of total error one might expect if the grid size, i.e., either Δx or Δt were altered.

In Figure (2-A) is shown the solution of $V(0,t)$ for the experimental data of Run M2-C-12 for three grid sizes. (See Figure 23, Chapter V.) The smallest grid size is $\Delta x = 19.025$ cm , $\Delta t = .01$ sec, and it produces the most output. The intermediate grid,
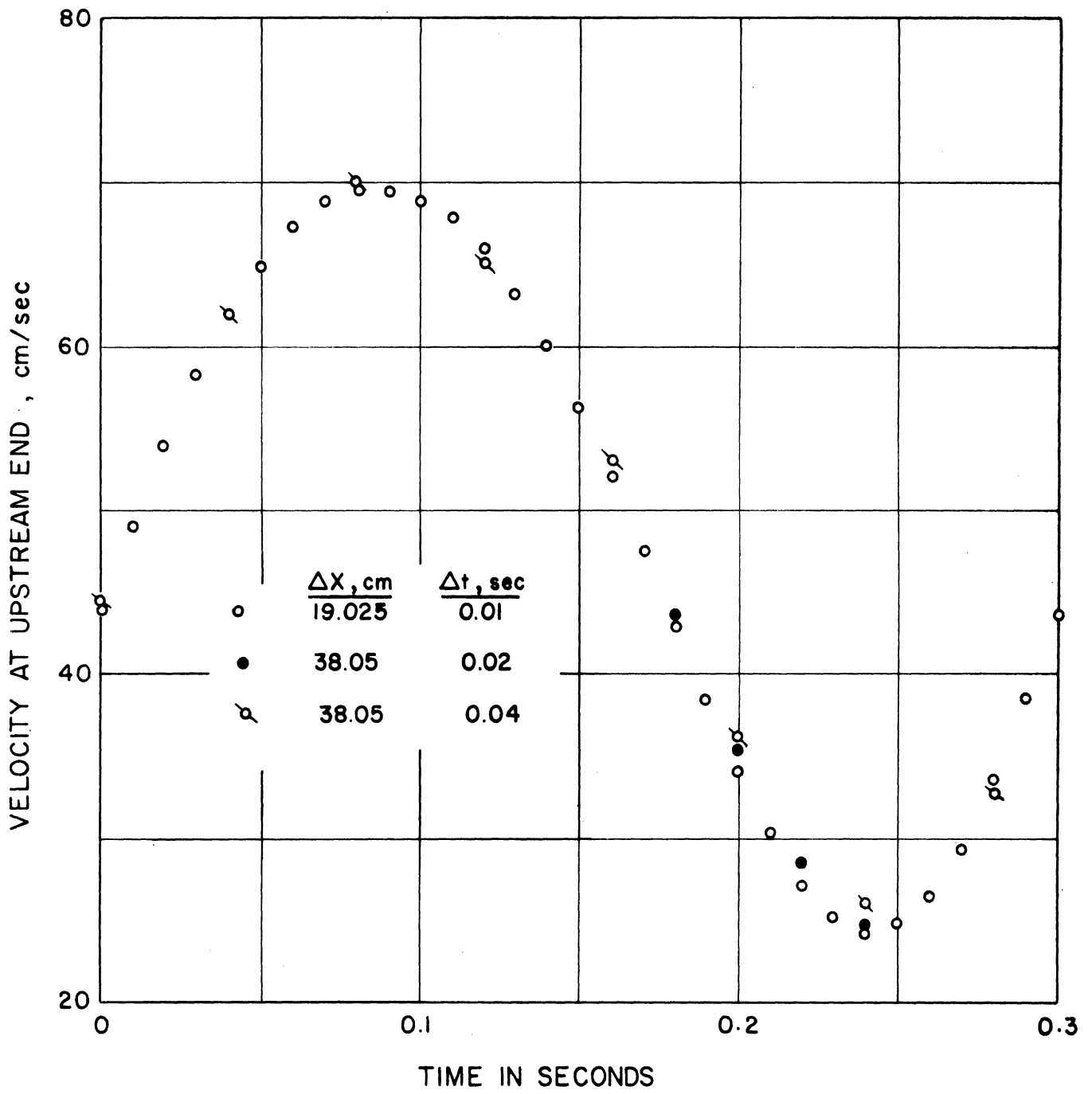
Figure 2-A. Velocity versus Time for Various Grid Sizes.

$\Delta x = 38.05$ cm, $\Delta t = .02$ sec, deviates slightly from the finest grid for only a portion of the flow cycle. The largest grid -- which yields the least information -- has $\Delta x = 38.05$ cm, $\Delta t = .04$ sec. It is seen to follow the pattern of the smallest grid but shows some deviation.

In the analysis of the experimental data of Chapter V, the intermediate grid is used. It is reasonably accurate, and the time increment is small enough so that a good comparison can be made with the recorded flow curves, see Figure 23.

Convergence and stability criteria appear to be satisfied, since for three different grid sizes, the solutions tend to remain the same, and they approximate the recorded flow curve.

APPENDIX B

FINITE-DIFFERENCE APPROXIMATION OF HYPERBOLIC EQUATIONS

Consider the characteristic equations in which $H = H(x,t)$ and $V = V(x,t)$ are the dependent variables:

$$\pm \frac{g}{a} \frac{dH}{dt} + \frac{dV}{dt} + \xi + \eta \pm \alpha = 0 , \qquad (16)$$

$$\frac{dx}{dt} - (V \pm a) = 0 . \qquad (17)$$

Assume A and a to be constant; referring to Figure (1-B), the finite-difference approximations are:

1. First-order accuracy,

$$\frac{g}{a} (H_P - H_R) + (V_P - V_R) + (\xi_R + \eta_R + \alpha_R)\Delta t = 0 , \qquad (B-1)$$

$$- \frac{g}{a} (H_P - H_S) + (V_P - V_S) + (\xi_S + \eta_S - \alpha_S)\Delta t = 0 ; \qquad (B-2)$$

2. Second-order accuracy,

$$\frac{g}{a} (H_P - H_R) + (V_P - V_R) + \left[\frac{1}{2} (\xi_P + \xi_R) + \frac{1}{2}(\eta_P + \eta_R) + \frac{1}{2}(\alpha_P + \alpha_R)\right] \Delta t = 0 , \qquad (B-3)$$

$$- \frac{g}{a} (H_P - H_S) + (V_P - V_S) + \left[\frac{1}{2} (\xi_P + \xi_S) + \frac{1}{2}(\eta_P + \eta_S) - \frac{1}{2}(\alpha_P + \alpha_S)\right] \Delta t = 0 . \qquad (B-4)$$

Equations (B-1) and (B-3) are valid along the C^+ characteristic, defined by $dx/dt = V + a$; similarly, Equations (B-2) and (B-4) are valid along the C^- characteristic, defined by $dx/dt = V - a$. Now, assume $a \gg V$, which is a reasonable restriction for a stiff tube (recall that in the experimental manifold $a \approx 388$ m/sec and the maximum velocities are about 1.15 m/sec). Then the characteristics become straight lines, and on the
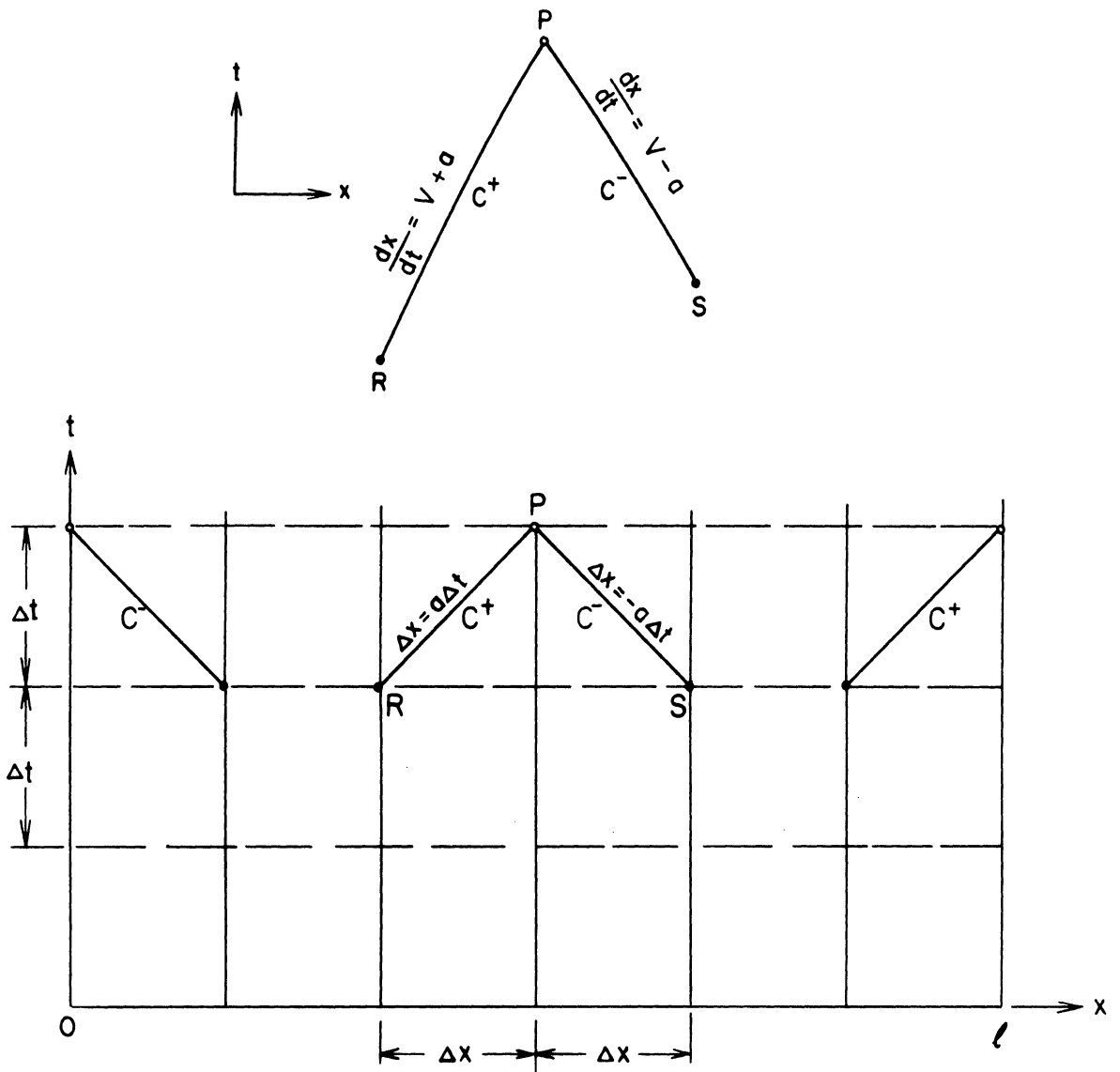
Figure 1-B. Finite-Difference Grid for Solution of Characteristic
Difference Equations.

finite grid, Equations (B-1) and (B-3) are valid on the C^+ characteristic $\Delta x = a \Delta t$, while Equations (B-2) and (B-4) are valid on the C^- characteristic $\Delta x = - a \Delta t$. (This simplification is not possible when consideration is given to flows in a distensible tube.)

If we consider a continuous manifold and utilize the orifice relation, the solution of H_P at an interior point is obtained by subtracting Equation (B-4) from (B-3) and noting that $\alpha_P = \frac{A}{a} q_P$:

$$- q_P = C_1 H_P - C_2 , \qquad (B-5)$$

$$C_1 = \frac{2Ag}{a^2 \Delta t} ,$$

$$C_2 = \left(\frac{A}{a\Delta t}\right) \left[\frac{g}{a} (H_R + H_S) + (V_R - V_S) \right.$$

$$\left. - \frac{\Delta t}{2} (\xi_R - \xi_S + \eta_R - \eta_S + \alpha_R + \alpha_S) \right] . \qquad (B-6)$$

Now,

$$q_P = C_d b \sqrt{2gH_P} = B \sqrt{H_P} , \qquad (B-7)$$

and combining Equations (B-5) and (B-7), one obtains

$$H_P = \frac{1}{(2C_1)^2} \left[(2C_1 C_2 + B) - \sqrt{(2C_1 C_2 + B)^2 - 4(C_1 C_2)^2} \right] . \qquad (B-8)$$

An iterative method must be used to solve for V_P, since in the second-order approximation ξ_P and η_P are expressed implicitly. The first-order relations can be used to approximate V_P; then ξ_P and η_P based on this value are used in the second-order equations to determine a better V_P. Note that α_P is known since H_P has been determined. The resulting iterative solution is obtained by respectively

adding Equations (B-1) and (B-2), and Equations (B-3) and (B-4):

$$V_P = \frac{1}{2}(V_R + V_S) + \frac{g}{2a}(H_R - H_S) - \frac{\Delta t}{2}(\xi_R + \xi_S + \eta_R + \eta_S + \alpha_R - \alpha_S) \ , \qquad (B-9)$$

$$V_P = \frac{1}{2}(V_R + V_S) + \frac{g}{2a}(H_R - H_S)$$
$$- \frac{\Delta t}{4}(2\xi_P + \xi_R + \xi_S + 2\eta_P + \eta_R + \eta_S + \alpha_R - \alpha_S) \ . \qquad (B-10)$$

At the upstream boundary, if H_P is a function of time, then again an iterative procedure solves V_P. Using Equations (B-2) and (B-4) along the C^- characteristic, one gets

$$V_P = V_S + \frac{g}{a}(H_P - H_S) - \Delta t(\xi_S + \eta_S - \alpha_S) \ , \qquad (B-11)$$

$$V_P = V_S + \frac{g}{a}(H_P - H_S) - \frac{\Delta t}{2}(\xi_P + \xi_S + \eta_P + \eta_S - \alpha_P - \alpha_S) \ . \qquad (B-12)$$

At the downstream end, if H_P is a function of time, then a solution similar to Equations (B-11) and (B-12) can be derived. As an alternative, consider $V_P = 0$ at the downstream end. Then ξ_P and η_P are zero. Let

$$C_1 = \frac{2Ag}{a^2 \Delta t} \ , $$

$$C_2 = \left(\frac{2A}{a\Delta t}\right)\left[\frac{g}{a} H_R + V_R - \frac{\Delta t}{2}(\xi_R + \eta_R + \alpha_R)\right] \ ; $$

$$\left.\begin{array}{c} \\ \\ \\ \\ \end{array}\right\} (B-13)$$

then the solution of H_P is given by Equation (B-8). At any point on the x-t grid, the lateral outflow can be computed using Equation (B-7).

By applying the second-order approximation to the coefficients of the characteristic equations, one is essentially utilizing the trapezodial rule to integrate along each characteristic. For example, along

the C^- characteristic the approximation of the term $\int \alpha dt$ is

$$\int_{t_S}^{t_P} \alpha dt \approx \frac{1}{2}(\alpha_S + \alpha_P)\, \Delta t$$

for the second-order approximation, whereas the first-order one is

$$\int_{t_S}^{t_P} \alpha dt \approx \alpha_S \Delta t \; .$$

For most hydraulic problems a first-order approximation is usually sufficient, but in the case that lateral outflow is present, α in Equation (16) may introduce instability if the second-order one were not used.

REFERENCES

1. Acrivos, A., Babcock, B. D., and Pigford, R. L. "Flow Distributions in Manifolds," _Chemical Engineering Science_, 10 (1959), 112-124.

2. Arden, B. W. _An Introduction to Digital Computing_. Reading, Massachusetts: Addison-Wesley Publishing Co., Inc., 1963.

3. Attinger, E. O., and Anne, A. "Simulation of the Cardiovascular System," _Annals of the New York Academy of Sciences_, 128, Art. 3 (1966), 810-829.

4. Douglas, J., Jr. "A Survey of Numerical Methods for Parabolic Differential Equations," _Advances in Computers_, Vol. 2, New York: Academic Press, Inc., 1961.

5. Forsythe, G. E., and Wasow, W. R. _Finite-Difference Methods for Partial Differential Equations_. New York: John Wiley and Sons, Inc., 1960.

6. Gray, C. A. M. Discussion of "Water Hammer Analysis Including Fluid Friction, by V. L. Streeter and Chintu Lai," _Journal of the Hydraulics Division_, ASCE, 89, No. HY1 (January, 1963), 211-214.

7. Horlock, J. H. "An Investigation of the Flow in Manifolds with Open and Closed Ends," _Journal of the Royal Aeronautical Society_ (November, 1956), 749-753.

8. Lambossy, P. "Oscillations Forcées d'un Liquide Incompressible et Visqueux dans un Tube Rigide et Horizontal. Calcul de la Force de Frottement," _Helvetica Physica Acta_, 25 (1953), 371-386.

9. Lister, M. "The Numerical Solutions of Hyperbolic Partial Differential Equations by the Method of Characteristics," _Mathematical Methods for Digital Computers_, New York: John Wiley and Sons, Inc., 1960.

10. McDonald, D. A. _Blood Flow in Arteries_. Baltimore: The Williams and Wilkins Co., 1960.

11. McNown, J. S. "Mechanics of Manifold Flow," _Transactions ASCE_, 119 (1954), 1103-1142.

12. McNown, J. S., and Hsu, E. "Application of Conformal Mapping to Divided Flow," _Proceedings First Midwestern Conference on Fluid Dynamics_, Ann Arbor: Edwards Brothers, Inc., 1951.

13. Markland, E. "The Analysis of Flow from Pipe Manifolds," _Engineering_, _187_ (January 30, 1959), 150-151.

14. Miller, M. E. _Anatomy of the Dog_. Philadelphia: W. B. Saunders Company, 1964.

15. Moore, R. K. _Traveling-Wave Engineering_. New York: McGraw-Hill Book Company, Inc., 1960.

16. Rich, G. R. _Hydraulic Transients_. New York: Dover Publications, Inc., 1963.

17. Rudinger, G. "Review of Current Mathematical Methods for the Analysis of Blood Flow," _Biomedical Fluid Mechanics Symposium_, ASME, New York (1966).

18. Smith, C. D. _Numerical Solution of Partial Differential Equations_. London: Oxford University Press, 1965.

19. Streeter, V. L. _Fluid Mechanics_. New York: McGraw-Hill Book Company, Inc., 1966.

20. Streeter, V. L., Keitzer, W. F., and Bohr, D. F. "Pulsatile Pressure and Flow Through Distensible Vessels," _Circulation Research_, Vol. XIII, No. 1 (July, 1963).

21. Streeter, V. L., and Wylie, E. B. _Hydraulic Transients_. New York: McGraw-Hill Book Company, Inc., 1967 (in press).

22. Tolstov, G. P. _Fourier Series_. Englewood Cliffs, New Jersey: Prentice-Hall, Inc., 1962.

23. Wiggert, D. C., and Keitzer, W. F. "Pulsatile Flow in Cylindrical and Tapered Rubber Tubing," ASME Paper No. 64-WA/HUF-1, New York (1964).

24. Wylie, E. B. "Flow Through Tubes with Nonlinear Wall Properties," _Symposium on Biomechanics_, ASME, New York (1966).

25. Zielke, W. "Frequency Dependent Friction in Transient Pipe Flow," (Ph.D. dissertation, University of Michigan, 1966).